REPORT NO.
UCB/EERC-92/07
AUGUST 1992

EARTHQUAKE ENGINEERING RESEARCH CENTER

A BEAM ELEMENT FOR SEISMIC DAMAGE ANALYSIS

by

ENRICO SPACONE
VINCENZO CIAMPI
FILIP C. FILIPPOU

A Report to the National Science Foundation
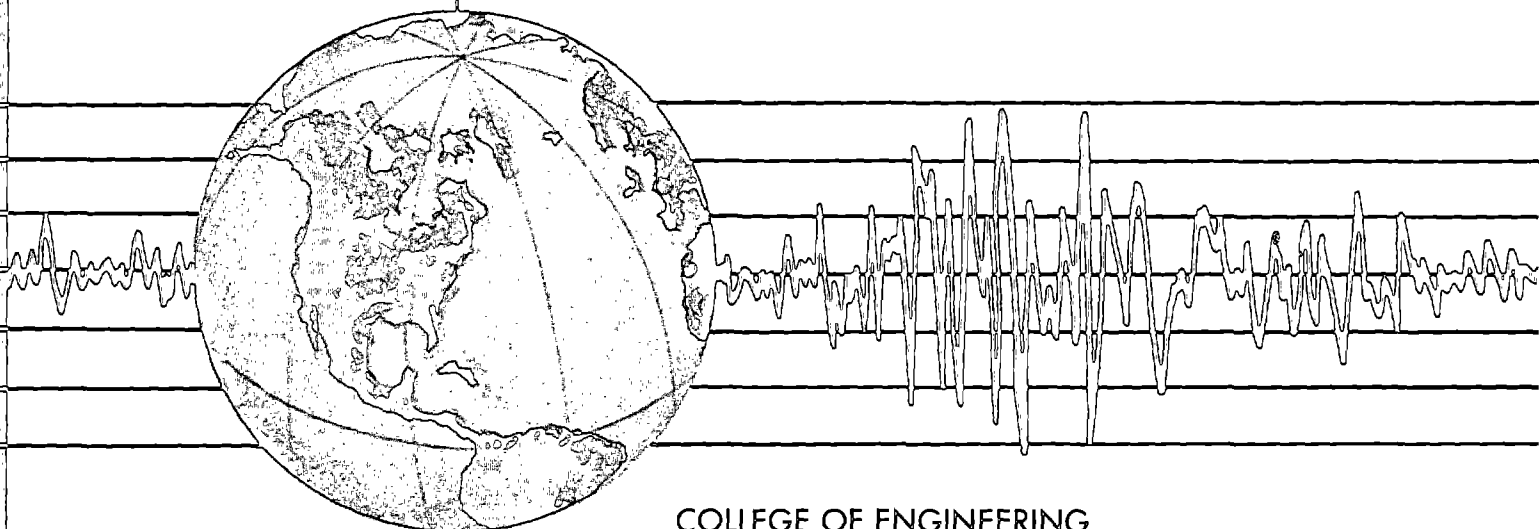
COLLEGE OF ENGINEERING

UNIVERSITY OF CALIFORNIA AT BERKELEY

A BEAM ELEMENT FOR SEISMIC DAMAGE ANALYSIS

by

Enrico Spacone
Doctoral Student, University of California, Berkeley

Vincenzo Ciampi
Professor, Università di Roma "La Sapienza"

and

Filip C. Filippou
Associate Professor, University of California, Berkeley

August 1992

ABSTRACT

This study proposes a beam finite element model with distributed inelasticity and two nonlinear end rotational springs for the nonlinear dynamic analysis of frame structures under earthquake excitations. The beam element is based on the assumption that deformations are small and shear deformations are neglected. The axial behavior is assumed linear elastic and is uncoupled from the flexural behavior. The element is derived with the mixed method of finite element theory. The force distribution within the element is based on interpolation functions that satisfy equilibrium. The relation between element forces and corresponding deformations is derived from the weighted integral of the constitutive force-deformation relation. While the element can also be derived with the virtual force principle, the mixed method approach has the advantage of pointing the way to the consistent numerical implementation of the element state determination.

The constitutive force-deformation relation of the control sections of the beam and of the end rotational springs has the form of a differential relation that is derived by extending the simple standard solid model according to the endochronic theory. This constitutive model can describe a wide range of hysteretic behaviors, such as strain hardening, "pinching" and degradation of mechanical properties due to cycles of deformation reversals. The deterioration of the mechanical properties of structural elements due to incurred damage is an evolutionary process that can be readily accounted for in the proposed incremental force-deformation relation. Damage is defined as the weighted sum of the dissipated plastic work and the maximum previous deformation excursions. Several examples highlight the effect of the various parameters of the proposed constitutive law.

A special nonlinear algorithm for the state determination is proposed that yields the stiffness matrix and the resisting forces of the flexibility based beam element. The proposed algorithm is general and can be used with any nonlinear section force-deformation relation. The procedure involves an element iteration scheme that converges to a state that satisfies the constitutive relations within the specified tolerance. During the element iterations element equilibrium and compatibility are always satisfied in a strict sense. The proposed method is computationally stable and robust and can trace the complex hysteretic behavior of structural

members, such as strain hardening, "pinching" and softening under cyclic nodal and element loads.

The study concludes with a demonstration of the ability of the proposed model to trace the softening response of a cantilever beam without numerical difficulties and with correlation studies of the response of the model with the experimental behavior of two reinforced concrete cantilever beams that highlight the flexibility of the constitutive law in the description of the hysteretic behavior of structural members.

ACKNOWLEDGEMENTS

TABLE OF CONTENTS

LIST OF FIGURES

LIST OF TABLES

CHAPTER 1

INTRODUCTION

1.1 General

The simulation of the hysteretic behavior of structures under severe seismic excitations is a very challenging problem. In addition to the problem of modeling the structural system and the interaction between its different components, there is the difficulty of representing the hysteretic behavior of the critical regions in the structure that undergo several cycles of inelastic deformation. Most experimental work in the last years is devoted to the understanding of the hysteretic behavior of critical regions in the structure, such as the ends of girders and columns under the combination of bending moment, shear and axial force, but very few experiments have addressed the study of entire lateral force resisting systems, because of the prohibitive cost of such studies. It is, therefore, implicit in this approach to improving the understanding of the seismic behavior of structural systems, that analytical models for the hysteretic behavior of critical regions will be derived from the experimental results, which will then be used in the simulation of the seismic behavior of entire structures. Unfortunately, the capabilities of computer hardware have limited such attempts to the simplest possible member models, which assume that all inelastic behavior is concentrated in a hinge of zero length. In conjunction with this approach, models of different degree of complexity were proposed for the description of the hysteretic moment-rotation relation of the hinge.

Models proposed to date suffer from several shortcomings that tend to undermine the credibility of analytical results: (a) the neglect of the spread of inelastic deformations as a function of loading history; (b) the neglect of the presence of distributed gravity loads on the inelastic behavior of the member; (c) the inability to account for the interaction between bending moment, shear and axial force in a rational manner; (d) the inability to account for strength loss and softening, because of numerical difficulties; and, (e) the inability of proposed hysteretic laws to simulate the evolution of damage and its effect on the subsequent hysteretic behavior of the inelastic region.

The continuous and precipitous increase in the computing power of engineering workstations calls for a match in the software capabilities of simulating the seismic behavior of structures. Since computing power is less of an issue nowadays, it is important to develop rational models of the hysteretic behavior of structural members, which are formulated in a clear, efficient and consistent manner, so as to ensure their robust numerical behavior in the nonlinear static and dynamic analysis of structures with many degrees of freedom.

1.2   Review of Previous Studies

The Finite Element Method of analysis is now the most widespread and general numerical method of structural analysis. Several models have been proposed to date for the simulation of the seismic behavior of steel and concrete structures. These range from simple nonlinear springs which lump the behavior of an entire story in a single degree of freedom to complex three dimensional finite elements that attempt to describe the behavior of a structural member by integrating the stress-strain relation of the constituent materials. An intermediate class of elements, often referred to as discrete finite elements, constitutes a compromise between these two families of models, by providing often sufficient detail of member behavior without the undue computational cost and the heavy demand on data storage and processing of three dimensional finite elements. Discrete finite elements represent a class of member models that use a priori assumptions about the force and/or displacement field of the member which result in considerable simplification of the element formulation. An extensive review of the discrete finite elements proposed to date is presented in the introduction of the companion study by Taucer et al. (1991) and is not repeated here.

The classical displacement method of analysis is most commonly used in the formulation of discrete finite elements. For frame elements the assumed displacement field consists of Hermitian polynomials that represent the exact solution for a prismatic member with uniform linear elastic material properties. Hermitian polynomials correspond to a linear curvature distribution in the member. Under nonlinear behavior this assumption deviates significantly from the actual curvature distribution giving rise to serious numerical problems. For members under cyclic deformation reversals and members that exhibit softening at the critical sections, displacement-based models are known to suffer from the existence of spurious solutions and from numerical instability and convergence problems. These problems persist even in the case that the finite element mesh is refined in the inelastic region of the member in an attempt to approximate better the actual curvature distribution.

In recent years growing interest has been directed at the force (flexibility) method of analysis for the formulation of beam finite elements. Beams are well suited for the application of the force method because the force distribution in the member is known exactly from the satisfaction of the equilibrium conditions. For end forces acting on an element without rigid body modes the axial force is constant and the bending moment distribution is linear. The internal force distribution is exactly known even in the presence of distributed element loads, whose treatment in nonlinear displacement-based models creates many challenges. Early proposals (Mahasuverachai and Powell 1982, Kaba and Mahin 1984, Zeris 1986, Zeris and Mahin 1988 and 1991) suggest different formulations and identify the advantages of the force method in the formulation of nonlinear frame elements. These studies, however, fail to give a clear and theoretically consistent formulation for the implementation of a flexibility based element in a general purpose finite element analysis program that is based on the direct stiffness method of analysis. The lack of a clear formulation plagues these models with numerical instability problems.

This study presents a new approach to the formulation of nonlinear flexibility-based frame elements. At present the nonlinear nature of the element derives from the material behavior of control sections that constitute the integration points of the element. Extensions of the method to geometrically nonlinear problems are possible, but are beyond the scope of this study. A general differential constitutive relation that derives from the endochronic theory describes the hysteretic behavior of control sections. The approach is, however, general and can be applied to any nonlinear section constitutive law. In fact, a companion study by Taucer et al. (1991) addresses the implementation of this method in the context of a fiber beam-column element for reinforced concrete members under cyclic deformation reversals.

The theoretical work in this report derives to a great extent from the original framework established by Professor Vincenzo Ciampi and his collaborators at the University "La Sapienza" of Rome, Italy. The original work is reordered, refined and extended in this study to produce a unified theory. An important extension of the model is its derivation from the formal framework of mixed finite element methods that clarifies the strong connection between formulation and numerical implementation and also opens the door to future extensions of the model. The extension of this formulation to a fiber beam-column element for reinforced concrete members is presented in the companion report by Taucer et al. (1991).

A significant advantage of the new formulation is its ability to accommodate a section constitutive relation of any level of complexity. In fact, the method is not limited to explicit constitutive relations and is amenable to incremental and differential relations. This offers the opportunity of exploring the potential of differential (evolutionary) constitutive relations in the damage analysis of structures under seismic excitations.

The differential model in this study was first presented as a section constitutive model by Brancaleoni et al. (1983). Carlesimo (1983) formulated a linear beam element with nonlinear rotational springs at the ends and used the model to describe the hysteretic behavior of the end springs. The first beam element with distributed plasticity that was based on this model was proposed by Ciampi and Carlesimo (1986) and was refined in its implementation details by Paronesso (1986), who also extensively tested the model.

An interesting aspect of the proposed differential model is its ability to trace the evolution of damage using the concept of intrinsic time from the endochronic theory of Valanis (1971). The accumulated damage continuously alters the strength and stiffness parameters of the hysteretic section relation in evolutionary fashion, thus, mimicking the actual behavior of the material. The damage index is defined as the weighted sum of the normalized energy dissipation and the normalized cyclic deformation ductility of the section. In this context, parameter identification methods are very useful in the selection of the monotonic and, particularly, the hysteretic parameters of the model. Such a method for the proposed endochronic model with strength and stiffness deterioration was proposed by Ciampi and Nicoletti (1986). Damage analysis is a major research area nowadays and several models have been proposed for the definition of the degree of damage at either the member or the structure level under seismic loading conditions. While the present study does not deal in depth with the subject, but intends, instead, to demonstrate the potential of the proposed model in seismic damage analysis, a short review of proposed damage models is presented below for the sake of completeness.

Damage is usually measured by means of a damage function (or damage index) D which varies from 0 to 1, where 0 indicates no damage and 1 indicates failure. Following a broad classification it is possible to order the proposed damage models in three classes: (a) one-parameter models, in which damage is a function of ductility or inelastic energy dissipation; (b) two-parameter models, in which damage is a function of, both, cyclic deformation ductility and inelastic energy dissipation; and, (c) low cycle fatigue models.

Models belonging to class (a) are based on cyclic deformation ductility or inelastic energy dissipation. *Cyclic ductility* is defined in Mahin and Bertero (1981) as

$$\mu_c = \frac{x_{max,c}}{x_y}$$

where $x_{max,c}$ is the maximum plastic excursion and x_y is the yield displacement. The damage function D_μ associated with cyclic ductility is

$$D_\mu = \frac{\mu_c}{\mu_{u,mon} - 1}$$

where $\mu_{u,mon}$ is the ultimate ductility in a monotonic test. Mahin and Bertero (1981) similarly define *hysteretic ductility* as

$$\mu_e = \frac{E_h}{F_y x_y} + 1$$

where F_y is the yield strength of the structural model and E_h is the total inelastic energy dissipation. The corresponding damage function D_e is

$$D_e = \frac{\mu_e - 1}{\mu_{e,u,mon} - 1}$$

where $\mu_{e,u,mon}$ is the attainable hysteretic ductility in a monotonic test.

A well known damage model in class (b) was proposed by Park and Ang (1985) who introduced a damage function that is the linear combination of the maximum displacement (deformation) ductility and the inelastic energy dissipation

$$D_{PA} = \frac{x_{max}}{x_{u,mon}} + \beta \frac{E_h}{F_y x_{u,mon}} = \frac{\mu_s + \beta(\mu_e - 1)}{\mu_{u,mon}}$$

β is a parameter that depends on the level of shear and axial force in the member and on the amount of longitudinal and transverse reinforcement. Another interesting set of damage functions in class (b) were proposed by Banon and Veneziano (1982).

Damage models in class (c) consider, in a simplified way, the distribution of inelastic cycles in the assessment of damage. Krawinkler and Zohrei (1987) and Krawinkler (1987) propose the following function as a measure of cumulative damage

$$D_K = A \sum_{i=1}^{n} (\mu_i - 1)^b$$

where $A = \left(\mu_{u,mon} - 1\right)^{-b}$, b is a structural coefficient, n is the total number of inelastic cycles and μ_i is the cyclic ductility corresponding to the i-th inelastic cycle.

The above damage indices represent an overall measure of the level of damage that a member or the entire structure have sustained during a seismic excitation. These indices are, therefore, used in the estimation of the impact of ground motions on a given structure or on a class of structures with similar material properties and structural configuration.

In the technical literature the term damage model is also used to denote hysteretic rules which account for the gradual strength and stiffness deterioration in the material or section behavior as a result of inelastic deformation reversals. Such hysteretic rules for material models which are expressed in terms of a stress-strain or section moment curvature relation are based on expressions that resemble the damage indices discussed above.

A number of degrading constitutive laws have been proposed to date. These are either based on continuum mechanics principles or on more phenomenological rules. The work of Lemaitre and Mazars in damage mechanics (Mazars 1989, Lemaitre 1992) is characteristic of extensive recent work in the first category. Representative of models in the second category is the work of Roufaiel and Meyer (1987), who modify a Takeda-type hysteretic moment-curvature relation to account for the strength deterioration during cyclic loading. In the modified model the target point of the reloading branch includes a strength reduction relative to the last point on the moment-curvature envelope with the same inelastic deformation.

1.3   Objectives and Scope

The present study proposes a beam element with distributed nonlinearity and two rotational springs at the ends of the member for the analysis of structural members under cyclic deformation reversals in flexure in combination with low values of axial load. In this case it is possible to approximate the actual behavior by uncoupling the effect of axial force from the flexural behavior. While the axial behavior is approximated as linear elastic, the flexural behavior of the element is represented at several control sections in the member and at the two end rotational springs by a differential moment curvature law that is based on the evolutionary concept of intrinsic time of the endochronic theory. The proposed beam element is implemented in nonlinear analysis program with a consistent nonlinear solution algorithm for the element state determination. While the model is suitable for structural members of any

material, the emphasis in this study is on reinforced concrete structures, which might exhibit pronounced strength and stiffness deterioration under cyclic deformation reversals.

The main objectives of this study are:

- to derive a flexibility-based beam element from the formal framework of mixed finite element methods based on force interpolation functions that strictly satisfy the equilibrium of the member;

- to develop a robust nonlinear solution algorithm for the state determination of flexibility-based elements;

- to develop a differential moment-curvature relation for the hysteretic behavior of the control sections of the element that is evolutionary in nature and, thus, includes the progression of damage and its effect on the hysteretic behavior;

- to develop a nonlinear algorithm for the numerical implementation of the differential moment-curvature relation within the context of the proposed element state determination;

- to develop appropriate parameters for representing the "pinching" and strength deterioration of the hysteretic section relation;

- to illustrate the capabilities of the proposed hysteretic model to describe the behavior of reinforced concrete members under inelastic deformation reversals

- to illustrate the capabilities of the proposed beam element to describe the softening behavior of reinforced concrete members without numerical problems.

Following the introduction, Chapter 2 presents the flexibility formulation of the beam element and illustrates the proposed nonlinear solution algorithm for the element state determination. The mixed formulation of the beam element completes Chapter 2. Chapter 3 introduces a differential moment-curvature relation based on the endochronic theory. The differential constitutive relation is then numerically solved and a nonlinear algorithm is proposed for the correction of the local error. The beam formulation and the incremental constitutive relation of the section are combined in Chapter 4 in the derivation of a beam element with spread inelasticity and two nonlinear rotational springs at the ends of the member. Chapter 5 describes the parameters of the nonlinear constitutive law and introduces a method for accounting for the "pinching" and degradation of the hysteretic moment-curvature relation. Chapter 6 discusses three applications of the proposed element: the first

concerns a cantilever beam with softening to illustrate the capabilities of the proposed algorithm; the other two applications deal with the correlation of analytical with experimental results on reinforced concrete cantilever beams in order to illustrate the capabilities of the proposed damage model. The conclusions of the study and suggestions for future research are presented in Chapter 7.

CHAPTER 2

BEAM ELEMENT FORMULATION

2.1 General

This chapter discusses three different methods for the formulation of beam finite elements. All formulations assume that deformations are small and that plane sections remain plane and normal to the longitudinal axis during the loading history. The classical stiffness and flexibility methods are compared first, followed by the presentation of a two-field mixed method. Most finite elements proposed to date are based on the stiffness method, because of the relative ease of implementation in finite element programs that are typically based on the direct stiffness method of structural analysis.

Stiffness-based elements have, however, shortcomings that are associated with the displacement field approximation in the finite element. These shortcomings become particularly serious in the nonlinear range, especially for cyclic load histories. Fine mesh subdivisions must be selected and convergence problems are not uncommon.

Recent studies on frame analysis have shown that flexibility-based elements may help overcome these problems, because the assumed beam force distributions are exact in the absence of element loads, irrespective of the linear or nonlinear behavior of the element. The implementation of flexibility-based elements in a finite element program is, however, not easy. The state determination for a flexibility-based element typically involves the determination of the element flexibility matrix and the deformation vector that corresponds to the applied forces. For an element that is implemented in a finite element program, this means the determination of the element stiffness matrix and force vector that correspond to given deformations at the element ends. The models proposed to date basically differ in the state determination procedure, but lack a clear and theoretically sound formulation.

This chapter presents the general flexibility-based formulation of a beam finite element. The formulation is initially derived from the classical flexibility method of structural analysis and leads to a new state determination procedure. It is later recast in the more general

form of a mixed method which illustrates better the state-determination process for the nonlinear analysis algorithm and opens the way to future generalizations and possible improvements. The main advantage of the proposed element over previous models is a theoretically founded formulation and the consequent computational stability that permits the numerical solution of highly nonlinear problems, such as the softening flexural response of poorly reinforced RC members under high axial forces.

2.2   Element Forces and Deformations

The element formulations in this chapter refer to the general 3D beam element shown in Figure 2.1 through Figure 2.3. The global reference frame for the element is the coordinate system X, Y, Z, while x, y, z denotes the local reference system. The element is straight and the longitudinal axis x is the union of geometric centroids of the cross sections. The following notation is adopted for forces, displacements and deformations: forces are represented by uppercase letters and corresponding deformations or displacements in the work sense are denoted by the same letter in lowercase. Normal face letters denote scalar quantities, while boldface letters denote vectors and matrices. The element in Figure 2.1 includes rigid body modes. The nodal forces and displacements refer to the global system and are grouped in the following vectors

$$\mathbf{P} = \left\{ P_1 \quad P_2 \quad \cdots \quad P_{11} \quad P_{12} \right\}^T \qquad (2.1)$$

$$\mathbf{p} = \left\{ p_1 \quad p_2 \quad \cdots \quad p_{11} \quad p_{12} \right\}^T \qquad (2.2)$$

In Figure 2.2 the nodal forces and displacements of the element with rigid body modes refer to the local coordinate system and are grouped in the following vectors

$$\overline{Q} = \left\{ \overline{Q}_1 \quad \overline{Q}_2 \quad \cdots \quad \overline{Q}_{11} \quad \overline{Q}_{12} \right\}^T \qquad (2.3)$$

$$\overline{q} = \left\{ \overline{q}_1 \quad \overline{q}_2 \quad \cdots \quad \overline{q}_{11} \quad \overline{q}_{12} \right\}^T \qquad (2.4)$$

Finally, Figure 2.3 shows the forces and displacements of the element without rigid body modes in the local reference system. Throughout this discussion the torsional response is assumed as linear elastic and uncoupled from the other degrees of freedom. It is, thus, omitted in the remainder of this discussion for the sake of brevity. Without torsion the element has five degrees of freedom: one axial extension, q_5, and two rotations relative to the chord at each end node, (q_1, q_3) at one and (q_2, q_4) at the other. For simplicity's sake the displacements in Figure 2.3 are called element generalized deformations or simply element

deformations. Q_1 through Q_5 represent the corresponding generalized forces: one axial force, Q_5, and two bending moments at each end node, (Q_1, Q_3) at one, and (Q_2, Q_4) at the other. The element generalized forces and deformations are grouped in the following vectors:
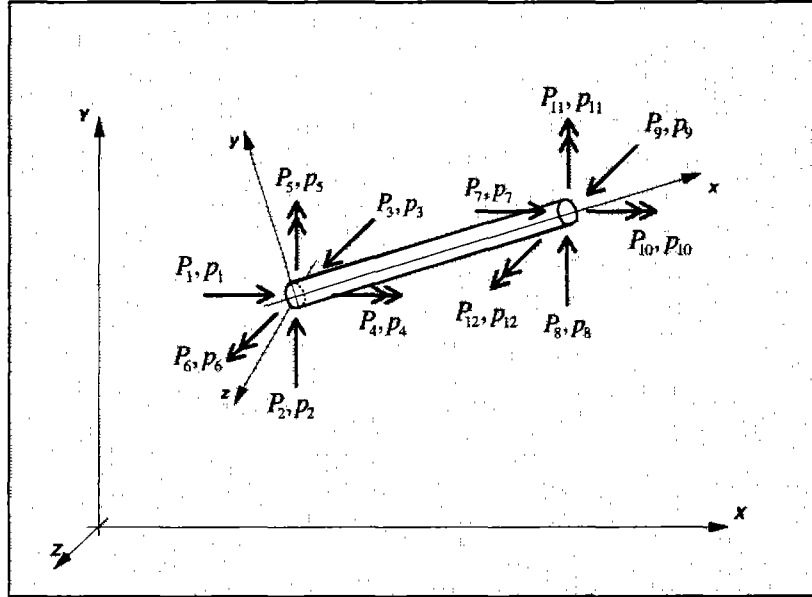
FIGURE 2.1   FORCES AND DISPLACEMENTS OF THE ELEMENT WITH
              RIGID BODY MODES IN THE GLOBAL REFERENCE SYSTEM

$$Q = \begin{Bmatrix} Q_1 & Q_2 & Q_3 & Q_4 & Q_5 \end{Bmatrix}^T \qquad (2.5)$$

$$q = \begin{Bmatrix} q_1 & q_2 & q_3 & q_4 & q_5 \end{Bmatrix}^T \qquad (2.6)$$

Figure 2.3 also shows the generalized forces and deformations at a section of the element. Since shear deformations are neglected, the deformation is represented by three strain resultants: the axial strain $\varepsilon(x)$ along the longitudinal axis and two curvatures $\chi_z(x)$ and $\chi_y(x)$ about two orthogonal axes z and y, respectively. The corresponding force resultants are the axial force $N(x)$ and two bending moments $M_z(x)$ and $M_y(x)$. The section generalized forces and deformations are grouped in the following vectors:

$$D(x) = \begin{Bmatrix} M_z(x) & M_y(x) & N(x) \end{Bmatrix}^T \qquad (2.7)$$

$$d(x) = \begin{Bmatrix} \chi_z(x) & \chi_y(x) & \varepsilon(x) \end{Bmatrix}^T \qquad (2.8)$$

The equations that relate the element forces with the corresponding deformations are essential for the implementation of the beam element in a finite element program. The

element deformation vector q can be derived from the element displacement vector $\mathbf{p}$ with two transformations.
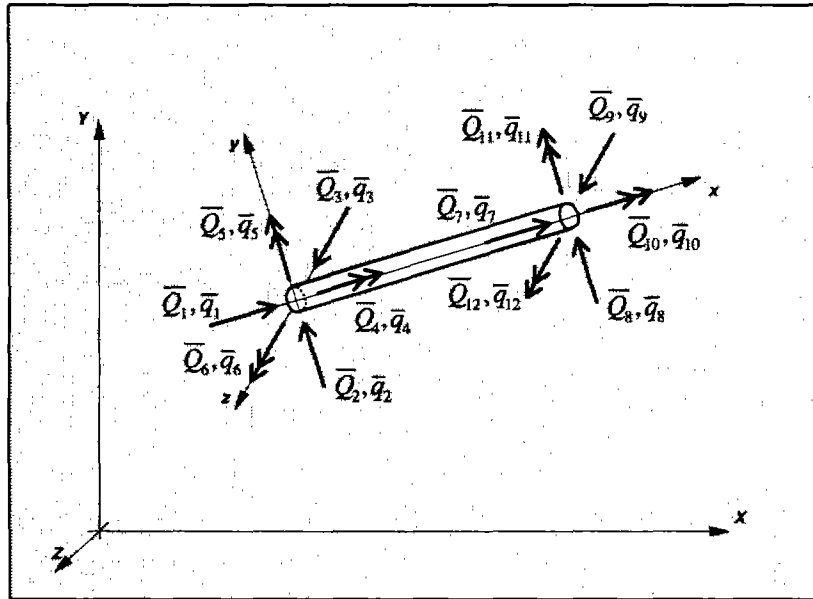
FIGURE 2.2   FORCES AND DISPLACEMENTS OF THE ELEMENT WITH
             RIGID BODY MODES IN THE LOCAL REFERENCE SYSTEM
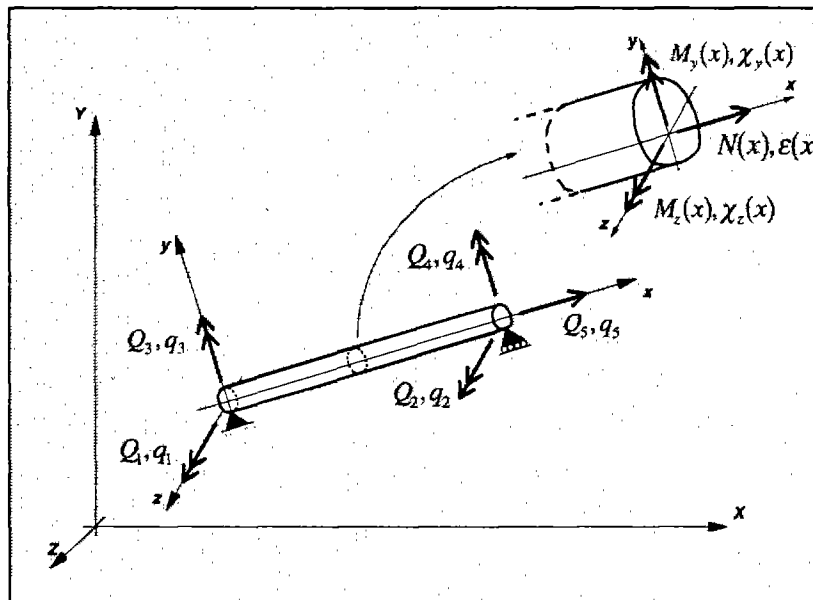
FIGURE 2.3   ELEMENT AND SECTION FORCES AND DEFORMATIONS IN THE
             LOCAL REFERENCE SYSTEM WITHOUT RIGID BODY MODES

(a)   Transformation from $\mathbf{p}$ to $\overline{q}$

$$\bar{q} = L_R \, \mathbf{p} \qquad\qquad (2.9)$$

where L_R is a rotation matrix that is defined by

$$L_R = \begin{bmatrix} R & 0 & 0 & 0 \\ 0 & R & 0 & 0 \\ 0 & 0 & R & 0 \\ 0 & 0 & 0 & R \end{bmatrix}$$

Submatrix R has the form

$$R = \begin{bmatrix} C_x & C_y & C_z \\ -\dfrac{C_x\,C_y\,\cos\alpha + C_z\,\sin\alpha}{C_{xz}} & C_{xz}\cos\alpha & \dfrac{-C_y\,C_z\,\cos\alpha + C_x\,\sin\alpha}{C_{xz}} \\ \dfrac{C_x\,C_y\,\sin\alpha - C_z\,\cos\alpha}{C_{xz}} & -C_{xz}\sin\alpha & \dfrac{C_y\,C_z\,\sin\alpha + C_x\,\cos\alpha}{C_{xz}} \end{bmatrix}$$
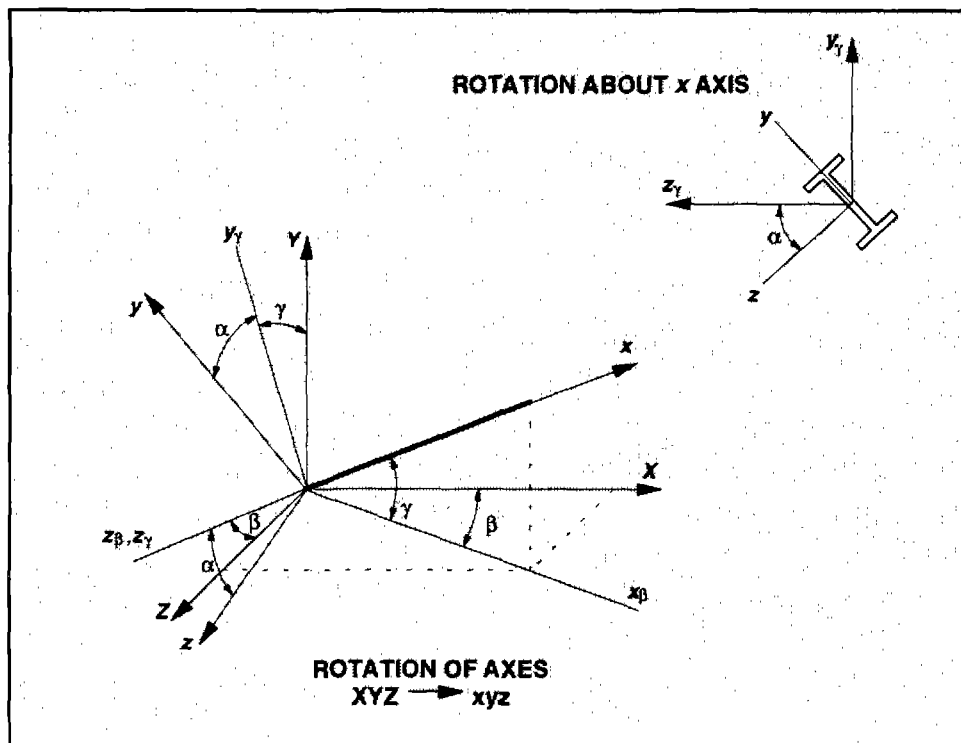
FIGURE 2.4   ROTATION OF AXES FOR A BEAM ELEMENT IN THREE DIMENSIONAL SPACE

C_x, C_y and C_z are the direction cosines of the axis of the member, $C_{xz} = \sqrt{\left(C_x\right)^2 + \left(C_z\right)^2}$, and α is the angle that defines the rotation about the element axis x. The rotation matrix L_R

describes three successive rotations α, β, γ, as illustrated in Figure 2.4. The first two rotations through angles β and γ (about the Y and z_β axes, respectively) are the same as those used for a space truss element. The third transformation consists of a rotation through the angle α about the beam axis x, causing the y and z axes to coincide with the principal axes of the cross section. This last rotation is illustrated at the top of Figure 2.4, which shows a cross section view of an I-beam pointing in the negative x direction. In the special case of a vertical member, $C_x = 0$, $C_z = 0$ and $C_{xz} = 0$, and R becomes indeterminate. The following alternative expression should be used in this case:

$$R = \begin{bmatrix} 0 & C_y & 0 \\ -C_y\cos\alpha & 0 & \sin\alpha \\ C_y\sin\alpha & 0 & \cos\alpha \end{bmatrix}$$

(b)   Transformation from $\bar{q}$ to q

$$q = L_{RBM}\,\bar{q} \tag{2.10}$$

L_{RBM} is the transformation matrix for the inclusion of rigid body modes. Accounting for the torsional degrees of freedom and omitting second order effects, L_{RBM} becomes

$$L_{RBM} = \begin{bmatrix} 0 & 1/L & 0 & 0 & 0 & 1 & 0 & -1/L & 0 & 0 & 0 & 0 \\ 0 & 1/L & 0 & 0 & 0 & 0 & 0 & -1/L & 0 & 0 & 0 & 1 \\ 0 & 0 & -1/L & 0 & 1 & 0 & 0 & 0 & 1/L & 0 & 0 & 0 \\ 0 & 0 & -1/L & 0 & 0 & 0 & 0 & 0 & 1/L & 0 & 1 & 0 \\ -1 & 0 & 0 & 0 & 0 & 0 & 1 & 0 & 0 & 0 & 0 & 0 \\ 0 & 0 & 0 & -1 & 0 & 0 & 0 & 0 & 0 & 1 & 0 & 0 \end{bmatrix} \tag{2.11}$$

The following global relations hold

$$q = L_{RBM}\,L_R\,\mathbf{p} = L_{ele}\,\mathbf{p} \tag{2.12}$$

$$\mathbf{P} = L_R^T\,L_{RBM}^T\,Q = L_{ele}^T\,Q \tag{2.13}$$

where

$$L_{ele} = L_{RBM}\,L_R \tag{2.14}$$

With the transformation matrix L_{ele}, the local stiffness matrix K for the element without rigid body modes can be transformed to the global stiffness matrix $\mathbf{K}$ of the element with rigid body modes:

$$\mathbf{K} = L_{ele}^T\,K\,L_{ele} \tag{2.15}$$

The element stiffness matrix in Eq. (2.15) can now be assembled into the structure stiffness matrix.

2.3 Beam Element Formulation

This section presents the formulation of a beam element based on three different methods. Because the problems of interest in this study are nonlinear, the formulations are presented in incremental form. Even though tangent stiffness matrices appear in the nonlinear incremental solutions, the extension to other types of linearization is rather straightforward. It is also important to point out that the nonlinear response in this chapter arises only from the nonlinear material behavior. The formulation is first derived with the classical stiffness and flexibility methods. A mixed method is, then, presented which illustrates better the consistent implementation of the state determination procedure for flexibility-based elements.

The implementation of the beam element in a standard finite element program requires different state determination procedures for the stiffness and flexibility method. Since standard finite element programs are commonly based on the direct stiffness method of analysis, the solution of the global equilibrium equations yields the displacements of the structural degrees of freedom. These, subsequently, yield the end deformations of each element. The process of finding the stiffness matrix and the resisting forces of each element for given deformations is known as element state determination and is typically performed on the element without rigid body modes.

2.3.1 Stiffness Method

The beam formulation according to the stiffness method involves three major steps in the following order:

a)   *Compatibility*. The beam deformation field is expressed as a function of nodal deformations

$$d(x) = a(x)q \qquad (2.16)$$

Typically, in the formulation of a Bernoulli beam, the transverse displacements are described by cubic polynomials and the axial displacements by linear polynomials. Consequently, $a(x)$ contains linear functions of the end rotations and a constant function of the axial extension.

b)   *Section Constitutive Law.* The incremental section constitutive law is written as

$$\Delta D(x) = k(x) \Delta d(x) \tag{2.17}$$

c)   *Equilibrium.* Starting from a force distribution in equilibrium, the relation between element force and deformation increments is obtained with the principle of virtual displacements

$$\delta q^T \Delta Q = \int_0^L \delta d^T(x) \Delta D(x) dx \tag{2.18}$$

The substitution of Eqs. (2.16) and (2.17) in Eq. (2.18) and the fact that the latter must hold for arbitrary δq lead to

$$\Delta Q = K \Delta q \tag{2.19}$$

where K is the element stiffness matrix

$$K = \int_0^L a^T(x) k(x) a(x) dx \tag{2.20}$$

The state determination procedure is straightforward for a stiffness-based element. The section deformations $d(x)$ are determined from the element deformations q with Eq. (2.16). The corresponding section stiffness $k(x)$ and section resisting forces $D_R(x)$ are determined from the section constitutive law, which is assumed explicitly known in this chapter without loss of generality. The element stiffness matrix K is obtained by application of Eq. (2.20), while the element resisting forces Q_R are determined with the principle of virtual displacements that leads to

$$Q_R = \int_0^L a^T(x) D_R(x) dx \tag{2.21}$$

It is important to note that, in the nonlinear case, this method leads to an erroneous element response. This problem is illustrated in Figure 2.5 which shows the evolution of the structure, element and section states during one load increment ΔP_E^k that requires several iterations i. Throughout this study the Newton-Raphson iteration method is used at the global degrees of freedom. At each Newton-Raphson iteration structural displacement increments are determined and the element deformations are extracted for each element.
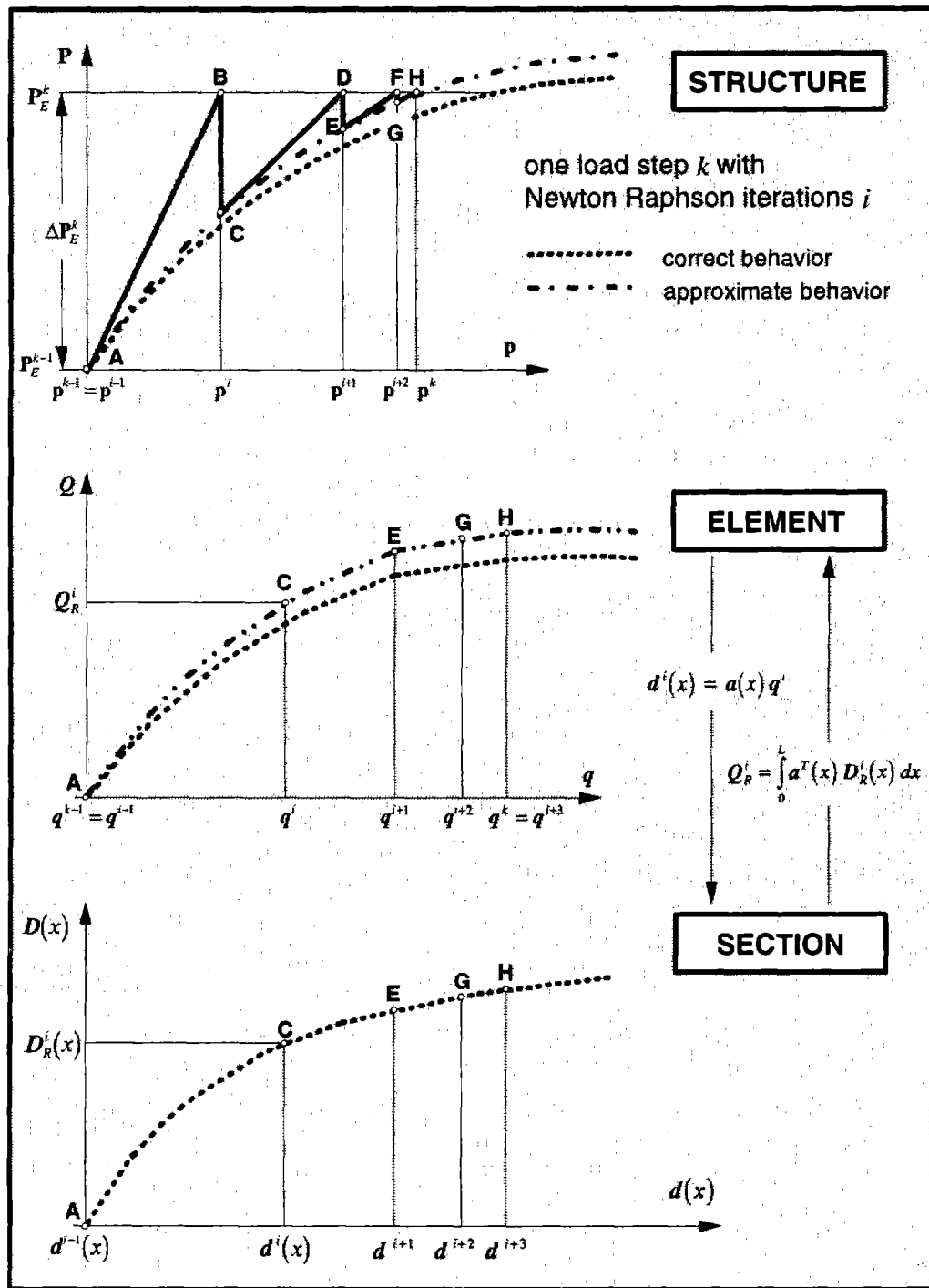
FIGURE 2.5   ELEMENT STATE DETERMINATION FOR STIFFNESS METHOD

The state determination process is made up of two nested phases: a) *the element state determination*, when the stiffness matrix and resisting forces of the element are determined

for given end deformations, and b) *the structure state determination*, when the stiffness matrix and resisting forces of the element are assembled to form the stiffness matrix and resisting force vector of the structure . Once the structure state determination is complete, the resisting forces are compared with the total applied loads and the difference, if any, yields the unbalanced forces which are then applied to the structure in an iterative solution process, until external loads and internal resisting forces agree within a specified tolerance.

At the i-th Newton-Raphson iteration, the global system of equations $\mathbf{K}^{i-1} \Delta \mathbf{p}^i = \mathbf{P}_U^{i-1}$ is solved, where $\mathbf{P}_U$ is the vector of unbalanced forces and $\mathbf{K}^{i-1}$ is the tangent stiffness matrix of the structure. From the total displacements at the structure degrees of freedom $\mathbf{p}^i$ the deformation vector $\mathbf{q}^i$ is determined for each element. Using Eq. (2.16) for each beam element the deformation field $\mathbf{d}^i(x)$ is computed. This is the first approximation of the element state determination, since $a(x)$ is exact only in the linear elastic case of a prismatic member.

Assuming that the section constitutive law is explicitly known, the section stiffness $k^i(x)$ and resisting forces $D_R^i(x)$ are readily computed from $d^i(x)$. Using Eqs. (2.20) and (2.21) the element stiffness matrix K^i and resisting forces Q_R^i are determined. Since $a(x)$ is approximate, the two integrals yield approximate results. The approximation of the deformation field leads to a stiffer solution, which is reflected in the behavior of Figure 2.5. Note that the curve labeled "correct" is only exact within the assumptions of the section constitutive law and the kinematic approximations of the problem, such as small kinematics, plane section deformations, etc..

To overcome the numerical errors that arise from the approximation of the deformation field, analysts resort to fine mesh discretization of the structure, especially, in frame regions that undergo highly nonlinear behaviors, such as the ends of members. Even so, numerical convergence problems persist.

2.3.2 Flexibility Method

The beam formulation according to the flexibility method involves three major steps in the following order:

a)   *Equilibrium*. The beam force field is expressed as a function of the nodal forces

$$D(x) = b(x)Q \tag{2.22}$$

In the absence of element loads $b(x)$ contains force interpolation functions that enforce a linear bending moment and a constant axial force distribution.

b)   *Section Constitutive Law.* The linearized section constitutive law is written as

$$\Delta d(x) = f(x) \Delta D(x) \tag{2.23}$$

c)   *Compatibility.* Starting from a compatible state of deformation, the element relation between force and corresponding deformation increments is obtained by application of the principle of virtual forces

$$\delta Q^T \Delta q = \int_0^L \delta D^T(x) \Delta d(x) dx \tag{2.24}$$

The substitution of Eqs. (2.22) and (2.23) in Eq. (2.18) and the fact that the latter must hold for arbitrary δQ lead to

$$\Delta q = F \Delta Q \tag{2.25}$$

where F is the element stiffness matrix defined by

$$F = \int_0^L b^T(x) f(x) b(x) dx \tag{2.26}$$

It is important to point out that the equilibrium equation (2.22) is exact in a strict sense when no element loads are present. This is a major advantage of the flexibility method over the stiffness method. The force interpolation matrix $b(x)$ is exact irrespective of the element material behavior, while the deformation interpolation matrix $a(x)$ is only exact in the linear elastic case of a prismatic member. Another advantage of the flexibility method is the ease of including element loads by enhancing $b(x)$ with additional force interpolation functions that can be readily derived from equilibrium considerations. The major obstacle of the flexibility formulation is its numerical implementation in a standard finite element analysis program that imposes kinematic, rather than static, boundary conditions at the element ends. For its complexity and importance this aspect is treated in a separate section.

2.3.3   State Determination for Flexibility-Based Elements

Most studies to date concerned with the analysis of frame structures are based on finite element models that are derived with the stiffness method. Recent studies on the analysis of reinforced concrete frames have focused on the advantages of flexibility-based

models (Zeris and Mahin 1988), but have failed to give a clear and consistent method of determining the resisting forces from given element deformations. This problem arises when the formulation of a finite element is based on the application of the principle of virtual forces. While the element is flexibility-dependent, the computer program into which it is inserted is based on the direct stiffness method of analysis. In this case the element is subjected to kinematic, rather than, static boundary conditions, and the implementation of the flexibility method, which is straightforward in the latter case, becomes challenging.

The determination of the stiffness matrix does not present problems, at least from a theoretical standpoint, since it is accomplished by inversion of the element flexibility matrix,

$$K = F^{-1} \tag{2.27}$$

During the state determination the resisting forces of all elements in the structure need to be determined. Since in a flexibility-based element there are no deformation interpolation functions to relate the deformations along the element to the end displacements, the state determination is not straightforward and is not well developed in flexibility-based models proposed to date. This fact has led to some confusion in the numerical implementation of previous models.

In the present study the nonlinear algorithm consists of three distinct nested processes, which are illustrated in Figure 2.6. The two outermost processes denoted by indices k and i involve structural degrees of freedom and correspond to classical nonlinear analysis procedures. The innermost process denoted by index j is applied within each element and corresponds to the element state determination. Similarly to Figure 2.5, Figure 2.6 shows the evolution of the structure, element and section states during one load increment $\Delta \mathbf{P}_E^k$ that requires several Newton-Raphson iterations i.

In summary, the superscripts of the nested iterations are defined as follows:

k denotes the applied load step. The external load is imposed in a sequence of load increments $\Delta \mathbf{P}_E^k$. At load step k the total external load is equal to $\mathbf{P}_E^k = \mathbf{P}_E^{k-1} + \Delta \mathbf{P}_E^k$ with $k=1,...,nstep$ and $\mathbf{P}_E^0 = 0$;

i denotes the Newton-Raphson iteration scheme at the structure level, i.e. the structure state determination process. This iteration loop yields the structural displacements $\mathbf{p}^k$ that correspond to applied loads $\mathbf{P}_E^k$;

j denotes the iteration scheme at the element level, i.e. the element state determination process. This iteration loop is necessary for the determination of the element resisting forces that correspond to element deformations q^i during the i-th Newton-Raphson iteration.

The processes denoted by indices k and i are common in nonlinear analysis programs and will not be discussed further. The iteration process denoted by the index j, on the other hand, is special to the beam element formulation developed in this study and will be described in detail. It should be pointed out that any suitable nonlinear solution algorithm can be used for the iteration process denoted by index i. In this study the Newton-Raphson method is used. The selection of this method for iteration loop i does not affect the strategy for iteration loop j, which has as its goal the determination of the element resisting forces for the given element deformations.

In a flexibility-based finite element the first step is the determination of the element forces from the current element deformations using the stiffness matrix at the end of the last iteration. The force interpolation functions yield the forces along the element. The first problem is, then, the determination of the section deformations from the given section forces, since the nonlinear section force-deformation relation is commonly expressed as an explicit function of section deformations. The second problem arises from the fact that changes in the section stiffness produce a new element stiffness matrix which, in turn, changes the element forces for the given deformations.

These problems are solved in the present study by a special nonlinear solution method. In this method residual element deformations are determined at each iteration. Nodal compatibility requires that these residual deformations be corrected. This is accomplished at the element level by applying corrective element forces based on the current stiffness matrix. The corresponding section forces are determined from the force interpolation functions so that equilibrium is always satisfied in a strict sense along the element. These section forces cannot change during the section state determination so as not to violate equilibrium along the element. Consequently, the linear approximation of the section force-deformation relation about the present state results in residual section deformations.These are then integrated along the element to obtain new residual element deformations and the whole process is repeated until convergence occurs. It is important to stress that *equilibrium along the element is always satisfied in a strict sense in this process.* The nonlinear solution procedure for the element state determination is schematically shown in Figure 2.7 for one Newton-Raphson

iteration i. In Figure 2.7 convergence in loop j is reached in three iterations. The consistent notation between Figure 2.6 and Figure 2.7 highlights the relation between the corresponding states of the structure, element and section, which are denoted by uppercase Roman letters.
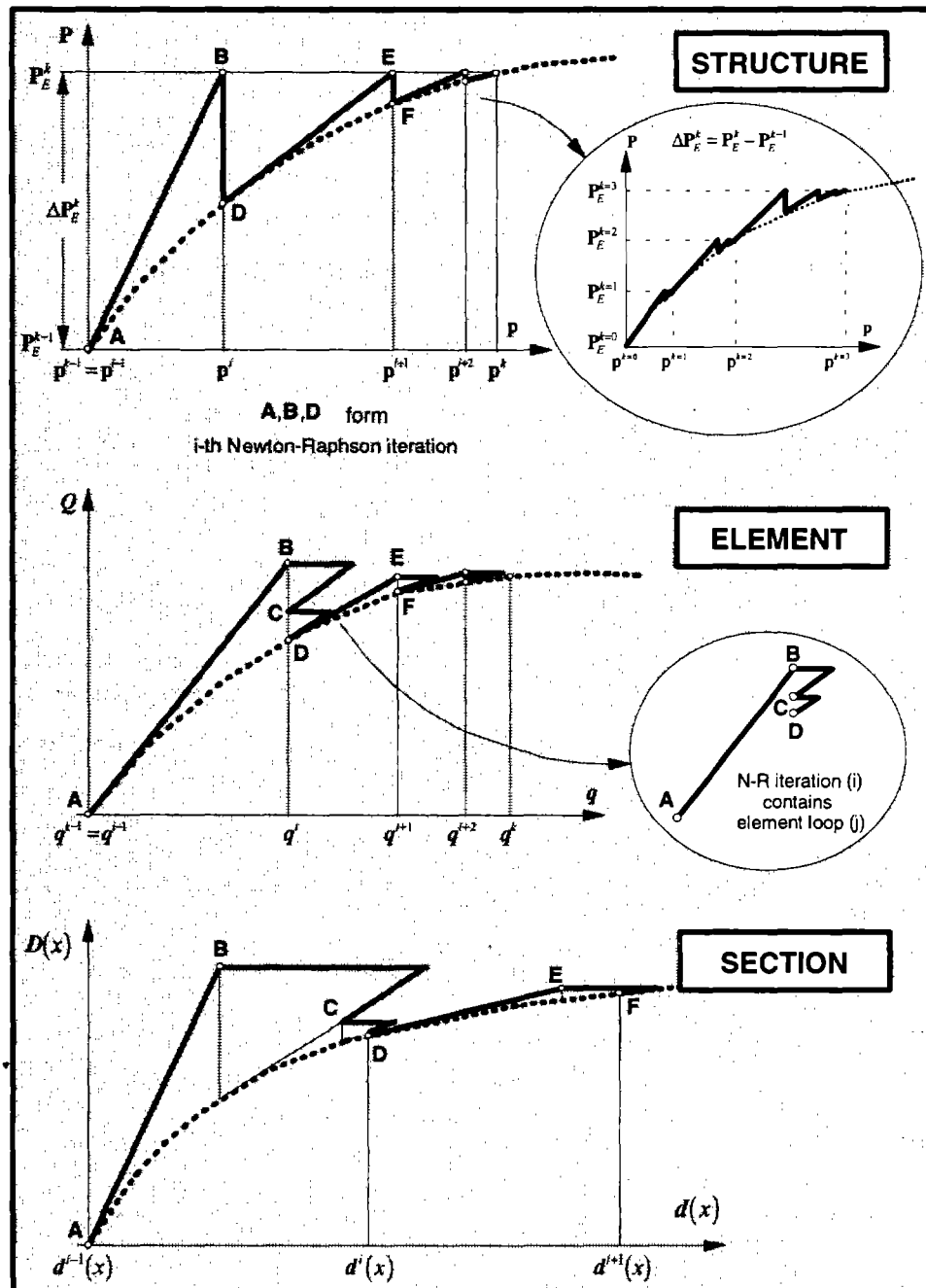
FIGURE 2.6   SCHEMATIC ILLUSTRATION OF STATE DETERMINATION AT THE STRUCTURE, ELEMENT AND SECTION LEVEL: k DENOTES THE LOAD STEP, i THE NEWTON-RAPHSON ITERATION AT THE STRUCTURE DEGREES OF FREEDOM AND j THE ITERATION FOR THE ELEMENT STATE DETERMINATION
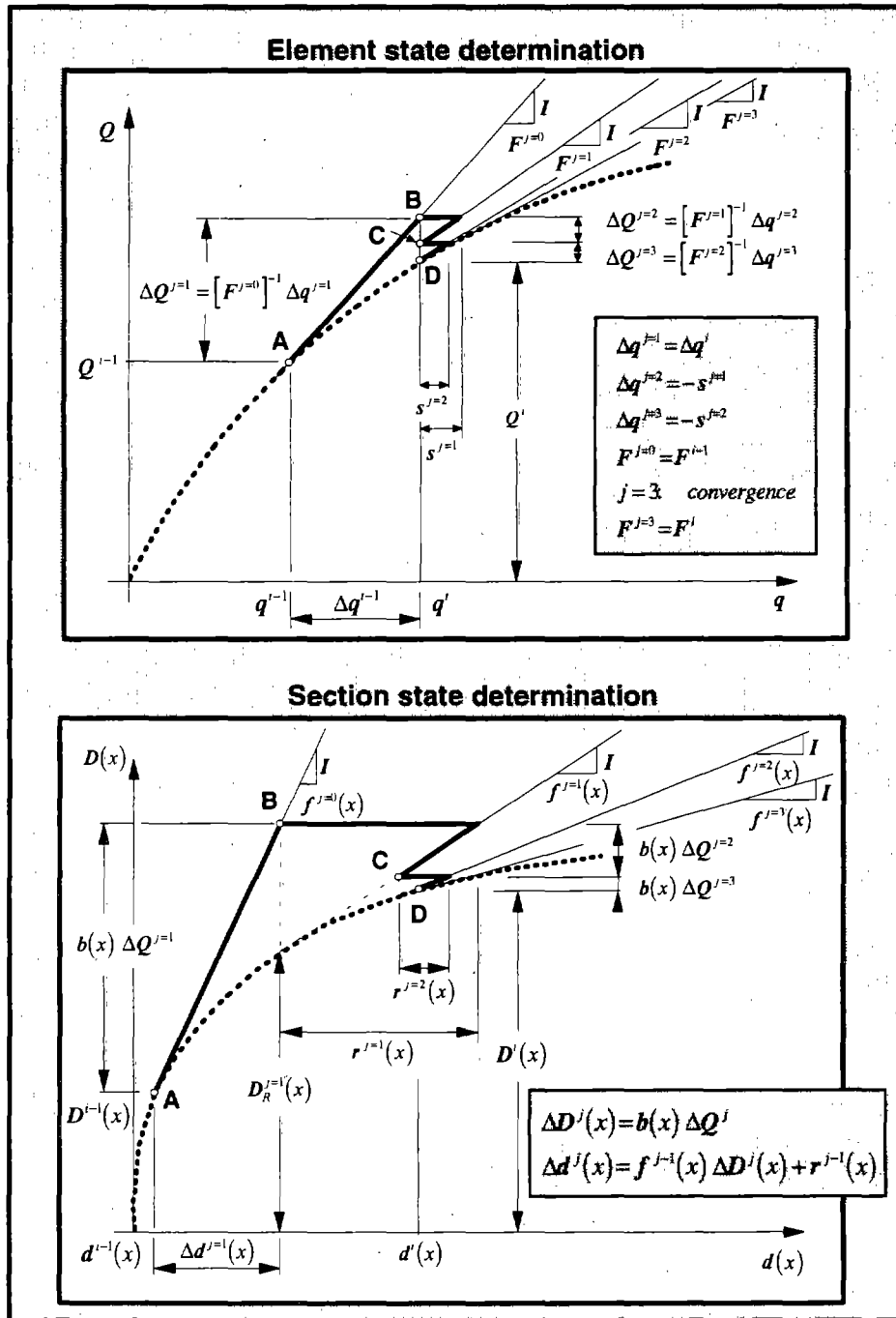
FIGURE 2.7   ELEMENT AND SECTION STATE DETERMINATION FOR FLEXIBILITY METHOD: COMPUTATION OF ELEMENT RESISTING FORCES Q^i FOR GIVEN ELEMENT DEFORMATIONS q^i

At the i-th Newton-Raphson iteration it is necessary to determine the element resisting forces for the current element deformations

$$q^i = q^{i-1} + \Delta q^i \qquad\qquad (2.28)$$

To this end an iterative process denoted by index j is introduced inside the i-th Newton-Raphson iteration. The first iteration corresponds to $j=1$. The initial state of the element, represented by point A and $j=0$ in Figure 2.7, corresponds to the state at the end of the last iteration of loop j for the $(i\text{-}1)$ Newton-Raphson iteration. With the initial element tangent stiffness matrix

$$\left[F^{j=0}\right]^{-1} = \left[F^{i-1}\right]^{-1}$$

and the given element deformation increments

$$\Delta q^{j=1} = \Delta q^i$$

the corresponding element force increments are:

$$\Delta Q^{j=1} = \left[F^{j=0}\right]^{-1} \Delta q^{j=1}$$

The section force increments can now be determined from the force interpolation functions:

$$\Delta D^{j=1}(x) = b(x)\,\Delta Q^{j=1}$$

With the section flexibility matrix at the end of the previous Newton-Raphson iteration

$$f^{j=0}(x) = f^{i-1}(x)$$

the linearization of the section force-deformation relation yields the section deformation increments $\Delta d^{j=1}(x)$:

$$\Delta d^{j=1}(x) = f^{j=0}(x)\,\Delta D^{j=1}(x)$$

The section deformations are updated to the state that corresponds to point B in Figure 2.7:

$$d^{j=1}(x) = d^{j=0}(x) + \Delta d^{j=1}(x)$$

According to the section force-deformation relation, which is here assumed to be explicitly known, section deformations $d^{j=1}(x)$ correspond to resisting forces $D_R^{j=1}(x)$ and a new tangent flexibility matrix $f^{j=1}(x)$ (Figure 2.7). In a finite element based on the stiffness method the section resisting forces $D_R^{j=1}(x)$ would be directly transformed to element resisting forces $Q^{j=1}$, thus, strictly violating the equilibrium along the element. Since this is undesirable, a new nonlinear solution method is proposed in this study. In this approach the section unbalanced forces are first determined

$$D_U^{j=1}(x) = D^{j=1}(x) - D_R^{j=1}(x)$$

and are then transformed to residual section deformations $r^{j=1}(x)$

$$r^{j=1}(x) = f^{j=1}(x) D_U^{j=1}(x) \qquad (2.29)$$

The residual section deformations are thus the linear approximation to the deformation error introduced by the linearization of the section force-deformation relation (Figure 2.7). While any suitable flexibility matrix can be used in the calculation of the residual deformations, the tangent flexibility matrix used in this study offers the fastest convergence rate.

The residual section deformations are integrated along the element according to the virtual force principle to obtain the residual element deformations:

$$s^{j=1} = \int_0^L b^T(x) r^{j=1}(x)\, dx \qquad (2.30)$$

At this point the first iteration $j=1$ of the corresponding iteration loop is complete. The final element and section states for $j=1$ correspond to point **B** in Figure 2.7. The residual section deformations $r^{j=1}(x)$ and the residual element deformations $s^{j=1}$ are determined in the first iteration, but the corresponding deformation vectors are not updated. Instead, they are the starting point of the subsequent steps within iteration loop j. The presence of residual element deformations $s^{j=1}$ violates compatibility. In order to restore compatibility corrective forces equal to $\left[F^{j=1} \right]^{-1} \left(-s^{j=1} \right)$ must be applied at the ends of the element, where $F^{j=1}$ is the updated element tangent flexibility matrix determined by integration of the section flexibility matrices according to Eq. (2.26). A corresponding force increment $b(x) \left[F^{j=1} \right]^{-1} \left(-s^{j=1} \right)$ is applied at all control sections inducing a deformation increment $f^{j=1}(x)\, b(x) \left[F^{j=1} \right]^{-1} \left(-s^{j=1} \right)$. Thus, in the second iteration $j=2$ the state of the element and the control sections change as follows: the element forces are updated to the value

$$Q^{j=2} = Q^{j=1} + \Delta Q^{j=2}$$

where

$$\Delta Q^{j=2} = \left[F^{j=1} \right]^{-1} \left(-s^{j=1} \right)$$

and the section forces and deformations are updated to the values

$$D^{j=2}(x) = D^{j=1}(x) + \Delta D^{j=2}(x)$$

and

$$d^{j=2}(x) = d^{j=1}(x) + \Delta d^{j=2}(x)$$

where

$$\Delta D^{j=2}(x) = b(x) \left[F^{j=1} \right]^{-1} \left(-s^{j-1} \right)$$

$$\Delta d^{j=2}(x) = r^{j=1}(x) + f^{j=1}(x) b(x) \left[F^{j=1} \right]^{-1} \left(-s^{j=1} \right)$$

The state of the element and the control sections at the end of the second iteration $j=2$ corresponds to point **C** in Figure 2.7. The new tangent flexibility matrices $f^{j=2}(x)$ and the new residual section deformations

$$r^{j=2}(x) = f^{j=2}(x) D_U^{j=2}(x)$$

are computed for all sections. The residual section deformations are then integrated to obtain the residual element deformations $s^{j=2}$ and the new element tangent flexibility matrix $F^{j=2}$ is determined by integration of the section flexibility matrices $f^{j=2}(x)$ according to Eq. (2.26). This completes the second iteration within loop j.

The third and subsequent iterations follow exactly the same scheme. Convergence is achieved when the specified convergence criterion is satisfied. With the conclusion of iteration loop j the element resisting forces for the given deformations q^i are established, as represented by point **D** in Figure 2.6 and Figure 2.7. The Newton-Raphson iteration process can now proceed with step $i+1$.

It is important to point out that during iteration loop j the element deformations q^i do not change except in the first iteration $j=1$, when increments $\Delta q^{j=1} = \Delta q^i$ are added to the element deformations q^{i-1} at the end of the previous Newton-Raphson iteration. These deformation increments result from the application of corrective loads ΔP_E^i at the structural degrees of freedom during the Newton-Raphson iteration process. For $j>1$ only the element forces change until the nonlinear solution procedure converges to the element resisting forces Q^i which correspond to element deformations q^i. This is illustrated at the top of Figure 2.7 where points **B**, **C** and **D**, which represent the state of the element at the end of subsequent iterations in loop j, lie on the same vertical line, while the corresponding points at the control sections of the element do not, as shown in the bottom of Figure 2.7. This feature of the proposed nonlinear solution procedure ensures compatibility.

The proposed nonlinear analysis method offers several advantages. Equilibrium along the element is always satisfied in a strict sense, since section forces are derived from element forces by the force interpolation functions according to Eq. (2.21). Compatibility is also satisfied in its integral form according to the virtual force principle

$$\Delta q = \int_0^L b^T(x) \ \Delta d(x) \, dx \tag{2.31}$$

It is straightforward to show that in the first step, $j=1$, the integral of the section deformation increments $\Delta d^{j=1}(x)$ is equal to $\Delta q^{j=1}$, while for $j>1$, the section deformation increments are determined from

$$\Delta q^j(x) = r^{j-1}(x) + f^{j-1}(x) \, b(x) \left[F^{j-1} \right]^{-1} \left(-s^{j-1} \right) \tag{2.32}$$

Upon substitution of Eq. (2.32) in Eq. (2.31) it is easy to verify that $\Delta q^j = 0$ for $j>1$, thus satisfying nodal compatibility. In other words, the element iterations adjust the element force and deformation distributions while maintaining the imposed nodal deformation increments $\Delta q^{j=1} = \Delta q^i$.

At this point it is important to point out that the element state determination algorithm can be regarded as an iterative Newton-Raphson process inside the element. A comparison of the iteration schemes at the structure and at the element level in Figure 2.6 reveals that, while the global iterative scheme is based on force corrections, the element scheme is based on deformation corrections. While the applied forces are kept fixed at the global level, it is the end deformations that are kept fixed at the element level.

A complete step-by-step summary of the element state determination is presented in Appendix A with the help of flow charts which illustrate the complete solution method for a nonlinear structural analysis problem that uses Newton-Raphson iterations at the structural degrees of freedom.

2.3.4 Mixed Method

This section presents a more general element formulation based on a two-field mixed method which uses the integral forms of the equilibrium and force-deformation relations to derive the matrix relation between element generalized forces and corresponding deformations. This approach provides a more direct and elegant way of relating the element formulation with the element state determination and opens the way to future extensions of the method.

One important difference between stiffness and flexibility method on one hand, and the mixed approach on the other, is the way the section constitutive law is treated. The stiffness and flexibility methods satisfy the section constitutive law exactly. In the flexibility

method the section constitutive relation is used to obtain the section deformations from the corresponding forces. Since it is not clear how to relate these deformations to the resisting forces of the element, inconsistencies appear in the numerical implementation of the method. To avoid these inconsistencies it is expedient to accept a deformation residual as the linearization error in the nonlinear section force-deformation relation. The analytical treatment of this error is well established within the framework of two-field mixed methods, as will be discussed in the following. Even though this approach was already introduced in ad hoc fashion for the state determination of the flexibility method in the previous section, it is conceptually more appropriate to associate it with the mixed method. It will be shown in the following that the formulation of the element within the framework of the mixed method leads directly to the consistent implementation of the state determination algorithm.

In the two-field mixed method independent interpolation functions are used in the approximation of the deformation and force fields within the element (Zienkiewicz and Taylor 1989). Denoting with Δ increments of the corresponding quantities, the two incremental fields are written

$$\Delta d(x) = a(x) \Delta q \qquad (2.33)$$

$$\Delta D(x) = b(x) \Delta Q \qquad (2.34)$$

where matrices $a(x)$ and $b(x)$ denote the deformation and force interpolation functions, respectively. In the mixed method formulation the integral forms of the equilibrium and section force-deformation relations are expressed first. These are then combined to obtain the matrix relation between element force and deformation increments. If the incremental section constitutive relation is written as

$$\Delta d^{j}(x) = f^{j-1}(x) \Delta D^{j}(x) + r^{j-1}(x) \qquad (2.35)$$

its weighted integral form becomes

$$\int_{0}^{L} \delta D^{T}(x) \left[\Delta d^{j}(x) - f^{j-1}(x) \Delta D^{j}(x) - r^{j-1}(x) \right] dx = 0 \qquad (2.36)$$

The section force-deformation relation appears in the flexibility form $\Delta d(x) = f(x) \Delta D(x)$ in order to ensure symmetry, as discussed in Zienkiewicz and Taylor (1989). First, Eqs. (2.33) and (2.34) are substituted in Eq. (2.35) and, after observing that Eq. (2.35) must hold for arbitrary δQ, the integral is equivalent to

$$T \Delta q^{j} - F^{j-1} \Delta Q^{j} - s^{j-1} = 0 \qquad (2.37)$$

where F is the element flexibility matrix in Eq. (2.26), s is the element residual deformation vector in Eq. (2.30) and T is a matrix that depends only on the interpolation functions

$$T = \int_0^L b^T(x)\, a(x)\ dx \qquad (2.38)$$

Eq. (2.37) is the matrix equivalent of the integral form of the linearized section force-deformation relation. The next involves the satisfaction of equilibrium of the beam element. In the classical two-field mixed method the integral form of the equilibrium equation is derived from the virtual displacement principle

$$\int_0^L \delta d^T(x)\left[D^{j-1}(x) + \Delta D^j(x)\right] dx = \delta q^T Q^j \qquad (2.39)$$

where Q^j is the vector of nodal forces in equilibrium with the new internal force distribution $D^{j-1}(x) + \Delta D^j(x)$. Eqs. (2.33) and (2.34) are substituted in Eq. (2.39) and, after observing that Eq. (2.39) must hold for arbitrary δq, the integral is equivalent to the following matrix expression

$$T^T Q^{j-1} + T^T \Delta Q^j = Q^j \qquad (2.40)$$

This is the matrix equivalent of the integral form of the element equilibrium equations. Rearrangement and combination of Eqs. (2.37) and (2.40) result in

$$\begin{bmatrix} -F^{j-1} & T \\ T^T & 0 \end{bmatrix} \begin{Bmatrix} \Delta Q^j \\ \Delta q^j \end{Bmatrix} = \begin{Bmatrix} s^{j-1} \\ Q^j - T^T Q^{j-1} \end{Bmatrix} \qquad (2.41)$$

If the first equation in (2.41) is solved for ΔQ^j and the result is substituted in the second equation, the following expression results

$$T^T \left[F^{j-1}\right]^{-1} \left(T \Delta q^j - s^{j-1}\right) = Q^j - T^T Q^{j-1} \qquad (2.42)$$

So far, the selection of interpolation functions $b(x)$ and $a(x)$ has not been addressed. It is straightforward to conclude that a linear bending moment and a constant axial force distribution satisfy the element equilibrium in the absence of element loads. Thus, with the definition of the generalized forces Q and $D(x)$ for the element and section, respectively, the interpolation function $b(x)$ is equal to

$$b(x) = \begin{bmatrix} \left(\dfrac{x}{L}-1\right) & \left(\dfrac{x}{L}\right) & 0 & 0 & 0 \\ 0 & 0 & \left(\dfrac{x}{L}-1\right) & \left(\dfrac{x}{L}\right) & 0 \\ 0 & 0 & 0 & 0 & 1 \end{bmatrix}$$
(2.43)

The selection of $a(x)$ does not affect the present element formulation for a Bernoulli beam, because of the choice of force and deformation resultants Q and q, respectively. These are conjugate variables from a virtual work standpoint, which means that the product $q^T Q$ represents the external work of the beam . The application of the virtual work principle to the beam, thus, yields

$$\delta q^T Q = \int_0^L \delta d^T(x) D(x) dx = \delta q^T \left[\int_0^L a^T(x) b(x) dx \right] Q = \delta q^T T Q$$
(2.44)

This implies that any choice of $a(x)$ yields $T = I$, where I is the 3x3 identity matrix. It is important to note that the above result is specific to the proposed Bernoulli beam element in which force and deformation resultants are conjugate measures. Using the notation of Pian (1964) and Spilker and Pian (1979), two-field mixed methods typically assume nodal displacements q as deformation resultants and some internal stresses β as force or stress resultants. In general, q and β are not conjugate generalized measures and, consequently, matrix T is non square and full.

With the simplification $T=I$, Eq. (2.42) becomes

$$\left[F^{j-1} \right]^{-1} \left(\Delta q^j - s^{j-1} \right) = \Delta Q^j$$
(2.45)

The final matrix equation (2.45) expresses the linearized matrix relation between the element force increments ΔQ^j and the corresponding deformation increments $\Delta q^j - s^{j-1}$. The element stiffness matrix is written in the form $[F]^{-1}$ to stress the fact that it is obtained by inverting the flexibility matrix. Eq. (2.45) clearly relates the proposed element formulation with the element state determination algorithm, since it contains, both, the imposed element deformation increments Δq^j and the residual deformations s^{j-1} that arise during the nonlinear state determination algorithm.

According to Eq. (2.45) when $\Delta q^1 \neq 0$ and $s^0 = 0$, as is the case in the first iteration ($j=1$), the force increments are equal to $\Delta Q^1 = \left[F^0 \right]^{-1} \Delta q^1$. In subsequent iterations ($j > 1$), $\Delta q^j = 0$ and $s^j \neq 0$, and the force increments are equal to $\Delta Q^j = \left[F^{j-1} \right]^{-1} \left(-s^{j-1} \right)$. These

expressions correspond exactly to the element state determination scheme that was presented earlier. It is now clear how the consistent element state determination process can be directly derived from the element formulation, if residual section deformations are included as the linearization error of the incremental section constitutive relation in Eq. (2.35).

It is interesting to note that, with the notation of Tabarrok and Assamoi (1987), the deformation distribution along the element is the sum of two terms: a homogeneous component $\Delta d_h(x)$ and a particular component $\Delta d_p(x)$. Wherever kinematic boundary conditions are imposed $\Delta d_h(x)$ vanishes, while $\Delta d_p(x)$ takes the value of the imposed non zero deformations. In the present state determination algorithm the particular solution arises from the imposed node displacements at the structural degrees of freedom and is added to the deformation field during the first element iteration $j=1$. The homogeneous component is given by the sum of the contributions of all subsequent iterations $j>1$ that adjust the element force and deformation fields while maintaining the imposed nodal deformations. These conclusions can be analytically expressed as follows

$$\Delta d(x) = \Delta d_p(x) + \Delta d_h(x)$$

$$\Delta d_p(x) = \Delta d^{j=1}(x) = f^0(x)\,\Delta D^1(x) \tag{2.46}$$

$$\Delta d_h(x) = \sum_{j=2}^{convergence} \Delta d^j(x) = \sum_{j=2}^{convergence} \left[f^{j-1}(x)\,\Delta D^j(x) + r^{j-1}(x) \right]$$

The validity of these relations can be confirmed by determining the node deformation increments Δq corresponding to $\Delta d(x)$, that is $\int_0^L b^T(x)\,\Delta d(x)\,dx$. It is easy to verify that

$$\int_0^L b^T(x)\,\Delta d_p(x)\,dx = \int_0^L b^T(x)\,\Delta d^{j=1}(x)\,dx = \Delta q^{j=1} = \Delta q^i$$

and

$$\int_0^L b^T(x)\,\Delta d_h(x)\,dx = \sum_{j=2}^{convergence}\left[\int_0^L b^T(x)\,\Delta d^j(x)\,dx\right] = 0$$

In conclusion, the incremental field of the element corresponds to non zero end deformations in the first iteration only, when the internal deformations correspond to the imposed node deformation increments Δq.

CHAPTER 3

A DIFFERENTIAL SECTION CONSTITUTIVE LAW

3.1 General

This chapter presents a differential constitutive relation based on a standard solid model. The relation is general and can be applied to any stress-strain or force-displacement law but is presented here as a moment-curvature relation in view of its application in the formulation of the beam element in Chapter 2. The actual implementation of the section constitutive relation in the element is postponed to Chapter 4.

The constitutive relation is derived from the standard solid model and is, then, modified by introducing the concept of intrinsic time according to the endochronic theory. The monotonic relation is subsequently extended to cyclic loading. Finally, the differential constitutive relation is numerically integrated to obtain an incremental moment-curvature relation.

It is implicitly assumed in this study that the axial and bending behavior of the beam element are completely uncoupled. This may not be a good approximation for reinforced concrete columns with high levels of axial load. In the latter case more elaborate constitutive relations that introduce coupling between axial force and bending moment should be sought. The axial behavior is assumed linear elastic and no further discussion is needed. The flexural behavior is based on a moment-curvature relation expressed in the differential form

$$\frac{dM}{d\chi} = g(M, \chi) \tag{3.1}$$

This form of constitutive law does not provide an explicit expression of the moment-curvature relation, but only its derivative. Clearly, this is a disadvantage from the computational standpoint, since an integration of Eq. (3.1) is required before the section moment can be related to the corresponding curvature. On the other hand, the differential form of Eq. (3.1) is ideally suited for the representation of evolutionary behavior and progressive damage. In the latter context a wide range of characteristic hysteretic behaviors of

structural members can be represented by appropriate selection of model parameters, as will be discussed in Chapters 5 and 6.

Following the characteristics of models that are based on the endochronic theory, the proposed law does not have an explicit yield function, but presents a smooth transition from the elastic to the plastic regime and uses a single relation for both loading and unloading conditions. The last fact makes the numerical implementation of such models relatively straightforward, since the different branches of the hysteretic response (transitions, loading, unloading, yielding surface intersection) do not need to be monitored.
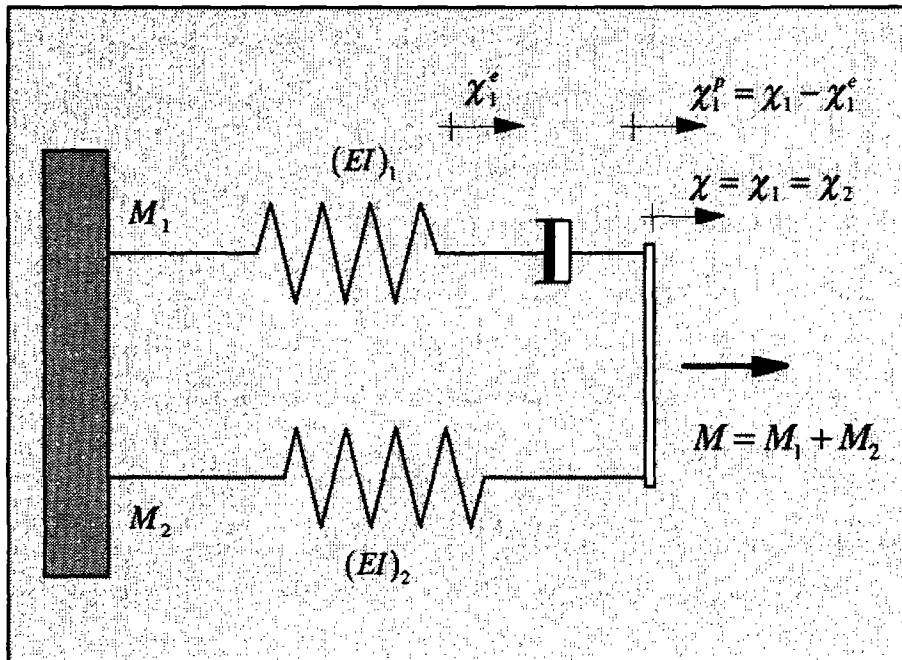
FIGURE 3.1   MOMENT-CURVATURE RELATION BASED ON THE
STANDARD SOLID MODEL: e = ELASTIC p = PLASTIC

The original form of the proposed model is presented in Brancaleoni et al. (1983) where the model is developed from the simple Maxwell model that is subsequently refined by the addition of a linear spring in parallel. The theory is based on a formulation that is formally identical to viscoelasticity, in which time is replaced by a deformation measure called "intrinsic time" leading to a differential constitutive equation. While the original presentation of the model gives a general overview of endochronic theory and outlines the formulation of the constitutive law, this chapter presents a step-by-step evolution of the formulation from the simple viscoelastic model to the final form of the governing differential equation.

3.2   A Differential Constitutive Law

The proposed constitutive relation is derived from the simple standard solid model shown in Figure 3.1. The model consists of two elements acting in parallel. Following the notation of Figure 3.1, element 2 is linear elastic, while element 1 is formed by a linear elastic and a viscous element connected in series.

The behavior of the viscous element is defined by the differential equation

$$\frac{d\chi_1^p}{dt} = \left(\frac{M_1}{M_0 \, k}\right)^n \tag{3.2}$$

where superscript p stands for plastic, M_1 is the force in the dashpot, M_0 is the yield moment and k is defined by

$$k = \frac{EI_1}{EI_1 + EI_2} \tag{3.3}$$

From the model characteristics and Eq. (3.2) the following relation is derived

$$\frac{d\chi}{dt} = \frac{d\chi_1^e}{dt} + \frac{d\chi_1^p}{dt} = \frac{1}{EI_1}\frac{dM_1}{dt} + \left(\frac{M_1}{M_0 \, k}\right)^n \tag{3.4}$$

where superscript e stands for elastic. Since $M_1 = M - (EI)_2 \, \chi$, Eq. (3.4) can be written as

$$\frac{d\chi}{dt} = \frac{1}{EI_1}\left(\frac{dM}{dt} - EI_2 \frac{d\chi}{dt}\right) + \left(\frac{M - EI_2 \, \chi}{M_0 \, k}\right)^n \tag{3.5}$$

Eq. (3.5) is solved with respect to dM/dt to obtain

$$\frac{dM}{dt} = \left(EI_1 + EI_2\right)\frac{d\chi}{dt} - EI_1\left(\frac{M - EI_2 \, \chi}{M_0 \, k}\right)^n \tag{3.6}$$

The differential equation of the solid model in Eq. (3.6) can be interpreted with the aid of Figures 3.2 and 3.3, where α is the strain hardening ratio defined by

$$\alpha = \frac{EI_2}{EI_1 + EI_2} = 1 - k \tag{3.7}$$

The product $\overline{M} = M_0 \, k$ represents the intersection point of the moment M axis with the straight line asymptote to the hardening branch. The effect of α on the shape of the curve is illustrated in Figure 3.3. The exponent n governs the sharpness of the transition between two essentially linear branches (elastic and elasto-plastic) and may take any positive value. As n

increases, the curve tends to a perfectly bilinear behavior.

$$\overline{M} = \left(EI_1 + EI_2\right)\chi_0 - EI_2\,\chi_0$$
$$= M_0 - \frac{EI_2}{EI_1 + EI_2}\,M_0$$
$$= \left(1 - \alpha\right) M_0$$
$$= k\,M_0$$
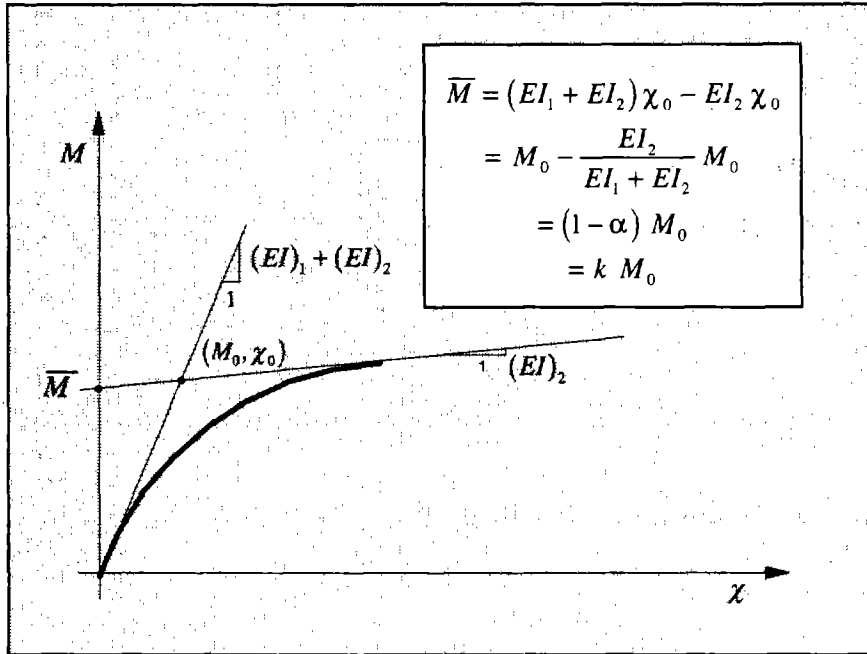
FIGURE 3.2   MOMENT-CURVATURE RELATION BASED ON EQ. (3.6)
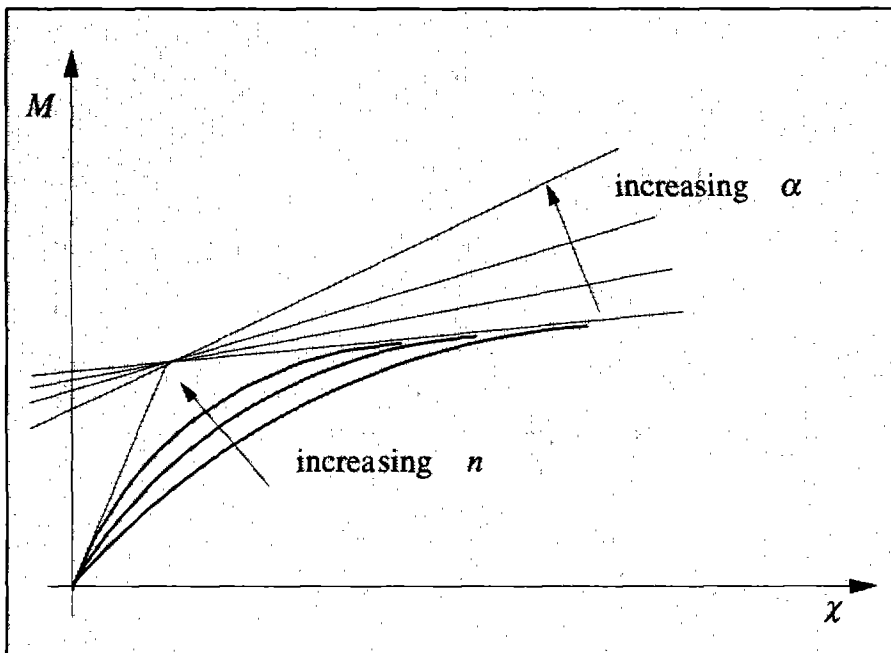
FIGURE 3.3   INFLUENCE OF n AND α ON THE MOMENT-CURVATURE RELATION

Eq. (3.6) is the basic expression of the monotonic constitutive relation and its derivation is general. The same steps are now retraced in an alternative procedure for the purpose of eliminating the time dependence from Eq. (3.6), and deriving the cyclic behavior of the model with the introduction of loading and unloading paths.

First, the concept of intrinsic time $z=t$ is introduced. According to the endochronic theory formulated in Valanis (1971) and later extended in Valanis and Lee (1984), the time is replaced by a monotonically increasing function of time. Typically, in a three dimensional stress-strain constitutive relation the time is replaced by the arc length of the path that describes the material loading history in strain space. In the one dimensional force-deformation relation the section curvature is the only deformation parameter, so that it naturally follows to select $dz = dt = |d\chi|$. After making this substitution and introducing a new parameter w which accounts for loading and unloading paths Eq. (3.2) can be written as

$$\frac{d\chi_1^p}{|d\chi|} = w \left| \frac{M_1}{M_0 \, k} \right|^n$$

(3.8)

where the absolute value of the normalized moment is used and parameter w is equal to

$$w = \frac{M_1}{|M_1|} \beta + \frac{d\chi}{|d\chi|} \gamma$$

(3.9)

β and γ are two constants that according to the original work by Brancaleoni et al. (1983) must satisfy the constraint

$$\beta + \gamma = 1$$

The effect of w on the loading and unloading paths is discussed later in the chapter. With Eqs. (3.8) and (3.9), Eq. (3.4) becomes

$$\frac{d\chi}{|d\chi|} = \frac{1}{(EI)_1} \frac{dM_1}{|d\chi|} + w \left| \frac{M_1}{M_0 \, k} \right|^n$$

(3.10)

Recalling that $M_1 = M - (EI)_2 \, \chi$ Eq. (3.10) is written as

$$\frac{d\chi}{|d\chi|} = \frac{1}{EI_1} \left(\frac{dM}{|d\chi|} - EI_2 \frac{d\chi}{|d\chi|} \right) + w \left| \frac{M - EI_2 \, \chi}{M_0 \, k} \right|^n$$

or,

$$\frac{d\chi}{|d\chi|} = \frac{1}{EI_1} \frac{d\chi}{|d\chi|} \left(\frac{dM}{d\chi} - EI_2 \right) + w \left| \frac{M - EI_2 \, \chi}{M_0 \, k} \right|^n$$

(3.11)

Finally, Eq. (3.11) is solved for $dM/d\chi$ to yield

$$\frac{dM}{d\chi} = (EI_1 + EI_2) - EI_1 \, w \, \frac{d\chi}{|d\chi|} \left| \frac{M - EI_2 \, \chi}{M_0 \, k} \right|^n$$

or,

$$\frac{dM}{d\chi} = (EI_1 + EI_2) \left\{ 1 - \frac{EI_1}{EI_1 + EI_2} \left(\frac{M - EI_2 \, \chi}{|M - EI_2 \, \chi|} \beta + \frac{d\chi}{|d\chi|} \gamma \right) \frac{d\chi}{|d\chi|} \left| \frac{M - EI_2 \, \chi}{M_0 \, k} \right|^n \right\} \quad (3.12)$$

With the notation introduced in Eqs. (3.3) and (3.7) and with the following definitions

$$EI_0 = EI_1 + EI_2$$

$$sgn(x) = \frac{|x|}{x}$$

the following equality holds true by noting that the product $M_0 \, k$ is always positive

$$sgn(M - EI_2 \, \chi) = sgn\left(\frac{M - EI_2 \, \chi}{M_0 \, k} \right)$$

Eq. (3.12) is written in the more compact form

$$\frac{dM}{d\chi} = EI_0 \left\{ 1 - (1-\alpha) \left[sgn\left(\frac{M - EI_2 \, \chi}{M_0 \, k} \right) sgn(d\chi) \, \beta + \gamma \right] \left| \frac{M - EI_2 \, \chi}{M_0 \, k} \right|^n \right\} \quad (3.13)$$

At this point a further simplification is obtained by introducing a convenient coordinate transformation

$$x = \frac{M - EI_2 \, \chi}{M_0 \, k} = \frac{M}{M_0(1-\alpha)} - \frac{\chi \, \alpha}{\chi_0(1-\alpha)} \quad (3.14)$$

which upon substitution in Eq. (3.13) yields

$$\frac{dM}{d\chi} = \frac{M_0}{\chi_0} \left\{ 1 - (1-\alpha)[sgn(d\chi) sgn(x)\beta + \gamma]|x|^n \right\} = \frac{M_0}{\chi_0} f(x) \quad (3.15)$$

where

$$f(x) = 1 - (1-\alpha)[sgn(d\chi) \, sgn(x) \, \beta + \gamma]|x|^n \quad (3.16)$$

The coordinate transformation in Eq. (3.14) helps to illustrate the model behavior. First, it is observed that the condition $x=const$ represents a straight line in the $M - \chi$ plane (see Figure 3.4) that is defined by the following equation

$$M = \left(\frac{M_0}{\chi_0} \alpha \right) \chi + M_0 (1 - \alpha) x \qquad (3.17)$$

As the value of x changes, Eq. (3.17) describes a family of parallel lines with inclination $\alpha M_0/\chi_0$. The axis $\chi - x$ or $\chi' - M$ can be selected as the new reference system. It is further observed that, since $f(x)$ is constant for given x, the $M - \chi$ curve crosses the line $x=0$ with the same initial tangent $\delta = M_0/\chi_0$ (Figure 3.4).

Two limit cases can be identified for function $f(x)$ when $x = \pm 1$. In the loading phase $f(1) = \alpha$, therefore

$$\frac{dM}{d\chi} = \frac{M_0}{\chi_0} \alpha \qquad \text{for} \quad x = 1 \qquad (3.18)$$
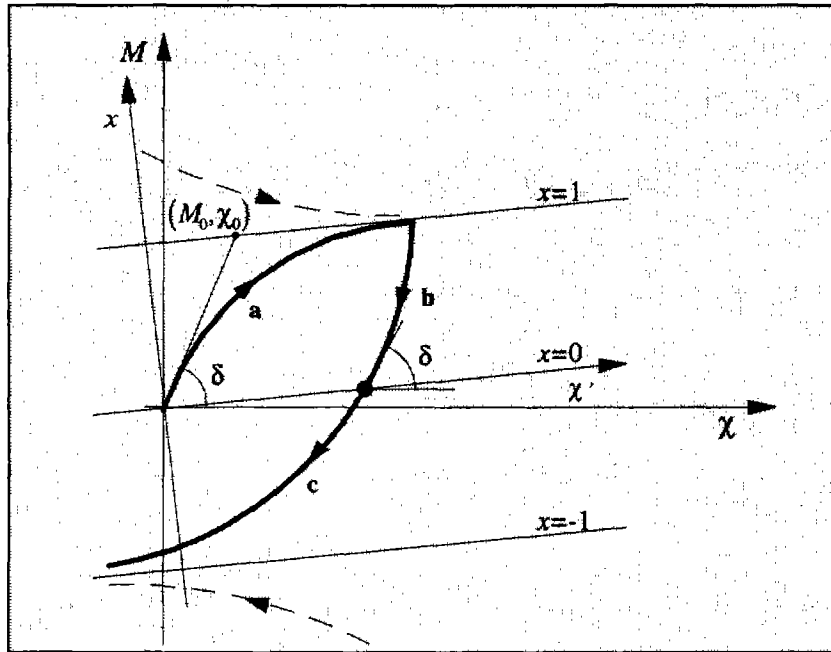
FIGURE 3.4   LOADING AND UNLOADING BRANCHES IN THE CONSTITUTIVE RELATION AND DEFINITION OF NEW AXIS x

Eqs. (3.17) and (3.18) imply that, in the loading phase, the M-χ curve tends asymptotically to the straight line $x=1$. Similar considerations can be repeated for the unloading phase, where the constitutive relation asymptotically tends to the straight line $x=-1$.

Figure 3.4 shows a possible moment-curvature diagram: other branches are described by Eq. (3.15) outside the $|x| < 1$ range, but they are of no physical interest. In Figure 3.4 the

ascending line marked **a** refers to a loading phase with $x>0$ and the descending line marked **c** refers to an unloading phase with $x<0$. In both cases

$$sgn(d\chi)\ sgn(x)\ \beta + \gamma = 1$$

and β, γ have no influence on the shape of the curve. On the contrary, the descending branch marked **b** describes an unloading path with $x>0$ and is influenced by β, γ since

$$sgn(d\chi)\ sgn(x)\ \beta + \gamma = -\beta + \gamma$$

To avoid the possibility that $f(x)$ becomes negative, the condition

$$-\beta + \gamma < 0$$

is imposed. Since $\beta + \gamma = 1$, it follows that $\gamma \leq 1/2$.

It is important to note that the proposed nonlinear model does not have an explicit yield surface. No distinction is necessary between loading and unloading branches and the same differential equation governs the behavior of the entire constitutive relation. The model derives from the original endochronic theory of Valanis (1971) and uses a simple definition of intrinsic time, since the strain (or deformation) space is onedimensional. In his 1980 work Valanis suggests a few improvements to the original formulation. First, he showed that the introduction of a Dirac delta function into the theory leads to the definition of a yield function. He also showed that classical plasticity models of isotropic and kinematic hardening could be derived as a special case of the endochronic theory. Finally, he corrected the original theory that violated Drucker's stability postulate. Because the model in this study is based on the endochronic theory in its original form, it suffers from these initial limitations. This aspect is discussed in more detail in Appendix B, but it should be noted that such errant behavior is not encountered in practical cases.

It is finally important to point out that the model can represent any force-deformation or stress-strain relation. It is used in the description of the moment-curvature relation because this study focuses on the formulation of a beam element whose cross section behavior is based on Eq. (3.15). In this context it is clear that the constitutive relation cannot be readily used in the beam element in the differential form of Eq. (3.15), because finite rather than infinitesimal moment and curvature increments are imposed. This problem is solved by integration of Eq. (3.15) as discussed in the next section. The resulting form of the section constitutive relation is very similar to the incremental constitutive law in Eq. (2.35) that forms the basis of the beam element formulation in Chapter 2.

3.3   Numerical Integration

The constitutive differential equation in Eq. (3.15) cannot be solved in closed form. Thus, numerical integration is used with a single step integration scheme. After expressing the constitutive law in the form of Eq. (3.1)

$$\frac{dM}{d\chi} = g(M,\chi)$$

and introducing subscripts i and i-1 to indicate different solution steps, Eq. (3.1) is approximated by the expression

$$M^i - M^{i-1} \cong \left(\chi^i - \chi^{i-1}\right) g\left(\chi_\theta^i, M_\theta^i\right) \tag{3.19}$$

or,

$$\Delta M^i \cong \Delta\chi^i g\left(\chi_\theta^i, M_\theta^i\right) \tag{3.20}$$

where

$$\chi_\theta^i = (1-\theta)\chi^{i-1} + \theta\,\chi^i$$

$$M_\theta^i = (1-\theta)M^{i-1} + \theta\,M^i \tag{3.21}$$

$$0 \le \theta \le 1$$

The integration scheme of Eq. (3.20) corresponds to the classical Euler forward method for $\theta = 0$, while $\theta = 0.5$ gives the central method and $\theta = 1$ an implicit backward difference method which is unconditionally stable (Dahlquist and Björck 1974). Even though the implicit backward difference with $\theta = 1$ is selected in this study, the dependence of Eq. (3.20) on θ is maintained in the following derivation in the interest of generality.

The error resulting from the change from an infinitesimal $(d\chi, dM)$ to a finite $(\Delta\chi, \Delta M)$ step size can be expressed in terms of an *error function* ψ that is defined by

$$\psi = \psi\left(\chi^i, M^i\right) = \Delta M^i - \Delta\chi^i g\left(\chi_\theta^i, M_\theta^i\right) \tag{3.22}$$

Starting from a point $\left(M^{i-1}, \chi^{i-1}\right)$ of the constitutive relation, the values M^i and χ^i need to be adjusted so as to minimize the *error function* to practically zero. To do so, a local iteration scheme is used within the global discretization scheme. Thus, two separate schemes are introduced: the global scheme, denoted by subscript i, provides the numerical solution of the moment-curvature differential relation in Eq. (3.19); the local scheme, denoted by subscript j, corrects the local error introduced by the numerical solution of Eq. (3.19). Intermediate

solutions of the local scheme are denoted by $\left(\chi^i\right)^j$, $\left(M^i\right)^j$. The *error function* at local iteration j is defined by

$$\left(\psi^i\right)^j = \left(\Delta M^i\right)^j - \left(\Delta \chi^i\right)^j \, g\left[\left(\chi_\theta^i\right)^j, \left(M_\theta^i\right)^j\right] \qquad (3.23)$$

where

$$\begin{aligned}
\left(\Delta\chi^i\right)^j &= \left(\chi^i\right)^j - \chi^{i-1} \\
\left(\Delta M^i\right)^j &= \left(M^i\right)^j - M^{i-1} \\
\left(\chi_\theta^i\right)^j &= (1-\theta)\,\chi^{i-1} + \theta\left(\chi^i\right)^j \\
\left(M_\theta^i\right)^j &= (1-\theta)\,M^{i-1} + \theta\left(M^i\right)^j
\end{aligned} \qquad (3.24)$$

Regarding the implementation of the constitutive relation in the beam element it is important to point out that the superscript notation is consistent with Chapter 2. Superscript i refers to the nonlinear solution algorithm at the structure degrees of freedom. Superscript j refers to the nonlinear state determination within the element. Since the section constitutive law is incorporated in the beam element formulation in the following chapter, the notation in the following description of the section constitutive law is simplified by omitting superscript i when it is not necessary. Thus, Eq. (3.23) is written as

$$\psi^j = M^j - M^{i-1} - \left(\chi^j - \chi^{i-1}\right) g\left(\chi_\theta^j, M_\theta^j\right) = \Delta M^j - \Delta\chi^j \, g\left(\chi_\theta^j, M_\theta^j\right)$$

The local iteration scheme is derived by Taylor series expansion of ψ^j about the initial point $\left(\chi^{j-1}, M^{j-1}\right)$ and truncation after the linear terms. Setting the resulting expression equal to zero results in

$$\psi^j = \psi^{j-1} + \left(\frac{\partial\psi}{\partial\chi}\right)^{j-1}\left(\chi^j - \chi^{j-1}\right) + \left(\frac{\partial\psi}{\partial M}\right)^{j-1}\left(M^j - M^{j-1}\right) = 0 \qquad (3.25)$$

The superscripts in $\left(\dfrac{\partial\psi}{\partial\chi}\right)^{j-1}$ and $\left(\dfrac{\partial\psi}{\partial M}\right)^{j-1}$ indicate that the partial derivatives of the *error function* ψ with respect to χ and M are determined at iteration j-1. Eq. (3.25) is rearranged and written in the more compact form

$$\Delta\chi^j = f^{j-1} \, \Delta M^j + r^{j-1} \qquad (3.26)$$

where

$$f^{j-1} = -\frac{\left(\dfrac{\partial \psi}{\partial M}\right)^{j-1}}{\left(\dfrac{\partial \psi}{\partial \chi}\right)^{j-1}} \qquad r^{j-1} = -\frac{\psi^{j-1}}{\left(\dfrac{\partial \psi}{\partial \chi}\right)^{j-1}} \tag{3.27}$$

Following the terminology of Chapter 2 the expressions in Eq. (3.27) can be regarded as the flexibility f^{j-1} and the residual deformation r^{j-1} at iteration $j-1$.

The two partial derivatives in Eqs. (3.25) and (3.27) can be expressed in explicit form using Eq. (3.23) for the *error function* ψ. The two derivatives become

$$\left(\frac{\partial \psi}{\partial M}\right)^{j-1} = 1 - \left(\frac{\partial g}{\partial M}\right)^{j-1} \Delta\chi^{j-1} \tag{3.28}$$

$$\left(\frac{\partial \psi}{\partial \chi}\right)^{j-1} = -\left(\frac{\partial g}{\partial \chi}\right)^{j-1} \Delta\chi^{j-1} - g^{j-1} \tag{3.29}$$

where $\Delta\chi^{j-1} = \chi^{j-1} - \chi^{i-1}$. The two partial derivatives of g can be written as

$$\left(\frac{\partial g}{\partial M}\right)^{j-1} = \left(\frac{\partial g}{\partial x_\theta}\right)^{j-1} \left(\frac{\partial x_\theta}{\partial M}\right)^{j-1} \tag{3.30}$$

$$\left(\frac{\partial g}{\partial \chi}\right)^{j-1} = \left(\frac{\partial g}{\partial x_\theta}\right)^{j-1} \left(\frac{\partial x_\theta}{\partial \chi}\right)^{j-1} \tag{3.31}$$

Recalling from Eq. (3.15) the expression for $g = M_0/\chi_0\, f(x)$, it can be written as

$$g(M_\theta, \chi_\theta) = \frac{M_0}{\chi_0} - (1-\alpha)\frac{M_0}{\chi_0}\left[sgn(\Delta\chi)\, sgn(x_\theta)\, \beta + \gamma\right]|x_\theta|^n \tag{3.32}$$

Thus, the derivative of g with respect to x_θ becomes

$$\left(\frac{\partial g}{\partial x_\theta}\right)^{j-1} = -(1-\alpha)\frac{M_0}{\chi_0}\, n\, sgn\left(x_\theta^{j-1}\right)\left[sgn\left(\Delta\chi^{j-1}\right) sgn\left(x_\theta^{j-1}\right)\beta + \gamma\right]\left|x_\theta^{j-1}\right|^{(n-1)} \tag{3.33}$$

From Eqs. (3.14) and (3.24) the derivatives of x_θ with respect to M and χ are

$$\left(\frac{\partial x_\theta}{\partial M}\right)^{j-1} = \frac{\theta}{M_0(1-\alpha)} \tag{3.34}$$

$$\left(\frac{\partial x_\theta}{\partial \chi}\right)^{j-1} = -\frac{\alpha\,\theta}{\chi_0(1-\alpha)} \tag{3.35}$$

Therefore,

$$\left(\frac{\partial g}{\partial M}\right)^{j-1} = -\frac{1}{\chi_0} n\theta \; sgn\left(x_\theta^{j-1}\right) \left[sgn\left(\Delta\chi^{j-1}\right) sgn\left(x_\theta^{j-1}\right)\beta + \gamma\right] \left|x_\theta^{j-1}\right|^{(n-1)} \qquad (3.36)$$

$$\left(\frac{\partial g}{\partial \chi}\right)^{j-1} = \frac{M_0}{\left(\chi_0\right)^2} \alpha n\theta \; sgn\left(x_\theta^{j-1}\right)\left[sgn\left(\Delta\chi^{j-1}\right) sgn\left(x_\theta^{j-1}\right)\beta + \gamma\right] \left|x_\theta^{j-1}\right|^{(n-1)} \qquad (3.37)$$

Finally, the two partial derivatives of the *error function* ψ in Eqs.(3.28) and (3.29) are written as

$$\left(\frac{\partial \psi}{\partial M}\right)^{j-1} = 1 + \frac{\Delta\chi^{j-1}}{\chi_0} n\theta \; sgn\left(x_\theta^{j-1}\right) \left[sgn\left(\Delta\chi^{j-1}\right) sgn\left(x_\theta^{j-1}\right)\beta + \gamma\right] \left|x_\theta^{j-1}\right|^{(n-1)} \qquad (3.38)$$

and

$$\left(\frac{\partial \psi}{\partial \chi}\right)^{j-1} = -\frac{M_0}{\chi_0} \left\{1 - (1-\alpha)\left[sgn\left(\Delta\chi^{j-1}\right) sgn\left(x_\theta^{j-1}\right)\beta + \gamma\right]\right\} \left|x_\theta^{j-1}\right|^n -$$

$$\Delta\chi^{j-1} \frac{M_0}{\left(\chi_0\right)^2} \alpha n\theta \; sgn\left(x_\theta^{j-1}\right) \left[sgn\left(\Delta\chi^{j-1}\right) sgn\left(x_\theta^{j-1}\right)\beta + \gamma\right] \left|x_\theta^{j-1}\right|^{(n-1)} \qquad (3.39)$$

The incremental constitutive law in Eq. (3.26) is used in the following chapter to describe the moment-curvature relation of a beam element with distributed plasticity based on the flexibility method presented in Chapter 2. Eq. (3.26) can describe a variety of monotonic and hysteretic behaviors by proper selection of parameters, as discussed in Chapter 5.

The differential constitutive law presented in this chapter is compared in Appendix B with the well-known Bouc-Wen model. The similarities in the formulation of the two models are discussed first, followed by the presentation of common features and limitations in the hysteretic behavior.

CHAPTER 4

FORMULATION OF A BEAM ELEMENT WITH
A DIFFERENTIAL MOMENT-CURVATURE RELATION

4.1 General

This chapter presents a beam element with distributed plasticity and two end rotational springs. The element is derived by incorporating the incremental moment-curvature relation of Chapter 3 in the beam finite element formulation of Chapter 2. The same incremental constitutive law is used to represent the moment-rotation relation of the end rotational springs. The nonlinear state determination of the entire element is also presented with particular emphasis on the determination of the stiffness matrix and the resisting forces for given element deformations.

The element is formulated under the assumption of small strains and displacements. The shear deformations are neglected. The axial force and bending moment are assumed completely uncoupled with linear elastic axial behavior and nonlinear bending behavior. The uniaxial bending case is presented, with its extension to the biaxial case being straightforward under the assumption that the two responses are uncoupled. Two nonlinear rotational springs are added at the element ends to represent the local nonlinear behavior at the interface between beam and column, as might arise from pull-out of reinforcing bars in concrete members and semi-rigid connections in steel construction. The moment-curvature behavior of the beam cross section and the moment-rotation relation of the end rotational springs follow the incremental relation of Chapter 3, but different material parameters can be specified for each, as necessary.

The independence between axial and flexural behavior and the assumption of linear elastic axial behavior imply that the axial behavior follows that of a simple truss element with constant axial deformation and without second order effects. Any further description of the axial behavior is, therefore, omitted in the following and only the flexural behavior is discussed. A detailed description of axial behavior and the truss element with constant axial deformation are found, among others, in Mondkar and Powell (1975a and 1975b).

4.2   Beam Element Formulation

The beam element is shown in Figs. 4.1 and 4.2 where the reference axis X and Y represent the global reference system, while x and y denote the local reference system. The formulation refers to the local reference system and no rigid body modes are considered. The rotation into the global reference system and the inclusion of rigid body modes are accomplished with standard geometric transformations, as described in Taucer et al. (1991).
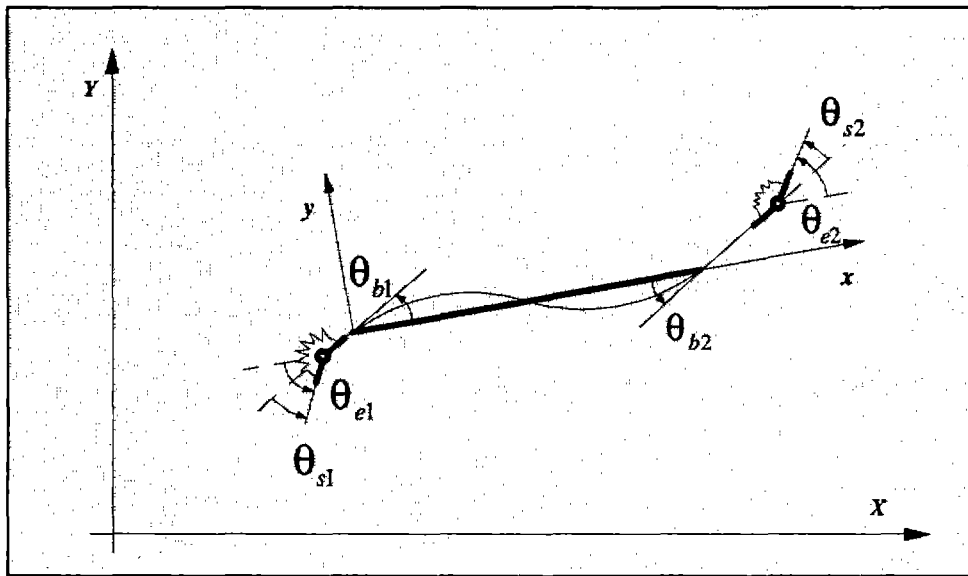
FIGURE 4.1   FORCES IN BEAM ELEMENT WITH DISTRIBUTED PLASTICITY
(e = ELEMENT, s = END SPRINGS, b = BEAM)
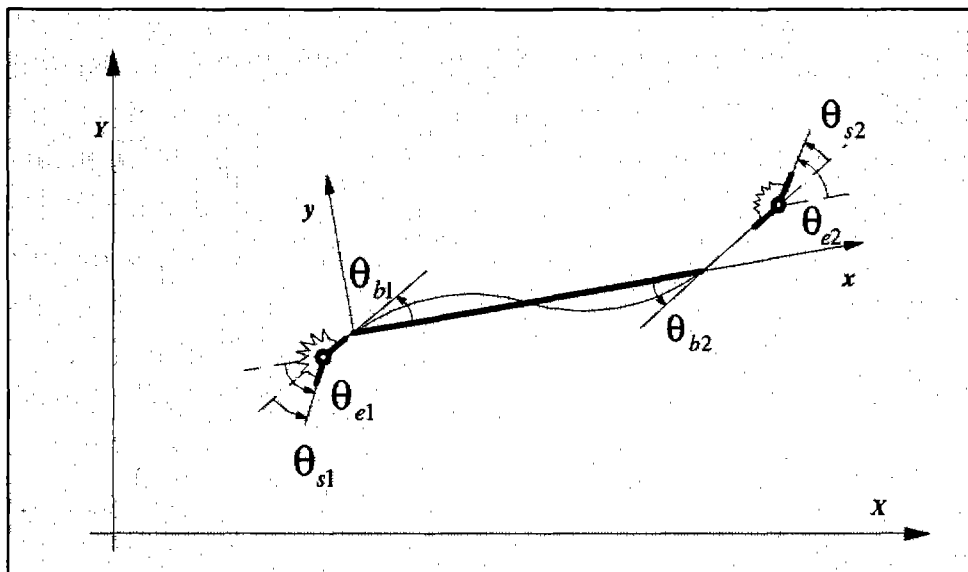
FIGURE 4.2   DEFORMATIONS IN BEAM ELEMENT WITH DISTRIBUTED PLASTICITY

The element, indicated by subscript e, consists of one beam (b) and two end rotational springs (s). The element has 2 degrees of freedom, the two end rotations θ_{e1} and θ_{e1}. For clarity's sake, these are called element generalized deformations or simply element deformations in the following discussion. The corresponding forces are the end moments M_{e1} and M_{e2}. The forces and deformations of the beam and the rotational springs are defined in similar fashion. The element, spring, beam and section forces and deformations are grouped in the following vectors:

Forces

$$\text{Element force vector} \quad Q = \{M_{e1} \quad M_{e2}\}^T$$

$$\text{Spring force vector} \quad Q_s = \{M_{s1} \quad M_{s2}\}^T$$

$$\text{Beam force vector} \quad Q_b = \{M_{b1} \quad M_{b2}\}^T \tag{4.1}$$

$$\text{Section force} \quad M(x)$$

Deformations

$$\text{Element deformation vector} \quad q = \{q_{e1} \quad q_{e2}\}^T$$

$$\text{Spring deformation vector} \quad q_s = \{q_{s1} \quad q_{s2}\}^T$$

$$\text{Beam deformation vector} \quad q_b = \{q_{b1} \quad q_{b2}\}^T \tag{4.2}$$

$$\text{Section deformation} \quad \chi(x)$$

The following compatibility and equilibrium conditions hold for these vectors:

$$q = q_b + q_s \tag{4.3}$$

$$Q = Q_b = Q_s \tag{4.4}$$

These relations represent a model in series and are fundamental for the derivation of the matrix relation between element force increments ΔQ and corresponding deformations Δq.

The beam element is formulated according to the mixed method discussed in Section 2.4. The procedure in repeated here only to the extent necessary for the incorporation of the incremental constitutive relations of the beam cross section and the rotational springs. Following Eq. (3.1) the incremental constitutive relations of the beam cross section and the rotational springs are written in the form

$$\frac{dM}{d\chi} = g[\chi(x), M(x)] \qquad (beam) \tag{4.5}$$

$$\frac{dM_{sl}}{d\theta_{sl}} = g_{sl}(\theta_{sl}, M_{sl}) \quad l = 1,2 \qquad (springs) \qquad (4.6)$$

For the beam cross section the constitutive law describes a differential moment-curvature relation, while for the end rotational springs it represents a differential moment-rotation relation. According to the numerical integration procedure in Chapter 3, Eqs. (4.5) and (4.6) become

$$\Delta\chi^j(x) = f^{j-1}(x)\Delta M^j(x) + r^{j-1}(x) \qquad (beam) \qquad (4.7)$$

$$\Delta\theta_{sl}^j = f_{sl}^{j-1}\Delta M_{sl}^j + r_{sl}^{j-1} \quad l = 1,2 \qquad (springs) \qquad (4.8)$$

where f is the section or spring flexibility and r denotes the residual curvature or rotation. The latter arises from the consistent linearization of the nonlinear constitutive laws in Eqs. (4.5) and (4.6), as discussed in detail in Chapter 3. Even though the formal representation of the force-deformation behavior of the beam cross section and the end rotational springs is the same, different material parameters can be used in each case, as necessary. The material parameters of the incremental constitutive relations were introduced in Chapter 3 and will be discussed in more detail in Chapter 5.

The matrix relation between forces and corresponding deformations of the end rotational springs can be readily obtained from the constitutive relation of each spring and the fact that the response of each spring is independent from the other. Consequently,

$$\Delta q_s^j = F_s^{j-1} \Delta Q_s^j + s_s^{j-1} \qquad (4.9)$$

where

$$F_s = \begin{bmatrix} f_{s1} & 0 \\ 0 & f_{s2} \end{bmatrix} \qquad s_s = \begin{Bmatrix} r_{s1} \\ r_{s2} \end{Bmatrix} \qquad (4.10)$$

The spring flexibility and the residual deformations are determined according to Eq. (3.29).

The matrix relation between end forces and corresponding deformations of the beam is derived in accordance with the mixed formulation of Chapter 2. The combination of the incremental constitutive law for the beam cross section in Eq. (4.7) with the mixed method of Section 2.4 results in the following matrix relation

$$\Delta q_b^j = F_b^{j-1} \Delta Q_b^j + s_b^{j-1} \qquad (4.11)$$

where F_b is the flexibility matrix of the beam and is obtained according to

$$F_b = \int_0^L b^T(x) f(x) b(x) \, dx \qquad (4.12)$$

while s_b are the residual deformations at the ends of the beam and are obtained according to

$$s_b = \int_0^L b^T(x) r(x) \, dx \qquad (4.13)$$

At this point the matrix relation between end force increments and corresponding deformations for the entire beam element can be established from the compatibility and equilibrium conditions in Eqs. (4.3) and (4.4), which are now written in incremental form

$$\Delta q^j = \Delta q_b^j + \Delta q_s^j \qquad (4.14)$$

$$\Delta Q^j = \Delta Q_b^j = \Delta Q_s^j \qquad (4.15)$$

The combination of Eqs. (4.9), (4.11) and (4.14) yields the following relation

$$\Delta q^j = F_b^{\,j-1} \, \Delta Q_b^j + s_b^{\,j-1} + F_s^{\,j-1} \, \Delta Q_s^j + s_s^{\,j-1} \qquad (4.16)$$

or,

$$\Delta q^j = F^{\,j-1} \, \Delta Q^j + s^{\,j-1} \qquad (4.17)$$

where F is the flexibility matrix of the entire beam element, as the sum of the flexibilities of the beam and the end springs

$$F = F_b + F_s \qquad (4.18)$$

and s are the residual deformations of the entire beam element, as the sum of the corresponding residual deformations of the beam and the end springs

$$s = s_b + s_s \qquad (4.19)$$

Eq. (4.17) is the matrix relation between end force increments and corresponding deformations for the entire beam element. The corresponding element state determination is very similar to the procedure discussed in Chapter 2. At this point it is important to note that the end deformation increments are such that $\Delta q^{j=1} \ne 0$ and $\Delta q^{j>1} = 0$, as was discussed in Chapter 2. In the first element iteration the end deformation increments are obtained from the nodal displacement increments at the structural degrees of freedom. In the subsequent iterations the nodal displacements and corresponding deformations cannot change, so as not to violate compatibility. Since $\Delta Q^j = K^{j-1} \cdot \left(-s^{j-1}\right)$ for $j>1$ according to the state determination procedure in Chapter 2, it is easy to conclude from Eq. (4.17) that $\Delta q^{j>1} = 0$.

The element formulation in this study is almost identical to the procedure used in the

parallel study for a beam-column element by Taucer et al. (1991). The latter involves an explicit section constitutive law that is derived from the nonlinear material behavior of the fibers into which the section is divided and the hypothesis that plane sections remain plane. The stiffness matrix and resisting forces of the section are derived by integration of the stiffness and resisting stress of the fibers. The difference between applied and resisting forces at the section results in a force unbalance that yields a residual deformation when multiplied by the new section stiffness. By contrast, in the present study the section constitutive relation is only known in the incremental form of Eq. (4.7). While the overall element state determination procedure remains the same, the section state determination is clearly affected by the different section behavior.

4.3   Numerical Integration

All integrals in the element formulation are evaluated numerically with the Gauss-Lobatto integration scheme that is based on the expression

$$I = \int_{-1}^{1} g(\xi) \cdot d\xi = w_1 \cdot g(-1) + \sum_{h=2}^{m-1} w_h \cdot g(\xi_h) + w_m \cdot g(1) \qquad (4.20)$$

where h denotes the monitored section and w_h is the corresponding weight factor (Stroud and Secrest 1966). The Gauss-Lobatto scheme with m integration points permits the exact integration of polynomials of degree up to $(2m-3)$. This procedure is superior to the classical Gauss integration method, when it is important to include in the integration the end points of the element. Since inelastic behavior in beam-column elements often concentrates at the ends of the member, the monitoring of the end sections of the element offers advantages from the standpoint of accuracy and numerical stability.

4.4   Element State Determination

The state determination for the entire beam element follows the procedure described in Chapter 2. During this phase of the algorithm the task at hand is the determination of the element stiffness matrix and resisting forces for given end displacements. The numerical implementation of the element state determination is summarized in the following step-by-step description. It is important to recall that the nonlinear solution algorithm for the entire structure is subdivided into three nested loops:

Loop k denotes the sequence of load increments $\Delta\mathbf{P}_E^k$ for the application of external loads on the structure. At load step k the total applied load is $\mathbf{P}_E^k$.

Loop i denotes the iteration scheme at the structural degrees of freedom, i.e. the structure state determination. for the determination of the structural displacements $\mathbf{p}^k$ that correspond to the applied loads $\mathbf{P}_E^k$. In the present study the Newton-Raphson algorithm is used for the purpose.

Loop j denotes the iteration scheme at the element level, i.e. the element state determination process. These iterations are necessary for the determination of the element resisting forces that correspond to deformations $\mathbf{q}^i$ at the i-th Newton-Raphson iteration.

The relation and interaction among these three iteration processes is explained in more detail in Taucer et al. (1991) with a few illustrative diagrams. The following discussion is limited to one Newton-Raphson step i and concentrates on the steps of iteration loop j.

In Newton-Raphson step i the displacement increments $\Delta\mathbf{p}^i$ at the structural degrees of freedom are established first from the solution of the global equilibrium equations. The next task involves the determination of the stiffness matrix and resisting forces of the structure that correspond to the new structural displacements $\mathbf{p}^i$. This entails the following operations of state determination for each beam finite element:

(1)   *Determine the element deformation increments for Newton-Raphson step i.*

Using the compatibility matrix $\mathbf{L}_{ele}$ the element deformation increments $\Delta\mathbf{q}^i$ are determined from the nodal displacement increments $\Delta\mathbf{p}^i$ at Newton-Raphson step i

$$\Delta\mathbf{q}^i = \mathbf{L}_{ele}\,\Delta\mathbf{p}^i$$

The compatibility matrix $\mathbf{L}_{ele}$ performs, both, the elimination of rigid body modes and the rotation to the local reference system.

(2)   *Update the element deformations.*

$$\mathbf{q}^i = \mathbf{q}^{i-1} + \Delta\mathbf{q}^i$$

(3)   *Start the element state determination.*

Set the index of the first iteration: $j=1$.

(4)   *Determine the element force increments.*

The element force increments ΔQ^j are determined with the element stiffness matrix K^{j-1} at the end of the previous iteration in loop j. There are two cases:

a) for $j=1$

$$\Delta Q^{j=1} = K^{j=0}\ \Delta q^i$$

b) for $j>1$

$$\Delta Q^j = K^{j-1}\left(-s^{j-1}\right)$$

where s^{j-1} are the residual element deformations at the end of the previous iteration, as determined in step **(13)** below.

(5)   *Update the element forces.*

$$Q^j = Q^{j-1} + \Delta Q^j$$

When $j=1$, $Q^0 = Q^{i-1}$ where i-1 indicates the previous Newton-Raphson iteration. From equilibrium the forces in the beam and end springs are equal to the element forces, so that:

$$\Delta Q_s^j = \Delta Q_b^j = \Delta Q^j \qquad\qquad Q_s^j = Q_b^j = Q^j$$

(6)   *Determine the force increments at the control sections of the beam.*

The section force increments $\Delta M^j(x_h)$ are determined from the force interpolation functions $b(x)$ and the element force increments ΔQ^j. The section force $M^j(x_h)$ is then updated. These operations are repeated for all control sections or integration points m in the beam.

$$\Delta M^j(x_h) = b(x_h)\ \Delta Q^j \qquad\qquad h = 1, m$$

$$M^j(x_h) = M^{j-1}(x_h) + \Delta M^j(x_h) \qquad\qquad h = 1, m$$

(7)   *Determine the deformation increments at beam control sections and end springs.*

The deformation increments $\Delta\chi^j(x_h)$ and Δq_s^j are determined by adding the residual deformations from the previous iteration, $r^{j-1}(x_h)$ and s_s^{j-1}, to the deformation increments due to force increments $\Delta M^j(x_h)$ and ΔQ_s^j, respectively.

$$\Delta\chi^j(x_h) = f^{j-1}(x_h)\ \Delta M^j(x_h) + r^{j-1}(x_h) \qquad\qquad h = 1, m$$

$$\Delta q_s^{j} = F_s^{j-1} \, \Delta Q_s^{j} + s_s^{j-1}$$

The corresponding vectors are then updated

$$\chi^{j}(x_h) = \chi^{j-1}(x_h) + \Delta\chi^{j}(x_h) \qquad h = 1, m$$

$$q_s^{j} = q_s^{j-1} + \Delta q_s^{j}$$

(8) *Determine the error function and its derivatives.*

Compute the error function and its derivatives at the beam control sections, $\psi^{j}(x_h)$, $\dfrac{\partial\psi^{j}(x_h)}{\partial\chi}$ and $\dfrac{\partial\psi^{j}(x_h)}{\partial M}$ for $h=1..m$ and at the end springs, ψ_{sl}^{j}, $\dfrac{\partial\psi^{j}}{\partial\theta_{sl}}$ and $\dfrac{\partial\psi^{j}}{\partial M_{sl}}$ for $l=1..2$.

(9) *Determine the flexibility at the beam control sections and the end springs.*

Determine the section flexibility

$$f^{j}(x_h) = -\frac{\dfrac{\partial\psi^{j}(x_h)}{\partial M}}{\dfrac{\partial\psi^{j}(x_h)}{\partial\chi}} \qquad h = 1, m$$

and the diagonal spring flexibility matrix F_s^{j} with the following terms

$$f_{sl}^{j} = -\frac{\dfrac{\partial\psi^{j}}{\partial M_{sl}}}{\dfrac{\partial\psi^{j}}{\partial\theta_{sl}}} \qquad l = 1,2$$

(10) *Determine the residual deformations at the beam control sections and end springs.*

Determine the residual section deformations

$$r^{j}(x_h) = -\frac{\psi^{j}(x_h)}{\dfrac{\partial\psi^{j}(x_h)}{\partial\chi}} \qquad h = 1, m$$

and the residual spring deformation vector s_s^{j} with the following terms

$$r_{sl}^{j} = -\frac{\psi_{sl}^{j}}{\dfrac{\partial \psi^{j}}{\partial \theta_{sl}}} \qquad\qquad l = 1,2$$

(11)   *Determine the flexibility matrix of the beam and the entire element* .

The flexibility matrix of the beam is obtained by numerical integration of section flexibilities

$$F_{b}^{j} = \sum_{h=1}^{m}\left[w_{h}\ b^{T}(x_{h})\ f^{j}(x_{h})\ b(x_{h}) \right]$$

The flexibility matrix of the entire element is then established as the sum of the beam and end spring flexibility matrices

$$F^{j} = F_{b}^{j} + F_{s}^{j}$$

(12)   *Determine the element stiffness matrix.*

Invert the element flexibility to obtain the element stiffness matrix

$$K^{j} = \left[F^{j} \right]^{-1}$$

(13)   *Check for element convergence.*

a)   If the *error function* is sufficiently small at all control sections of the beam and at the end springs, the element state determination process has converged.

b)   If the *error function* exceeds the specified tolerance at one or more control sections, the residual deformations of the beam and the entire element, s_{b}^{j} and s^{j}, respectively are determined.

$$s_{b}^{j} = \sum_{h=1}^{m}\left[w_{h}\ b^{T}(x_{h})\ r^{j}(x_{h}) \right]$$

$$s^{j} = s_{b}^{j} + s_{s}^{j}$$

Steps **(4)** through **(13)** are repeated until the *error function* is sufficiently small at all control sections of the beam and at the end springs.
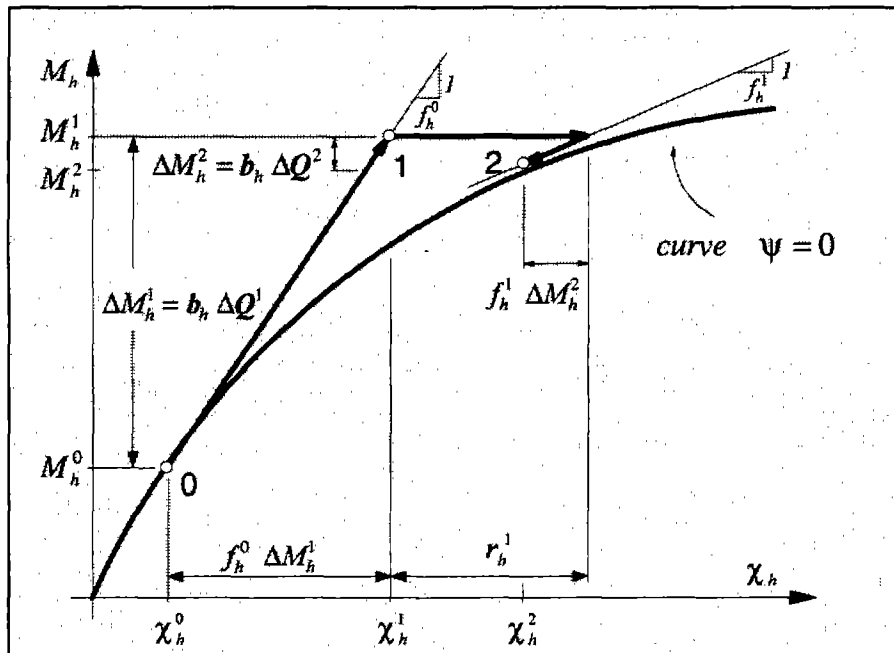
FIGURE 4.3   STATE DETERMINATION AT MONITORED SECTION h
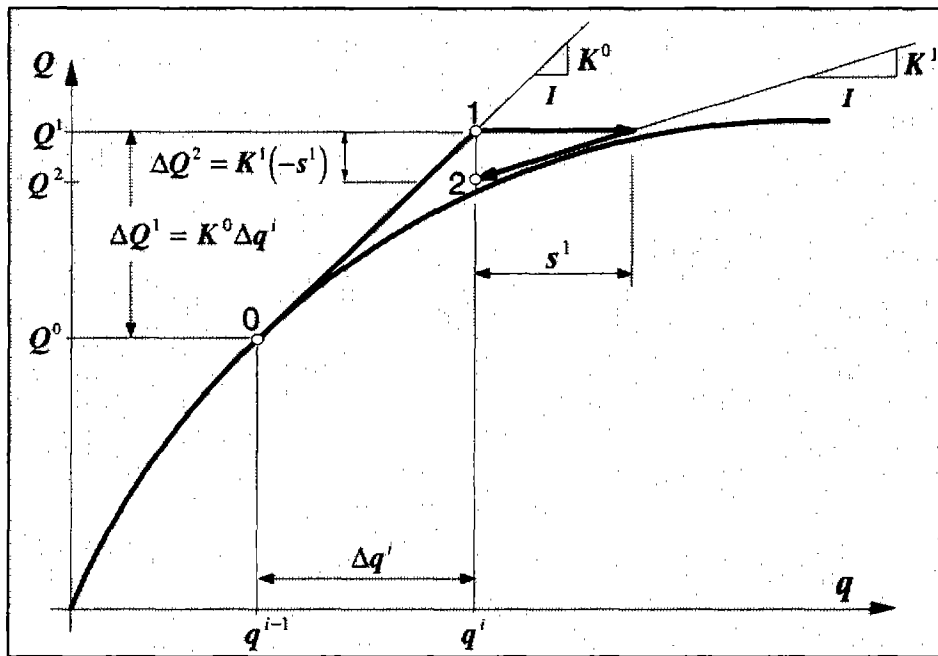
FIGURE 4.4   STATE DETERMINATION OF BEAM ELEMENT

The first two iterations of the element state determination are schematically shown in Figs. 4.3 and 4.4. Fig. 4.3 refers to monitored section h and Fig. 4.4 to the beam element. In both figures 0 denotes the initial point of the element state determination. For the first element iteration $j=1$, the section force increment $\Delta M_h^1 = b_h \, \Delta Q^1$ is determined from the

element force increment $\Delta Q^1 = K^0 \Delta q^i$ and the force field is updated to $M_h^1 = M_h^0 + \Delta M_h^1$. The initial flexibility f_h^0 yields the corresponding curvature increment $\Delta \chi_h^1 = f_h^0 \Delta M_h^1$ according to the consistent linearization of the constitutive relation. Given the initial point (χ_h^0, M_h^0) and the two increments $\Delta \chi_h^1$ and ΔM_h^1 the error function ψ_h^1 and its partial derivatives $\partial \psi_h^1 / \partial M^1$ and $\partial \psi_h^1 / \partial \chi^1$ can be established yielding the section flexibility f_h^1 and residual curvature r_h^1. In order to maintain compatibility at the element nodes the correction of the residual section curvatures is deferred to the next iteration in loop j. The section flexibility and the residual curvatures are integrated to obtain the beam flexibility F_b^1 and the residual deformations s_b^1. The same procedure is followed for the end springs yielding the spring flexibility F_s^1 and the residual deformations s_s^1. In the next step the element flexibility F^1 and the residual deformations s^1 are determined, thus completing the first iteration $j=1$. Point 1 corresponds to the final point of the first iteration in Figs. 4.3 and 4.4. The residual element deformations at the end of the previous iteration yield the element force increment for the iteration $j=2$ according to $\Delta Q^2 = K^1 (-s^1)$. The corresponding section force increment $\Delta M_h^2 = b_h \Delta Q^2$ is determined and the entire force field is updated to $M_h^2 = M_h^1 + \Delta M_h^2$. The section curvature increment is then determined with $\Delta \chi_h^2 = f_h^1 \Delta M_h^2 + r_h^1$ and the corresponding vector is updated. The new error function ψ_h^2 and its partial derivatives $\partial \psi_h^2 / \partial M^2$ and $\partial \psi_h^2 / \partial \chi^2$ are established yielding the new section flexibility f_h^2 and residual curvature r_h^2. The section flexibility and the residual curvatures are integrated to obtain the beam flexibility F_b^2 and the residual deformations s_b^2. The spring flexibility and residual deformations are also computed. Finally, the element flexibility F^2 and the residual deformations s^2 are established, thus completing the second iteration $j=2$. Point 2 corresponds to the final point of the second iteration in Figs. 4.3 and 4.4. The iterations continue until the error function becomes sufficiently small at all control sections of the beam and at the end springs.

It is important to point out that the deformations q of the entire element do not change during the iterations of the element state determination process. By contrast, the deformations of the beam and springs, q_b and q_s, respectively, change during these iterations. For the new element deformations $q^i = q^{i-1} + \Delta q^i$ the deformations of the beam and springs are adjusted until the corresponding constitutive relations are satisfied within the specified tolerance. During the iteration process compatibility is always maintained, since the sum of q_s and q_b is equal to q^i, even though the individual contributions vary. This is an important characteristic of the model showing the application of the flexibility-based method and the proposed state determination process to a finite element that is formed by a beam and two

end springs connected in series. Given the imposed nodal deformations q^i, the forces and deformations of the beam and end springs are adjusted until the element forces Q and the component deformations q_b and q_s satisfy the corresponding constitutive relations while maintaining compatibility between the components, as expressed by $q = q_b + q_s$, and equilibrium, as expressed by $Q = Q_b = Q_s$ and $M(x) = b(x)Q$. In this particular model implementation, the compatibility between the components need only be maintained at the end nodes, while the equilibrium is satisfied in a strict sense along the beam, as ensured by the internal force distribution $M(x) = b(x)Q$.

CHAPTER 5

MODEL PARAMETERS AND DEGRADATION SCHEME

5.1 General

This chapter discusses the selection of parameters for the incremental constitutive relation of Chapter 3. This constitutive relation was used in Chapter 4 to describe the moment-curvature relation of the beam control sections and the moment-rotation relation of the end springs. Since both constitutive relations are not necessarily symmetric, two sets of parameters are needed: one controls the behavior of the model in the positive load-deformation regime and the other in the negative. With the change in value of the control parameters during the loading history, the model can trace hysteretic loops of various shapes with different initial, unloading and post-yield stiffness.

The first part of the chapter discusses the basic constitutive law developed in Chapter 3. In the second part the basic model is extended to include the effect of "pinching". This effect of the hysteretic behavior is characteristic of materials that exhibit soft response under reloading for deformations that do not exceed the maximum previously imposed. Because of shear cracking and bond slip during cyclic loading, reinforced concrete is a material that exhibits such behavior. In the proposed model pinching is included by defining a lower intermediate level of yielding and a corresponding post-yield (pinching) stiffness. The last part of the chapter introduces the scheme of degradation of model parameters. As loading progresses, steel and concrete structural members often exhibit gradual degradation of strength and stiffness and a consequent loss of dissipative capacity. Damage is an evolutionary process that can be naturally included in an incremental constitutive relation. A damage coefficient is defined for each model parameter as the weighted sum of total plastic work and maximum deformation. Damage is assumed to be symmetric, so that the same damage coefficients affect the model parameters in the positive and negative load-deformation regime. The chapter concludes with a summary of the model and degradation parameters.

5.2   Parameters for Incremental Constitutive Law

Chapter 3 presented the development of an incremental constitutive law from a simple standard solid model. This constitutive relation was used in Chapter 4 to describe the moment-curvature relation of the beam control sections and the moment-rotation relation of the end springs. The parameters defining the incremental law are described in this section, limiting attention to the moment-curvature relation and keeping in mind that the moment-rotation relation of the end rotational springs has exactly the same form.

The moment-curvature relation in Eq. (3.17) can be written as follows after recalling that $M_0 = EI_0 \cdot \chi_0$

$$\frac{dM}{d\chi} = EI_0 \left\{ 1 - (1-\alpha) \left[sgn(d\chi) \, sgn(x) \, \beta + \gamma \right] |x|^n \right\} \tag{5.1}$$

where

$$EI_0 = EI_1 + EI_2 \tag{5.2}$$

$$\alpha = \frac{EI_2}{EI_0} \tag{5.3}$$

$$x = \frac{M}{M_0 (1-\alpha)} - \frac{\chi \, \alpha}{\chi_0 (1-\alpha)} \tag{5.4}$$

For the moment-rotation relation that characterizes the behavior of the end rotational springs, Eq. (5.1) can be written in the same way, by replacing EI_0 with k_0, χ with θ and using the definition of α in Eq. (5.3). In order to allow for non-symmetric load-deformation behavior two sets of parameters are needed for Eq. (5.1): one controls the behavior of the model in the positive load-deformation regime and the other in the negative. Only the unloading parameters γ and β have a single value. In the following description only the behavior of the model in the positive load-deformation regime will be discussed, the extension to the negative regime being straightforward. At the end of the chapter Table 1 summarizes the parameters that control the constitutive law of the beam cross sections and the end rotational springs.

The parameters in Eq. (5.1) are illustrated in Fig. 5.1. E is the initial elastic modulus of the material and I the moment of inertia of the cross section. EI_0 is the initial tangent stiffness of the moment-curvature relation and EI_2 is the post-yield stiffness. M_0 is the yield moment which for the model represents the bending moment at the intersection of the initial

tangent stiffness and the linear asymptote of the moment-curvature relation for very large curvature values. Parameter α represents the strain hardening ratio between the post-yield stiffness and the initial elastic stiffness of the model.
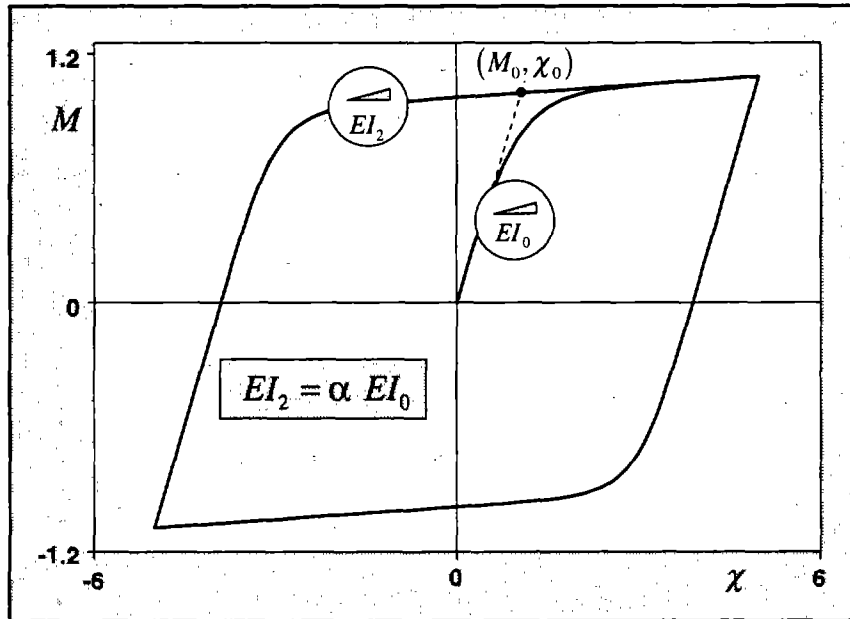
FIGURE 5.1   PARAMETERS DEFINING THE BEHAVIOR OF THE BASIC CONSTITUTIVE LAW
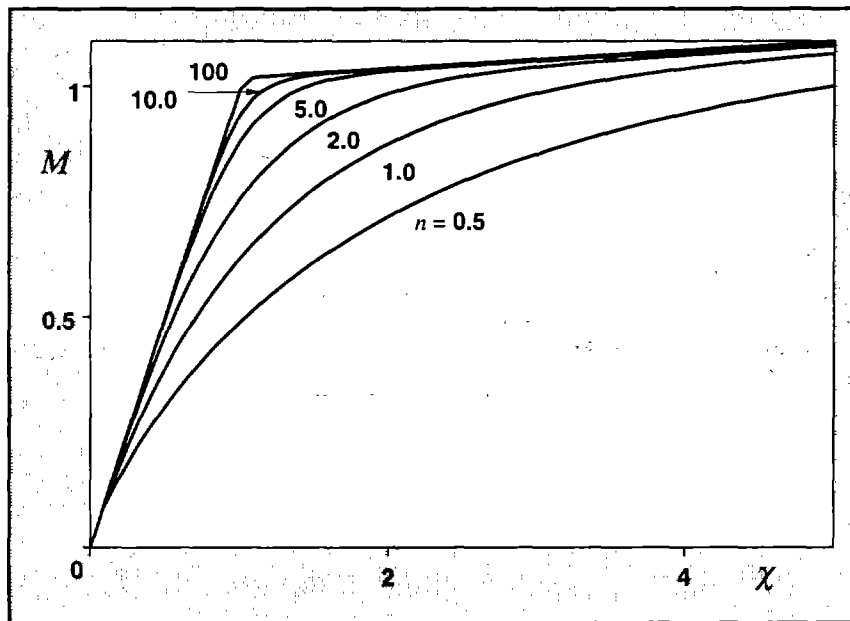
FIGURE 5.2   INFLUENCE OF n ON TRANSITION FROM ELASTIC TO PLASTIC BRANCH

Exponent n in Eq. (5.1) governs the transition from the elastic to the elasto-plastic branch. Its influence on the moment-curvature response is depicted in Fig. 5.2: small values of n lead to a smooth transition, but as n increases the transition becomes sharper tending to a perfectly bilinear behavior in the limit.

In Eq. (5.1) γ and β are two parameters that govern the initial phase of the unloading paths. Since their sum equals 1 according to the discussion in Section 3.2, only one parameter can be selected independently. In the following discussion γ in the variable parameter. The value $\gamma = 0.5$ is the default selection that gives rise to linear elastic unloading with the same slope EI_0 as the initial loading. If γ is assigned a value smaller than 0.5, the slope becomes steeper. It is important to recall that γ may take any positive or negative value smaller or equal to 0.5 according to Section 3.2. Fig. 5.3 shows three hysteretic loops corresponding to $\gamma = 0.5$, $\gamma = -3$ and $\gamma = -200$. The effect of γ on the hysteretic behavior may be rather sensitive to the size of unloading deformation increments. With larger increments the unloading path tends to perfectly elastic behavior, thus diminishing the effect of γ.
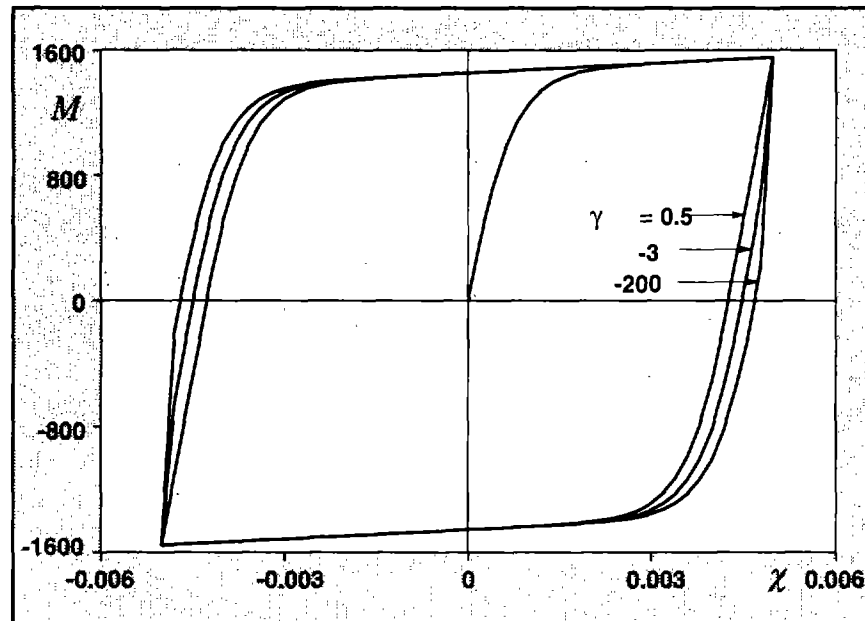
FIGURE 5.3   INFLUENCE OF UNLOADING PARAMETER γ ON $M - \chi$ CURVE

5.3   Pinching

The hysteretic behavior of some materials is characterized by soft response under reloading for deformations that do not exceed the maximum previously imposed. Because of

shear cracking and bond slip during cyclic loading, reinforced concrete is a material that exhibits such "pinching" behavior. The model of Chapter 3 can be modified to include the effect of "pinching" by introducing a new set of parameters. The idea is to define an intermediate fictitious yield level at the moment value that corresponds to the onset of "pinching" and an intermediate set of parameters similar to those described in Section 5.2. These intermediate values control the hysteretic behavior of the model until a specified deformation value is reached.

Formally, this is accomplished by rewriting Eq. (5.1) in the more general form

$$\frac{dM}{d\chi} = EI_0 \left\{ 1 - (1 - \tilde{\alpha}) \left[sgn(d\chi) \, sgn(\tilde{x}) \, \beta + \gamma \right] |\tilde{x}|^{\tilde{n}} \right\} \qquad (5.5)$$

where

$$\tilde{x} = \frac{M}{\tilde{M}_0 (1 - \tilde{\alpha})} - \frac{\chi \tilde{\alpha}}{\tilde{\chi}_0 (1 - \tilde{\alpha})} \qquad (5.6)$$

$$\tilde{\chi}_0 = \frac{\tilde{M}_0}{EI_0} \qquad (5.7)$$

$$\tilde{\alpha} = \frac{\tilde{EI}_2}{EI_0} \qquad (5.8)$$

$$\tilde{EI}_2 = EI_2^P + \left(EI_2 - EI_2^P \right) c \qquad (5.9)$$

$$\tilde{M}_0 = M_0^P + \left(M_0 - M_0^P \right) c \qquad (5.10)$$

$$\tilde{n} = n^P + \left(n - n^P \right) c \qquad (5.11)$$

Superscript P stands for "pinching". Fig. 5.4 illustrates these new parameters. M_0^P is the moment value at the intersection of the "pinching" branch with the bending moment axis, and EI_2^P is the stiffness of the "pinching" branch. Similar to n in Eq. (5.1), n^P is the exponent governing the transition from the elastic reloading branch to the "pinching" branch. EI_0, EI_2, M_0, n and γ are the same parameters defined in Section 5.2. Eqs. (5.9)-(5.11) depend on a parameter c, that relates the basic model parameters with the parameters for the "pinching" branch and defines the curvature value at the onset of "pinching". It is defined by the following expression:
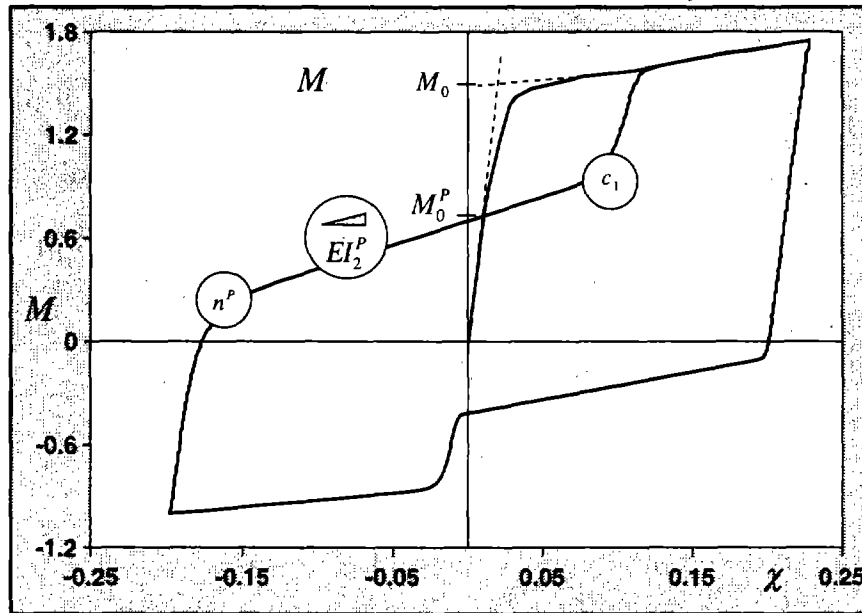
FIGURE 5.4   PINCHING PARAMETERS AND THEIR EFFECT ON CONSTITUTIVE LAW

$$c = \begin{cases} e^{c_1 \chi_{nor}} & \text{for} \quad \chi < c_2 \chi_{max} \\ 1 & \text{for} \quad \chi > c_2 \chi_{max} \end{cases} \tag{5.12}$$
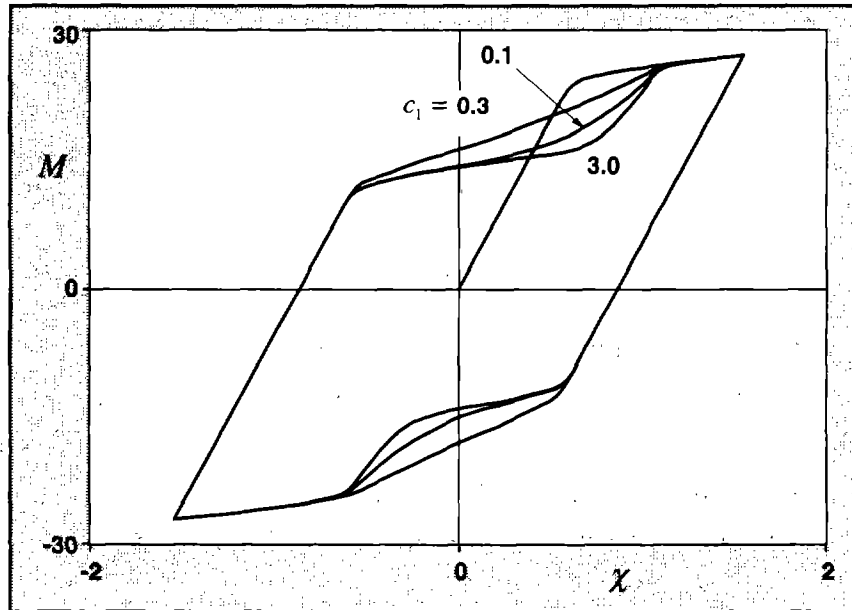
FIGURE 5.5   INFLUENCE OF PARAMETER c_1 ON TRANSITION FROM
PINCHING BRANCH TO PREVIOUS RELOADING BRANCH

where c_1 is an arbitrary coefficient whose effect on the shape of the "pinching" branch and the transition to the original reloading branch is shown is Fig. 5.5. $c_2 \chi_{max}$ is a limit deformation value that is specified below, and χ_{nor} is a normalized deformation given by the expression

$$\chi_{nor} = \frac{\chi \cdot sgn(d\chi) - c_2 \cdot \chi_{max}}{\chi_0} \qquad (5.13)$$

In Eqs. (5.12) and (5.13), c_2 is a positive coefficient and χ_{max} is the maximum deformation value in all previous loading cycles. Under negative deformation increments χ_{max} corresponds to the maximum negative deformation value in all previous loading cycles χ_{max}^-, and under positive deformation increments it corresponds to the maximum positive deformation value χ_{max}^+. The effect of different values of c_2 on the transition from the "pinching" branch to the original reloading branch is shown in Fig. 5.6. If $c_2 = 0$, the transition from the "pinching" branch to the original reloading branch initiates at zero curvature. At the other extreme, if $c_2 = 1$ the transition from the "pinching" branch to the original reloading branch is delayed until the maximum deformation value experienced in previous cycles. Even though it seems reasonable to assume that $c_2 \in [0,1]$, the model can also be assigned values of c_2 larger than 1, as shown in an application of the model in Chapter 6.
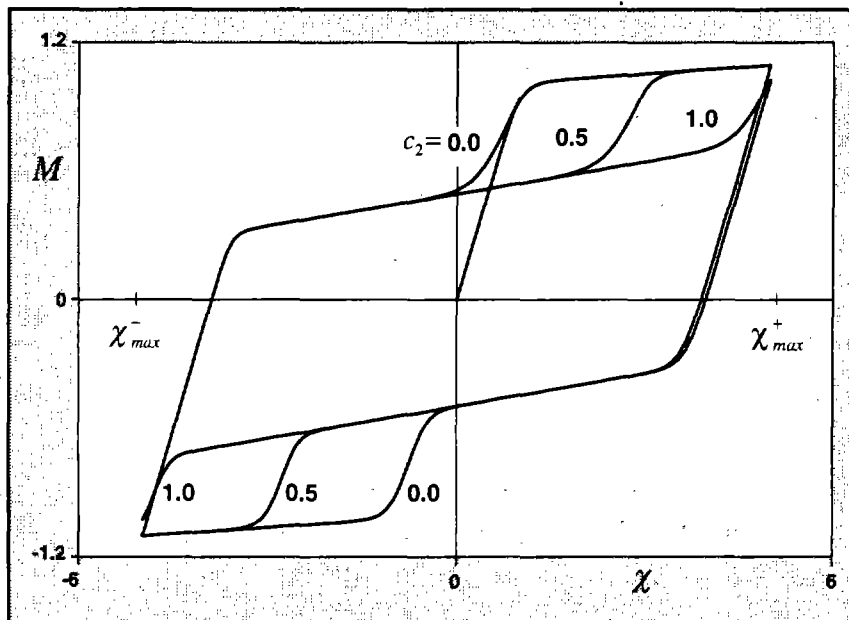
FIGURE 5.6   INFLUENCE OF PARAMETER c_2 ON TRANSITION FROM PINCHING BRANCH
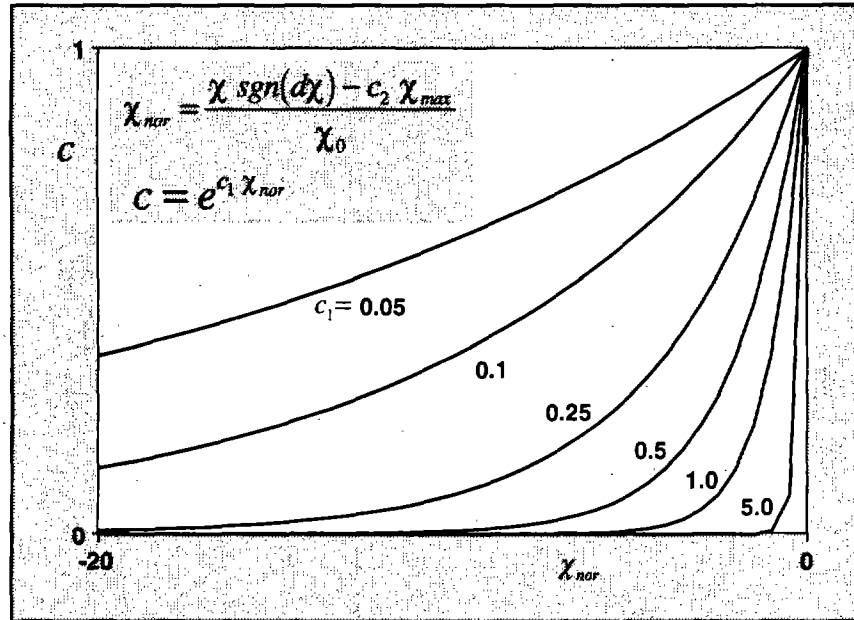
FIGURE 5.7   INFLUENCE OF c_1 ON c AS THE NORMALIZED

CURVATURE χ_{nor} INCREASES

The behavior of parameter $c = e^{c_1 \chi_{nor}}$ is analyzed in Fig. (5.7). For a small value of curvature χ, χ_{nor} assumes a very small negative value and c tends to zero, so that the parameters for the "pinching" branch dominate the response in Eq. (5.5). As the curvature χ increases and approaches the value $c_2 \chi_{max}$, χ_{nor} tends to zero and c tends to 1, so that the parameters of the initial reloading branch dominate the response in Eq. (5.5). The rate at which c increases form 0 to 1 depends on c_1. At the limit, as $c_1 \rightarrow \infty$, c becomes a delta function $c = \delta(\chi - c_2 \chi_{max})$, where $\delta(x)$ is the Dirac delta function, equal to 1 for $x=0$ and otherwise equal to zero.

5.4   Degradation Scheme

Experimental results of the hysteretic behavior of steel and reinforced concrete members show that repeated deformation cycles can cause deterioration of strength and stiffness of the member. Damage is an evolutionary process that can be naturally included in an incremental constitutive relation. A damage coefficient is defined for each model parameter as the weighted sum of total plastic work and maximum deformation. Damage is assumed to be symmetric, so that the same damage coefficients affect the model parameters in the positive and negative load-deformation regime. Typically, damage indices assume

values in the interval between 0 and 1 and decrease monotonically with increasing damage from the value of 1, which characterizes no damage, to the value of 0, which represents complete damage.

It it rather straightforward to introduce progressive damage in the constitutive relation that is defined by Eqs. (5.1) and (5.5). If Ω stands for the generic model parameter, Ω_n and Ω_{n+1} denote the parameter values at the end of the global load steps n and $n+1$, respectively, according to the notation of Chapter 3. The degradation scheme follows the equation

$$\Omega_{n+1} = \Omega_n \left(1 - \Delta \overline{W}_{n+1} \, d_1^{\Omega} \, d_2\right) \tag{5.14}$$

where d_1^{Ω} and d_2 are two parameters that will be defined subsequently, and $\Delta \overline{W}_{n+1}$ is the plastic work during the global step $n+1$. $\Delta \overline{W}_{n+1}$ is determined from the expression

$$\Delta \overline{W}_{n+1} = \left| \frac{\left(M_{n+1} + M_n\right) \Delta \chi_{n+1}^{p}}{2} \right| \tag{5.15}$$

where $\Delta \chi_{n+1}^{p}$ is the plastic deformation increment, which according to Eq. (3.9) is

$$\Delta \chi^{p} = w |\Delta \chi| \left| \frac{M - (EI)_2 \, \chi}{M_0 \, (1-\alpha)} \right|^{n} \tag{5.16}$$

The degradation scheme defined by Eq. (5.14) is applied to the following model parameters: EI_0, EI_2, M_0, M_0^p, α, n, n^p, c_1, c_2. Note that Eq. (5.14) is not dimensionally correct, because every term is dimensionless except for the plastic work increment $\Delta \overline{W}_{n+1}$. This increment could be normalized by dividing the right hand side of Eq. (5.15) by a measure of the work stored at yielding of the material, as defined by the product $M_0 \, \chi_0$. Since this correction is not necessary for low-cycle fatigue, which is the main focus of this study, it is not included in the present implementation of the element whose degradation scheme follows Eqs. (5.14) and (5.15) and should be used with care in cases of high-cycle fatigue.

The two coefficients d_1^{Ω} and d_2 in Eq. (5.14) control the weighting between plastic work and maximum deformation amplitude in the definition of damage. The first coefficient d_1^{Ω} varies in the range of [0,1]: if $d_1^{\Omega} = 0$, damage is only a function of maximum deformation amplitude and does not depend on plastic work; if $d_1^{\Omega} = 1$, the reverse is true. Superscript Ω stands for the generic model parameter to indicate that one damage coefficient is defined for each model parameter, without distinction between the parameters that control the behavior of the model in the positive and in the negative load-deformation regime. For example, $d_1^{EI_0}$ governs the degradation of, both, positive and negative initial stiffness, EI_0^+

and EI_0^-, respectively. All damage coefficients d_i^Ω that need to be specified for the definition of the hysteretic behavior of the constitutive relation are summarized in Table 1 at the end of this chapter.

The second coefficient d_2 is unique for all model parameters and is defined by

$$d_2 = \frac{1}{1 + e^{b_1\left(1 - \frac{\chi_{amp}}{b_2}\right)}} \qquad (5.17)$$

χ_{amp} is a deformation amplitude that controlls the degradation process and is, in turn, defined by

$$\chi_{amp} = \chi_{max}^+ - b_3\left(\chi_{max}^+ - |\chi_{max}^-|\right) \qquad (5.18)$$
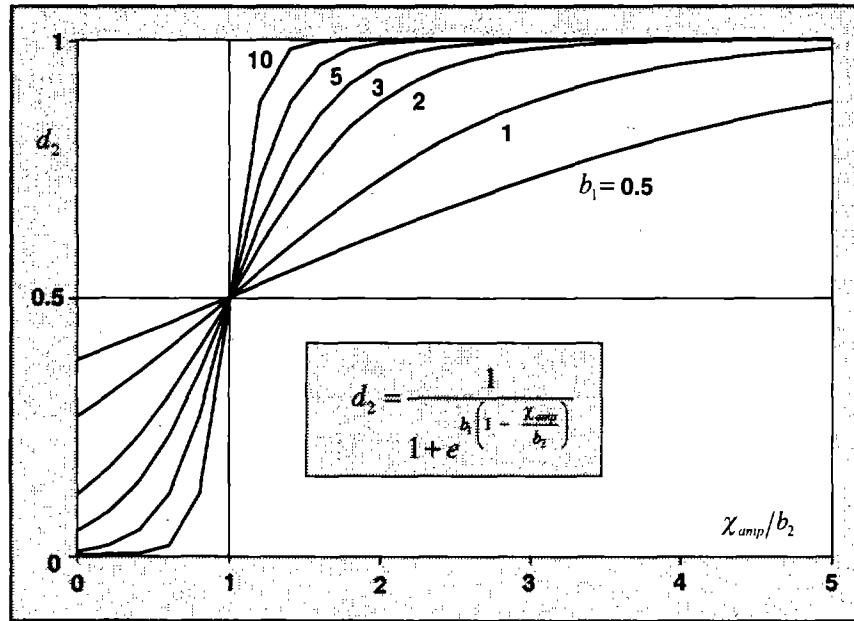
FIGURE 5.8   INFLUENCE OF PARAMETER b_2 ON d_2 FOR DIFFERENT VALUES OF b_1

b_3 is a coefficient that controlls the relative influence of the maximum and minimum deformation amplitudes on the degradation. Its value ranges from 0 to 1: the value of 0 ensures that degradation only depends on the maximum (positive) deformation amplitude, while the value of 1 limits the effect only to the minimum (negative) deformation amplitude. The value of 0.5 assigns equal weight to the extreme deformation values χ_{max}^+ and χ_{max}^-. Fig. 5.8 shows the effect of parameters b_1 and b_2 on the degradation parameter d_2. If b_1 is small, the degradation effect increases smoothly as the curvature amplitude increases. As b_1 becomes larger, d_2 tends to a unit step function equal to 0 for $\chi_{amp} < b_2$ and equal to 1 for

$\chi_{amp} > b_2$.
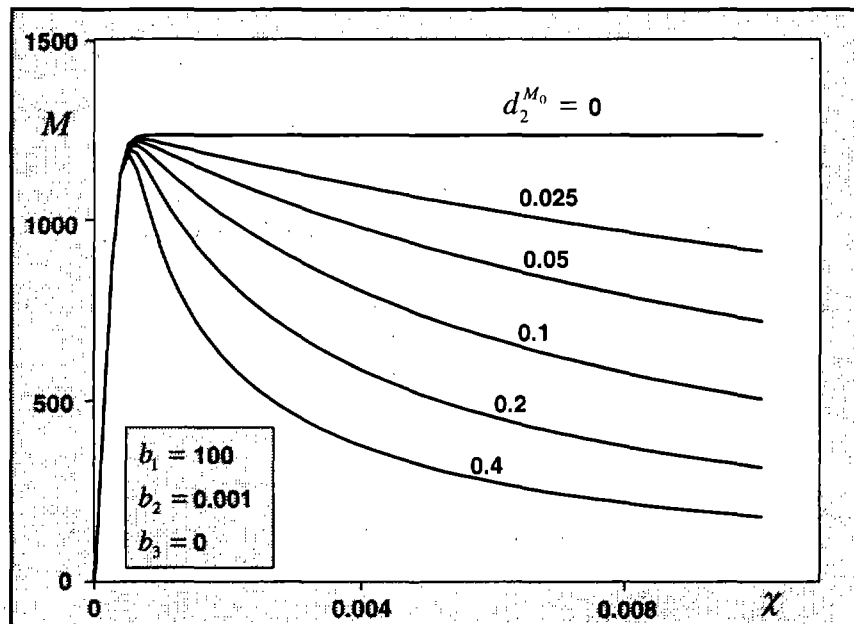
FIGURE 5.9   EFFECT OF DEGRADATION OF YIELD MOMENT M_0
ON YIELD AND POST-YIELD BEHAVIOR

The following figures illustrate the effect of the degradation degree of key model parameters on the hysteretic behavior of the model. Fig. 5.9 shows the monotonic behavior of the model for increasing values of $d_1^{M_0}$ and, thus, for increasing degradation of the yield moment M_0. As the imposed deformation increases, the yielding level decreases and the model exhibits a gradual loss of strength. This simulates well the characteristic strain softening behavior of certain materials, such as plain or reinforced concrete.

Fig. 5.10 shows the effect of degradation of yield moment and initial stiffness on the hysteretic behavior of the model under fixed deformation cycles of equal positive and negative amplitude. Fig. 5.10a isolates the effect of degradation of the yield moment only, Fig. 5.10b isolates the effect of degradation of the elastic stiffness, and Fig. 5.10c shows the combined effect of degradation of both parameters. The hysteretic behavior in Fig. 5.10 is obtained with a very low value for parameters $d_1^{M_0}$ and $d_1^{El_0}$, since, otherwise, the large value of plastic work during cyclic loading can quickly reduce the yield moment and the initial stiffness to zero and, thus, yield unrealistic results. For the cases of Fig. 5.10 which involve the degradation of yield moment, not only is the "pinching" level M^p equal to the yield moment M_0, but the same degradation function is used for both, i.e. $d_1^{M_0} = d_1^{M^p}$. If this is not the case, the hysteretic behavior changes to that in Fig. 5.11.

a) yield moment degradation   b) elastic stiffness degradation

c) degradation of yield moment and elastic stiffness
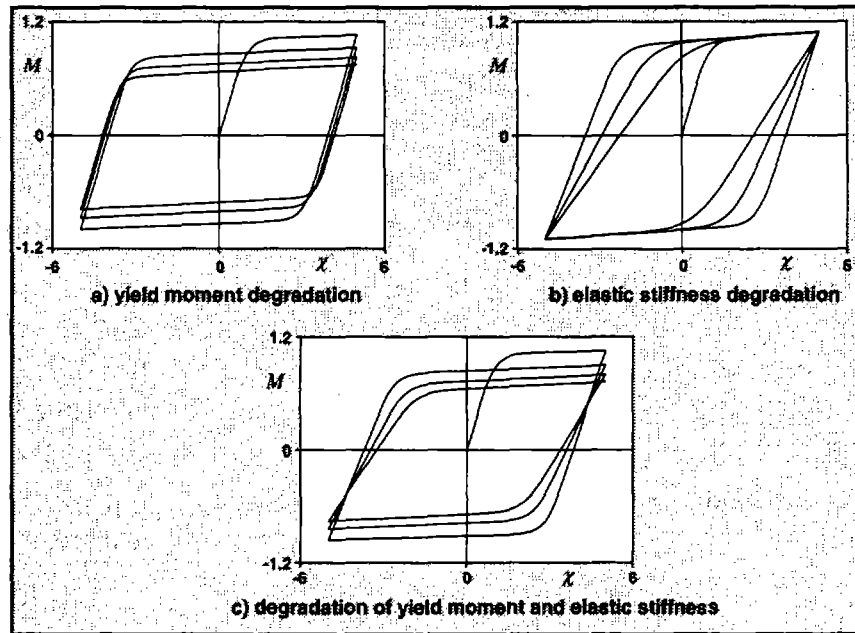
FIGURE 5.10   EFFECT OF DEGRADATION OF YIELD MOMENT M_0 AND ELASTIC STIFFNESS EI_0 FOR FIXED AND SYMMETRIC DEFORMATION CYCLES
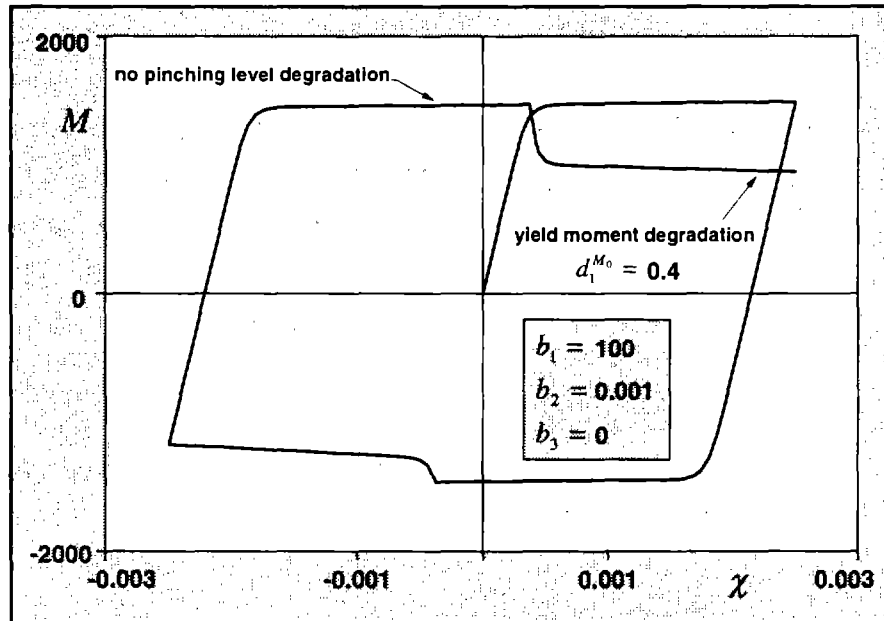
FIGURE. 5.11   CYCLE WITH DEGRADATION OF YIELD MOMENT M_0, BUT NOT OF PINCHING LEVEL M^P

Fig. 5.12 shows the strain softening example of Fig. 5.9 with $d_1^{M_0} = 0.4$ and three unloading-reloading cycles. In this case the post-yield stiffness is assigned a negative value. This becomes necessary for higher values of $d_1^{M_0}$ to facilitate convergence of the constitutive

model. Degradation of the elastic stiffness is also specified ($d_1^{EI_0} = 0.2$). Three unloading cycles to zero moment with reloading back to the envelope curve are specified. It is interesting to observe that the model shows a physical inconsistency in the failure of the unloading-reloading cycles to close. A detailed discussion of this phenomenon is presented in Appendix B in connection with the comparison of the proposed model with the Bouc-Wen model. It is possible to avoid this inconsistency by specifying a high initial value (see Fig. 5.2) and disallowing any degradation of exponent n, which controls the sharpness of the transition from the linear elastic to the post-yield range of response.
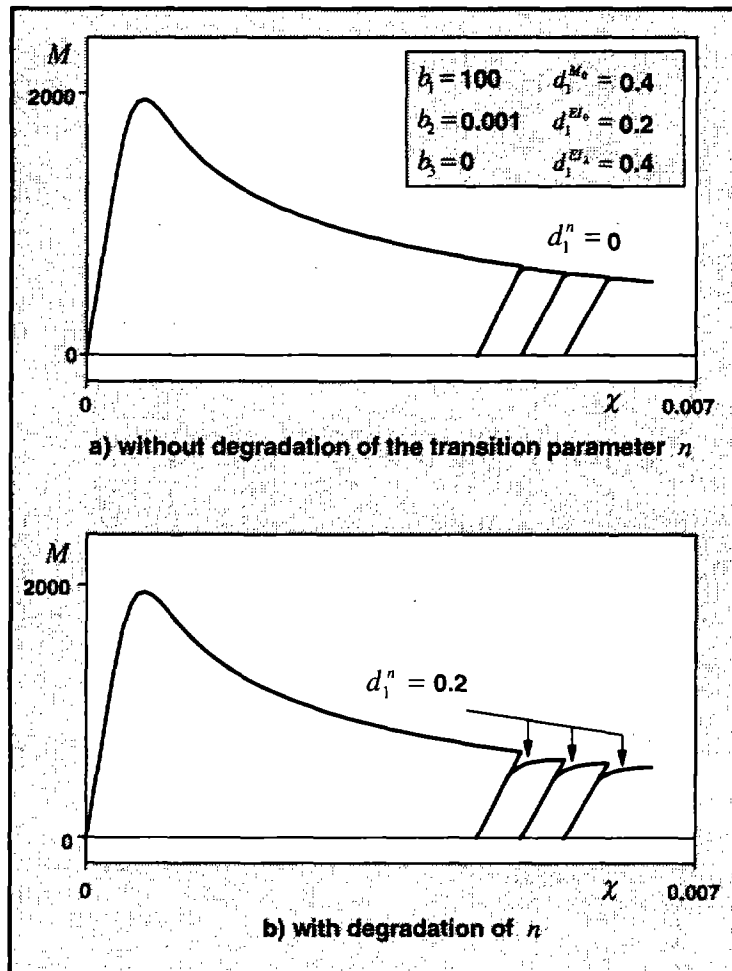
FIGURE 5.12   POST-YIELD CYCLES WITH AND WITHOUT DEGRADATION OF n:
DEGRADATION IS ALSO SPECIFIED FOR M_0, EI_0, AND EI_2

Finally, Fig. 5.13 shows that appropriate parameter selection enables the model to approximate the characteristic monotonic post-yield axial behavior of a steel coupon that exhibits a higher and lower yield stress and a plastic plateau followed by strain hardening.
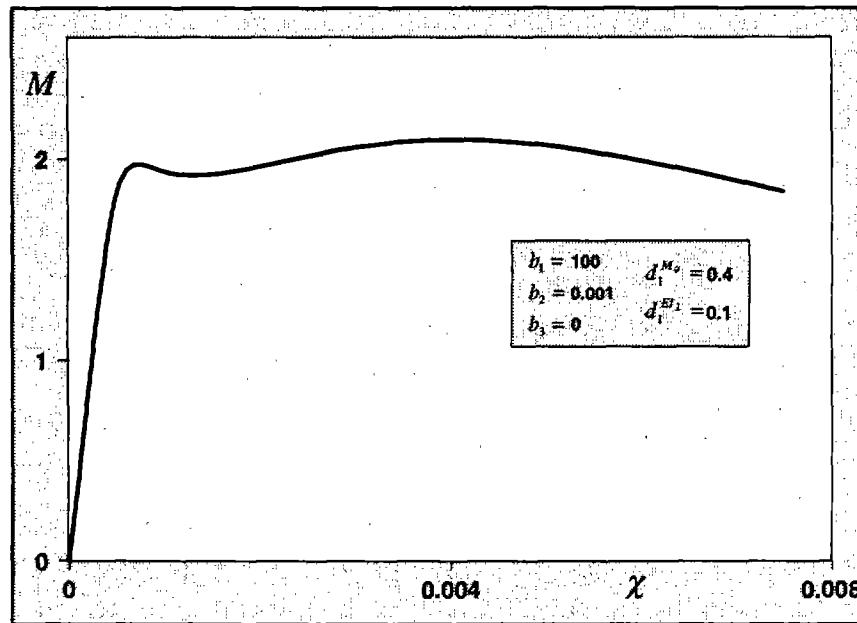
FIGURE 5.13   SIMULATION OF POST-YIELD BEHAVIOR OF

A STEEL COUPON UNDER MONOTONIC AXIAL LOADING

The few examples in this chapter demonstrate the inherent flexibility of the proposed constitutive model and the wide range of monotonic and hysteretic behaviors that it can simulate. Some correlation studies with experimental results are presented in the following chapter.

The demonstrated flexibility of the proposed model and the interaction between several parameters make the parameter selection by trial and error a difficult and lengthy process. It is possible to find several parameter combinations that match reasonably well the observed hysteretic behavior of a specimen. It is also possible to arrive at parameter combinations that lead to hysteretic behavior that is physically meaningless or even inconsistent with the basic rheological model that forms the foundation of the proposed constitutive relation. The latter problem arises, because of the purely empirical way of introducing the "pinching" effect in the basic model. So, while the introduction of the "pinching" effect in this chapter widens the range of hysteretic behaviors that the model can simulate, it also gives rise occasionally to physically inconsistent response. For these reasons objective and systematic methods of parameter selection are superior to the trial and error approach. Such an objective method is based on system-identification: given an initial set of parameters and a target moment-curvature relation, some user prescribed parameters are successively updated until the error between the target curve and the model response is

reduced to a prescribed minimum value. More details are provided in the work of Ciampi and Nicoletti (1986).

PARAMETER	SYMBOL		DAMAGE COEFFICIENT
cross section area	A		
integration scheme	θ		
beam unloading scheme	γ_b		
spring unloading scheme	γ_s		
tangent modulus	E^+	E^-	$d_1^{EI_0}$
moment of inertia	I^+	I^-	
yield moment	M_y^+	M_y^-	$d_1^{M_y}$
pinching moment	$\tilde{M}^+$	$\tilde{M}^-$	$d_1^{\tilde{M}}$
post-yield stiffness	EI_2^+	EI_2^-	$d_1^{EI_2}$
post-pinching stiffness	$\tilde{EI}^{p^+}$	$\tilde{EI}^{p^-}$	$d_1^{EI^p}$
transition at yielding	n^+	n^-	d_1^n
transition at pinching	n^{p^+}	n^{p^-}	$d_1^{n^p}$
transition at unloading	c_1^+	c_1^-	$d_1^{c_1}$
parameter extension of pinching	c_2^+	c_2^-	$d_1^{c_2}$
general degradation parameter 1			b_1
general degradation parameter 2			b_2
general degradation parameter 3			b_3

TABLE 5.1   SUMMARY OF PARAMETERS FOR INCREMENTAL CONSTITUTIVE RELATION AND OF CORRESPONDING DAMAGE INDICES

CHAPTER 6

APPLICATIONS

6.1   General

This chapter presents a few examples of the use of the proposed beam element in the simulation of the hysteretic behavior of structural members. The beam element is presently implemented in the general purpose finite element program ANSR. Details on the program can be found in Mondkar and Powell (1975a) and (1975b).

The example of a softening cantilever beam monotonically displaced beyond its point of maximum resistance is presented first. This is a test case for beam elements, because it is well known that stiffness based elements, which start from the compatibility rather than the equilibrium conditions along the element, encounter serious numerical difficulties in tracing the load-displacement behavior of softening members. The proposed beam element shows excellent agreement with the experimental results and convergence is attained in few iterations in every load step. Two more applications of the model are presented that compare the analytical results with experimental evidence from two reinforced concrete cantilever beams with non-symmetric longitudinal reinforcement. The first beam was cycled between fixed displacement values: in the experiment the beam failed in the second cycle when the bottom steel fractured. The second beam was cycled between symmetric displacements of increasing amplitude until failure took place. The finite element analysis of the two beams shows good agreement with the experimental results. The chapter concludes with a discussion about the selection of model parameters and damage coefficients and how these relate to the physical behavior of a reinforced concrete member.

6.2   A Softening Cantilever Beam

Several recent studies have dealt with the simulation of the softening behavior of reinforced concrete frame elements. Zeris and Mahin (1988) present a comprehensive review of these studies. The problem can be summed up as follows: when a cantilever element is subjected to an increasing displacement at the free end, the curvatures and bending moments

increase along the beam until the maximum resistance is reached at the built-in end. For the subsequent increase of tip displacement, the curvature amplitude increases in the neighborhood of the built-in end and decreases elsewhere in the beam, while the bending moment decreases along the beam, but remains linear in order to satisfy equilibrium. Thus, while the beam section at the built-in end softens, the remainder of the beam unloads, as the sections follow the decrease of bending moment in accordance with the reduction of the moment at the built-in end. The classical displacement method has difficulty tracing this behavior. In fact, following the common assumption of cubic displacement interpolation functions, that result in a linear curvature distribution, the element attempts to unload after the maximum resistance is reached at the built-in end. This unloading occurs in agreement with the imposed element compatibility condition and the resulting linear curvature distribution, whereas, in reality, it is the linear bending moment diagram that needs to be respected.

The response of a cantilever beam with the proposed finite element is shown in Fig. 6.1. The free end is supported on a very stiff spring to simulate an analysis under displacement control. The simple structure was studied with different mesh discretizations, but the response is mesh independent, as long as one rotational spring or one very short beam element is inserted at the built-in end to ensure that the length of the inelastic region (plastic hinge) remains constant. All beam sections have the same properties: the softening behavior is simulated by the degradation of the yield moment and by a negative post-yield stiffness. These two parameters need to be adjusted to obtain the desired degree of softening.

Fig. 6.1a shows the force-tip displacement relation. The softening behavior is governed by the moment-curvature history at the built-in section in Fig. 6.1b. After the maximum resisting moment is reached, the curvature at the built-in section continues increasing, whereas the resisting moment decreases. Accordingly, the tip displacement increases, while the shear force decreases. The behavior of a typical intermediate section is different in Fig. 6.1c. Since all sections respect the same constitutive relation and the bending moment diagram is linear, the sections along the beam are subjected to moment values less than the yield moment, when the built-in end reaches its maximum resistance. Once the bending moment decreases at the built-in section, all intermediate sections unload elastically to respect the imposed linear bending moment diagram. Fig. 6.1 shows that the proposed beam element can easily represent this physical behavior. Furthermore, convergence is very rapid, independent of mesh refinement and load step size. In fact, the load step size in the example of Fig. 6.1 was conditioned by the desire to obtain a smooth diagram.
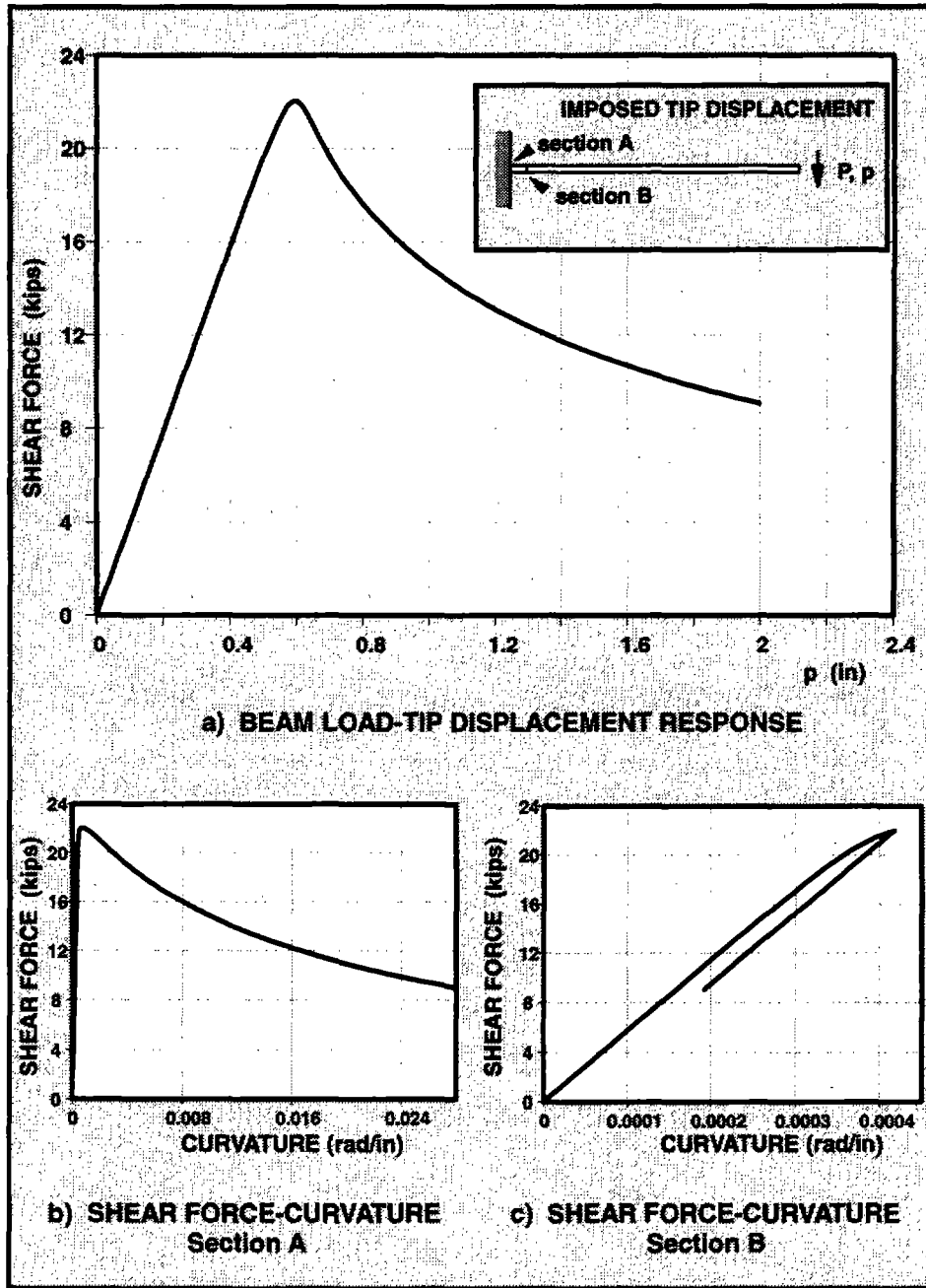
FIGURE 6.1   MONOTONIC LOADING OF A SOFTENING CANTILEVER BEAM:
                    BEHAVIOR AT THE BUILT-IN END AND AT AN INTERMEDIATE SECTION

This example makes clear why an approach based on force rather then displacement interpolation functions is better suited to describe softening. This derives from the fact that the bending moment diagram is always linear in a beam without element loads, independently of its material behavior. On the other hand the curvature diagram is linear for a prismatic

beam with uniform linear elastic material, but becomes highly nonlinear in the inelastic region of the section constitutive relation. In the classical displacement formulation of a two node beam finite element, the curvature diagram is assumed linear and the bending moment diagram, though initially linear, becomes nonlinear as the section constitutive enters the inelastic regime. This is in violation of the physical behavior. Even the proposed special methods, such as mesh refinement of the inelastic region of the member, do not free this type of elements from serious numerical problems.

6.3 Correlation Study with Two Cantilever Specimens

In this section the experimental responses of two cantilever beams under cyclic loading are compared with the results obtained from the finite element analysis of the same beams. The material properties, the geometry of the specimen and a discussion of the experimental results are available in the study by Ma et al. (1976). Both beams are half-scale models of a typical beam in the critical region of a 20 story ductile moment-resisting concrete frame. The beams have a rectangular cross section with non- symmetric longitudinal reinforcement: the top reinforcement consists of 4 #6 reinforcing bars and the bottom reinforcement consists of 3 #5 bars. Following the notation in Ma's work, the beams are referred to as specimens R-3 and R-4. Details on specimen geometry and reinforcement layout are given in Figs. 2.4 and 2.7 of Ma's work. The selection of these two specimens was
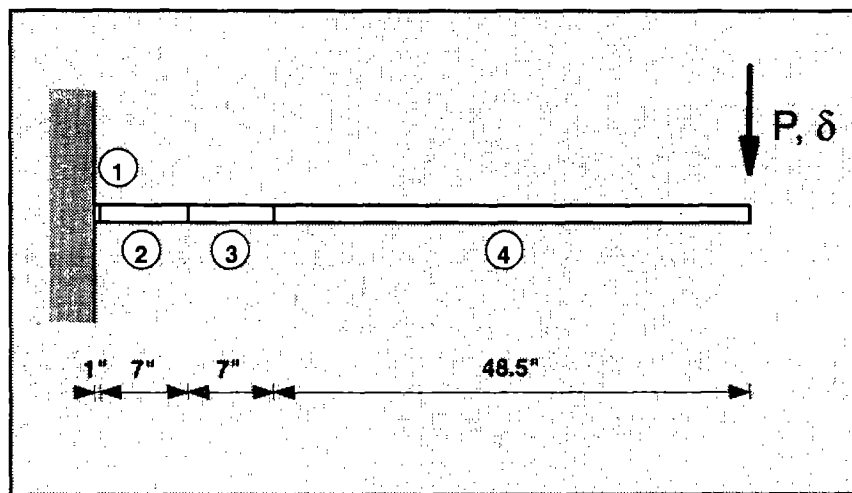
FIGURE 6.2   FINITE ELEMENT MESH FOR CANTILEVER SPECIMENS R-3 AND R-4

conditioned by the fact that their behavior was dominated by flexure and the effect of shear was rather small, because of the span to depth ratio. The finite element model for both beams is shown in Fig. 6.2. The cantilever beam is divided into 4 elements. The selection was conditioned by the fact that curvature measurements were undertaken in the tests over two segments of 7 in. length each, starting at a distance of 1 in. from the built-in end (Fig. 6.2). In addition, the first short element of 1 in. length permits a better monitoring of the hysteretic behavior near the built-in end. The numerical simulations were performed under displacement control by adding a very stiff spring at the free end of the cantilever and imposing forces of such magnitude as to induce the desired displacement value in the spring.

6.3.1   Specimen R-4

Beam R-4 was cycled between fixed symmetric tip displacement amplitudes, as shown in Fig. 6.3. In Fig 6.4 the experimental response of the beam is illustrated. Fig. 6.4a shows the measured load-tip displacement relation and Fig. 6.4b shows the measured bending moment-average curvature relation over the 7 in. segment nearest to the built-in end of the beam (element 2 in the finite element model of Fig. 6.2). These diagrams clearly reflect the presence of non-symmetric longitudinal reinforcement in the unequal moment strengths under positive and negative moments and the characteristic "pinching" of the hysteretic relation. Under the large end displacement, failure was reached after only one and a half cycles, and was initiated by inelastic buckling of the bottom reinforcing bars.
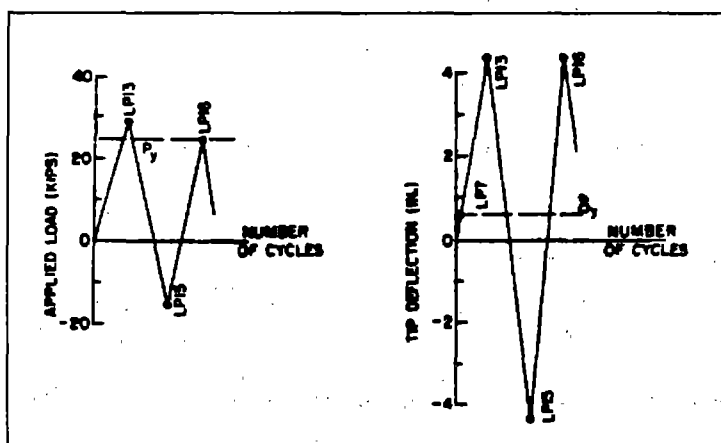
FIGURE 6.3   LOADING AND TIP DISPLACEMENT HISTORY
FOR SPECIMEN R-4 (FROM MA ET AL. 1976).

Because of the greater moment carrying capacity in the downward direction, the

concrete and reinforcing bars in the bottom of the beam were subjected to larger compressive forces than those at the top of the section. This resulted in the buckling of the bottom steel as evidenced by the difference in resisting force between points 13 and 16 in Fig. 6.4.

A) APPLIED LOAD-TIP DISPLACEMENT DIAGRAM

B) APPLIED LOAD-AVERAGE CURVATURE DIAGRAM IN ELEMENT 2
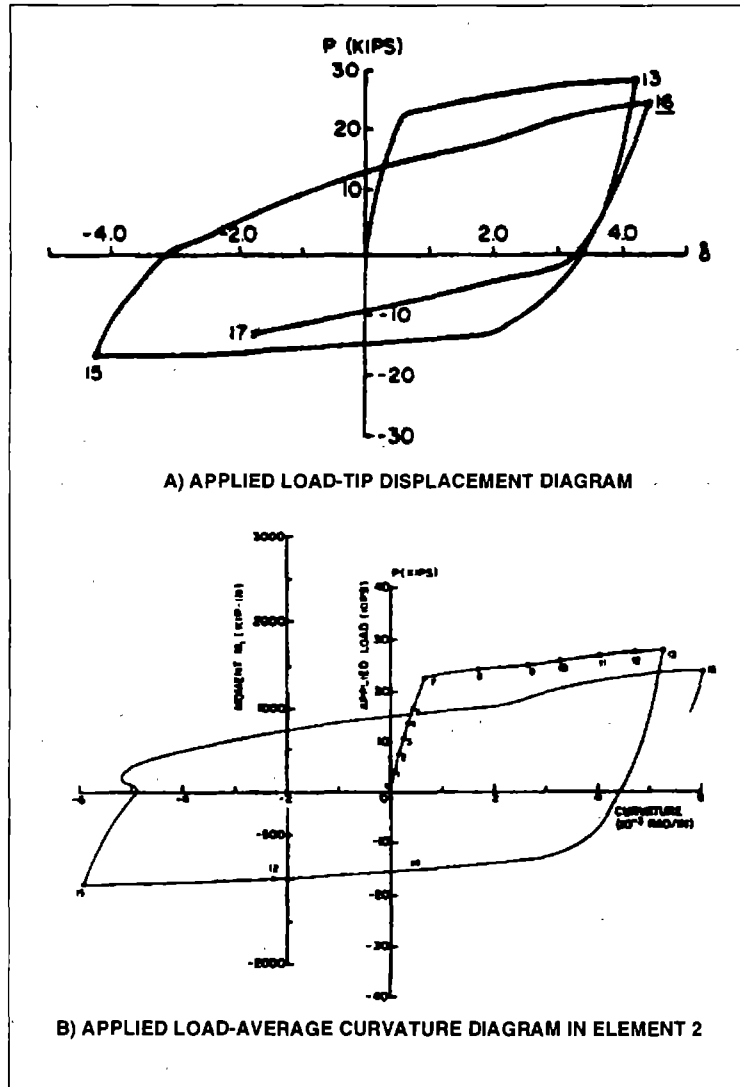
FIGURE 6.4   EXPERIMENTAL RESPONSE OF SPECIMEN R-4 (FROM MA ET AL. 1976):
            A) MEASURED LOAD-TIP DISPLACEMENT RELATION
            B) MEASURED LOAD- AVERAGE CURVATURE OVER 7 IN SEGMENT

"Pinching" was also observed during the downward reloading phase (from point 15 to 16), whereas little or no pinching was observed in the upward loading phase (point 13 to 14). In the upward loading phase cracks in the top part of the section do not close because the top steel can carry all the compressive force necessary to equilibrate the tensile force in the bottom reinforcement of the beam. In the following downward loading phase, the situation is

reversed, with the exception that the bottom steel in compression cannot equilibrate alone the tension in the top reinforcing steel. Consequently, the bottom reinforcement slips, until the crack closes and concrete starts contributing in compression. The response curve of Fig. 6.4 also indicates a clear loss of stiffness between the first and second loading cycle.
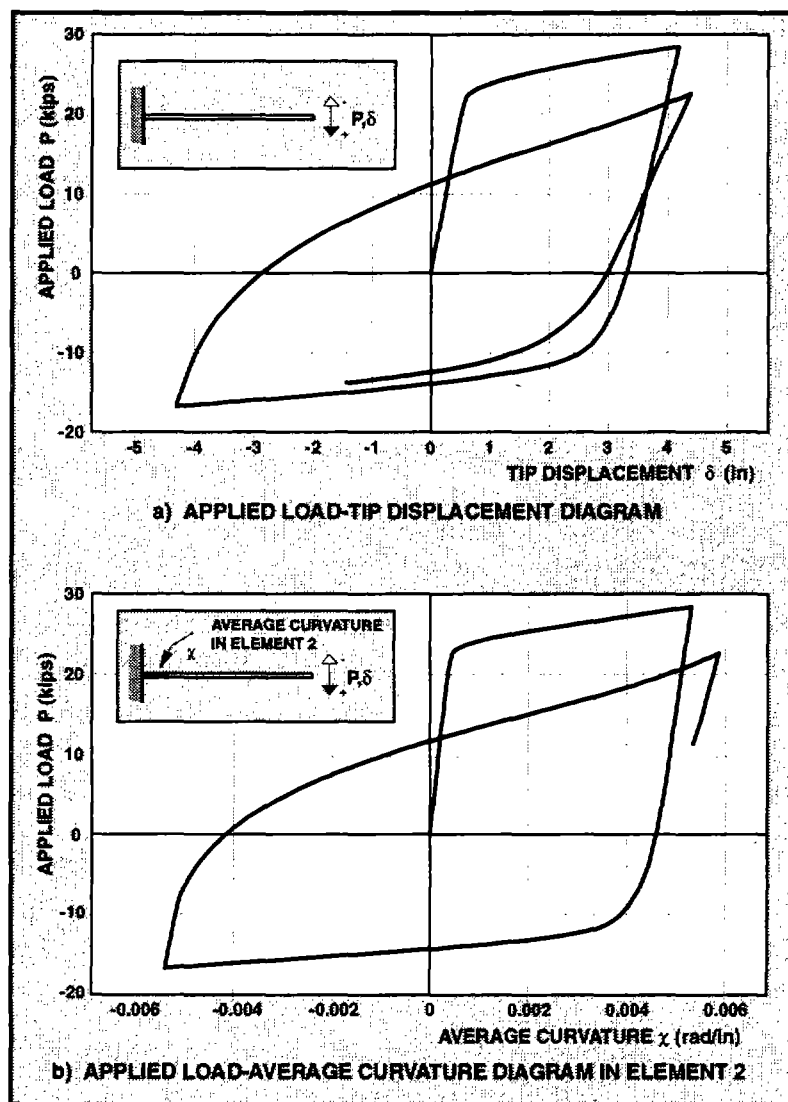
FIGURE 6.5   ANALYTICAL RESPONSE OF SPECIMEN R-4:
A) APPLIED LOAD-TIP DISPLACEMENT RELATION
B) APPLIED LOAD- AVERAGE CURVATURE IN ELEMENT 2

The selection of parameters of the proposed hysteretic section model was guided by these observations. The analytical results are shown in Fig. 6.5. As in Fig. 6.4, the plots represent the analytical load-tip displacement relation in Fig. 6.5a and the load-average curvature relation for element 2 in Fig. 6.5b. The analysis was performed with a degradation

parameter for the initial stiffness only ($d_1^{EI_0} = 0.08$ with $b_1 = 0$, $b_2 \cong 0$ and $b_3 = 1$). The numerical results agree closely with the experimental data. To simulate the "pinching" effect in the downward (positive) direction a pinching strength equal to about two thirds of the yield moment was specified in the model.

The buckling of the bottom reinforcing bars and the corresponding loss of moment strength between the first and second load cycle is simulated in the model by a very late return from pinching ($c_2 = 1.5$), which is a purely numerical solution. A more rational way of simulating this effect is the specification of a degradation parameter for yield strength. Since the model is presently limited to a single degradation parameter for, both, positive and negative yield strength, such a solution does not yield accurate results with the present model for cases involving a much higher degradation of yield strength in one loading direction, as happens for specimen R-4, which shows much higher degradation of yield strength in the positive than in the negative loading direction. The experimental results in Fig. 6.4 also show that a loss of moment strength takes place in the last unloading cycle from point 16 to point 17. This strength loss is not represented in the analytical results in Fig. 6.5a, because of the absence of a degradation parameter for yield strength in the constitutive relation of the beam section. The agreement between the experimental and the analytical moment-average curvature relation is very good in Figs. 6.4b and 6.5b. No experimental measurements are available for the moment-average curvature relation after the end of the first cycle when unloading starts at point 16 in Fig. 6.4b.

6.3.2 Specimen R-3

Specimen R-3 has the same geometry and reinforcement layout as specimen R-4, but was subjected to a different load history, as shown in Fig. 6.6. After a few cycles at very low deformation levels, the beam was subjected to cycles of gradually increasing tip displacement reversals that correspond to nearly equal forces in the positive and negative loading direction.

The experimental response of the beam is shown in Fig. 6.7, which depicts the measured load-tip displacement relation. The first few low deformation cycles did not affect the subsequent behavior of the specimen and are not included in the figure for the sake of clarity. Repeated load cycles under increasing tip displacement induced early spalling of concrete on the bottom side of the beam. Spalling of concrete and the kinking of the bottom bars by dowel action led to the final failure of the specimen by inelastic buckling of the bottom reinforcing bars. The buckling of the bottom bars was precipitated by the progressive

damage of the concrete cover under the large inelastic deformation reversals. A comparison of the experimental results for specimens R-3 and R-4 reveals that the specimen with several load cycles of increasing amplitude attained lower displacement ductility at failure.
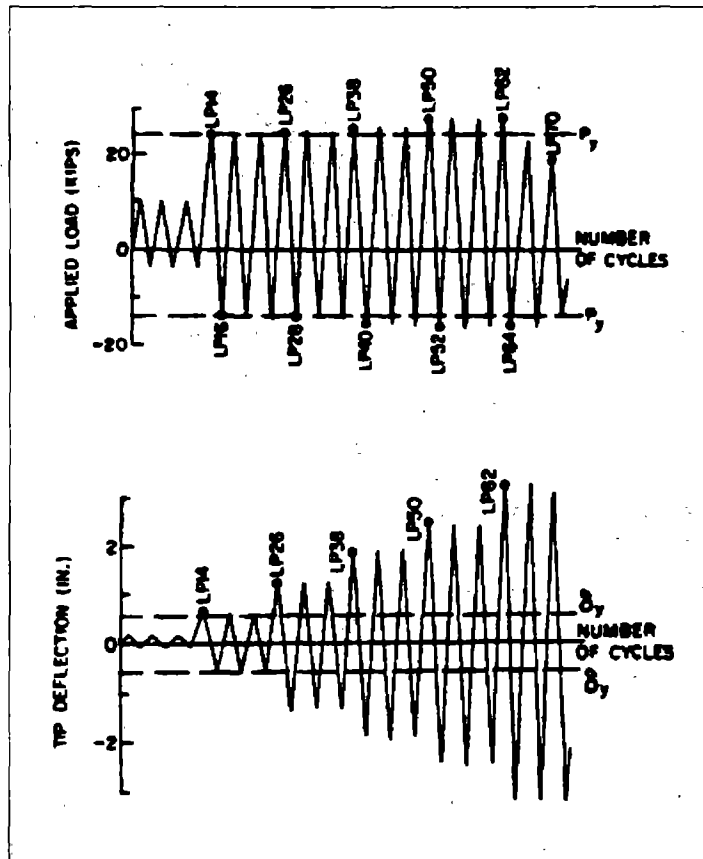
FIGURE 6.6   LOADING AND TIP DISPLACEMENT HISTORY
FOR SPECIMEN R-3 (FROM MA ET AL. 1976)

After the yield strength of the specimen was reached, gradual stiffness degradation and "pinching" of the hysteretic behavior are evident in the positive loading direction in Fig. 6.7. Similar to the behavior of specimen R-4, under imposed tip displacement in the downward direction, the previously opened bottom cracks need to close for the development of a compressive force sufficient to balance the tensile force developed by the top reinforcing bars. The cracks do not close in the negative (upward) loading direction, because the compression force in the top bars suffices to balance the tensile force in the bottom reinforcing steel. During this loading stage the moment resistance of the beam is provided by a pair of equal and opposite forces in the reinforcing steel with no participation of concrete. No notable degradation of yield strength takes place until the very last cycle, when the bottom

reinforcing bars buckled.
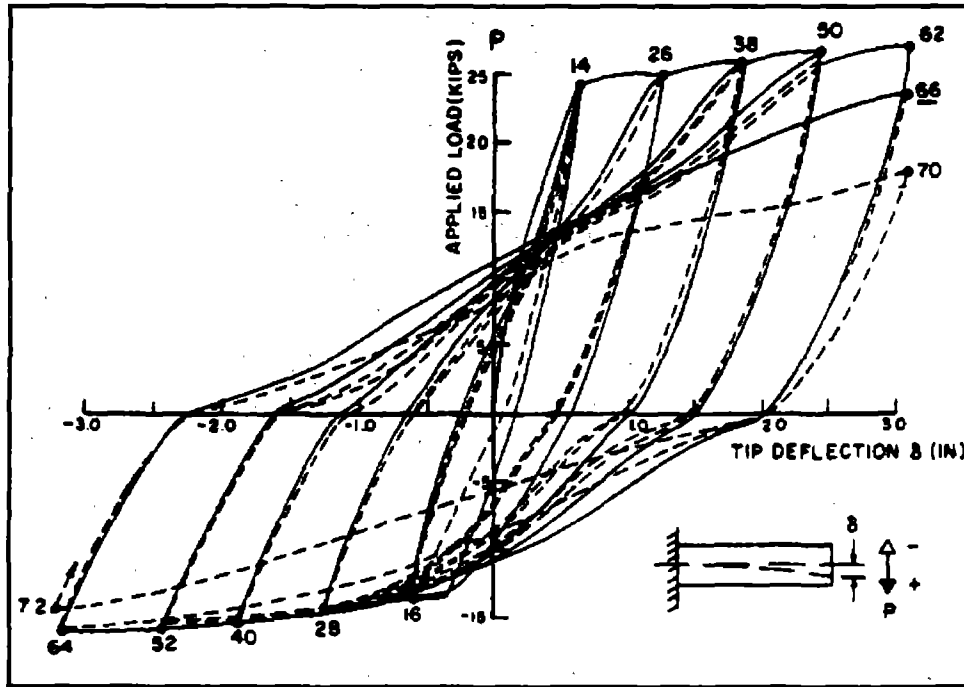
FIGURE 6.7   EXPERIMENTAL RESPONSE OF SPECIMEN R-3 (FROM MA ET AL. 1976):
                MEASURED LOAD-TIP DISPLACEMENT RELATION
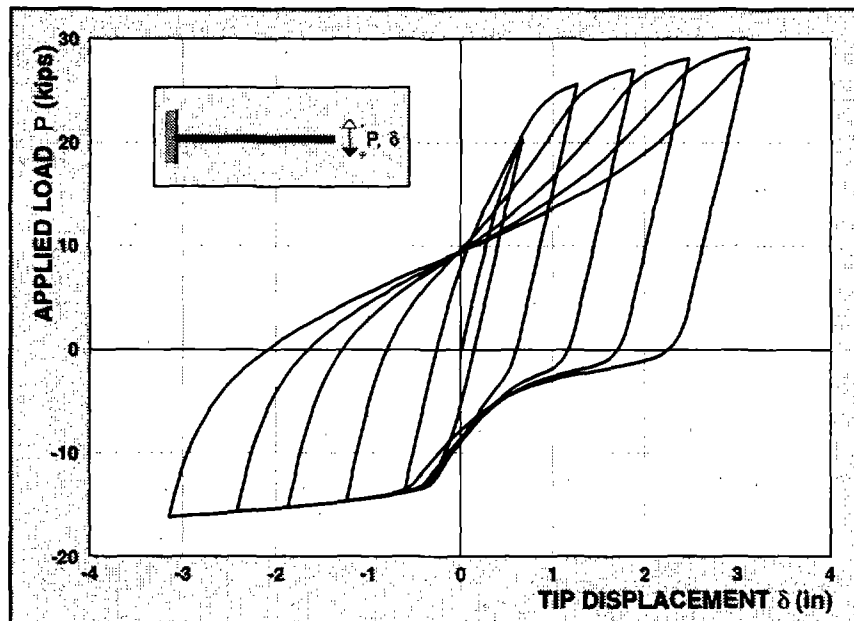
FIGURE 6.8   ANALYTICAL RESPONSE OF SPECIMEN R-3:
                LOAD-TIP DISPLACEMENT RELATION

The analytical results of the finite element model in Fig. 6.2 are shown in Fig. 6.8. The agreement with the experimental results is good, especially, if the energy dissipation per cycle is compared. The first cycle shows some discrepancies between analysis and experiment, because the effect of the first few cycles was not included in the analysis and the difficulty of establishing the right initial conditions for the model. All subsequent analytical cycles show good agreement with the experimental results. The analysis was performed with a degradation parameter for the initial stiffness only ($d_1^{EI_0} = 0.005$, with general parameters $b_1 = 1$, $b_2 = 0.001$ and $b_3 = 0.5$). A "pinching" strength under positive loading equal to approximately half the yield strength of the section was specified in the model accompanied by a late return to the plastic plateau ($c_2 = 1$). A "pinching" strength was also specified in the negative loading direction. However, the agreement is not as good in this case and numerical convergence problems arose when attempting to smooth out the transition to the "pinching" range.

The stiffness reduction of the model during unloading is not as pronounced as in the experimental results. While the model exhibits a practically straight unloading branch, the specimen displays a gradual loss of stiffness during unloading. This can be attributed to the following factors: (a) even though the model accounts for stiffness loss between cycles, it cannot accommodate graduate stiffness reduction during the unloading phase; thus, the unloading branch of the model is straight until reaching the "pinching" or yield strength; (b) the use of the same degradation parameter under, both, positive and negative loading fails to account for the different behavior of a reinforced concrete beam with unequal amounts of top and bottom reinforcement. Future improvements of the model need to address the effect of non-symmetric damage of parameters, or, else, a more refined section representation should be sought. For instance, the subdivision of the cross section into fibers with different material characteristics, constitutes a more suitable model for this case.

The failure of the specimen took place, when the bottom reinforcing bars buckled in compression at load point 66 in Fig. 6.7. While this phenomenon was captured in the analysis of specimen R-4 with the numerical device of a late return from pinching, such a solution is not possible in the analysis of specimen R-3, because of the large number of load reversals that will be impacted by this selection. This shows that alternative means for simulating failure in the model need to be sought in the future.

6.4   Remarks on Model Performance

The applications of the model and the comparisons of analytical with experimental results demonstrate the ability of the proposed beam element to describe several complexities of the hysteretic behavior of structural members, such as softening, "pinching", and stiffness degradation. While the simulation of the softening behavior of structural members is a direct result of the adopted constitutive law and the ability of the flexibility-based model to trace this behavior, the effect of "pinching" of the hysteretic behavior and of the damage degradation of key parameters is a feature of the proposed incremental constitutive relation.

The main difficulty in the use of the model consists in the selection of parameters. As Table 1 at the end of chapter 5 shows, the proposed constitutive relation depends on many parameters. Since some of these do not bear a direct relation to physical properties of the structural member, it is possible to arrive at physically unreasonable hysteretic behavior by injudicious selection. In addition, the proposed model is presently limited to the same degradation variable for a material parameter under positive and negative loading. This limitation is evident in the hysteretic behavior of non-symmetric sections, as is the case for specimens R-3 and R-4 in the correlation studies of this chapter. While the introduction of an additional degradation variable for each material parameter appears as the logical solution, it results in considerable increase of the number of model parameters.

The parameter selection not only affects the accuracy of the hysteretic constitutive relation of the section, but has an impact on the numerical convergence characteristics of the proposed element, as well. In the three examples of this chapter, convergence was always achieved very rapidly at each load step never requiring more than three iterations. The selection of the load step size was, therefore, governed by the desire to obtain a smooth load-displacement relation for the presentation of the results. Experience with the hysteretic model shows that failure to converge within a load step is almost always the result of aberrant behavior of the incremental constitutive law due to poor choice of degradation parameters: a high degradation value of one or more of the material parameters can result in a hysteretic behavior that is very difficult to trace numerically. The likelihood of this aberrant behavior increases with the number of load cycles, because of the monotonically increasing value of energy dissipation, which affects the degradation parameter. It is, thus, imperative that the degradation parameters be selected very carefully by calibration against a large set of experimental results from similar specimens, so as to ensure that numerical failure of the model corresponds to actual failure of the specimen. Since actual failure of the specimen

often depends on several factors, the calibration process is arduous and riddled with difficulties due to some fundamental limitations of the model. An extensive parameter study is, therefore, necessary, before the proposed hysteretic model can be used in large scale simulations of the seismic response of structures.

The difficulty in the selection of model parameters is alleviated by formal system identification methods, such as that proposed by Ciampi and Carlesimo (1986). Unfortunately, formal identification methods do not preclude the occurrence of physically unreasonable hysteretic behavior, so that the user needs to monitor the performance of the element during the analysis. At this stage of model complexity it appears reasonable to seek alternative descriptions of the hysteretic behavior of the section, such as the fiber section model proposed by Taucer et al. (1991).

CHAPTER 7

CONCLUSIONS

The objective of this study is to develop a reliable and computationally efficient beam finite element for the analysis of structural members under cyclic loading conditions that induce inelastic behavior in flexure. The nonlinear behavior of the element derives entirely form the uniaxial constitutive relation that governs the behavior of sections at integration points and of end rotational springs. The axial response of the element is assumed to remain linear elastic and completely independent of the response in flexure. Coupling between bending in two orthogonal directions and shear effects is also neglected. The nonlinear constitutive relation is incremental in nature and includes the effect of progressive damage on the hysteretic behavior. It is derived from a differential constitutive equation that arises from a simple unidimensional mechanical model formulated according to the endochronic theory. The numerical solution of the differential equation yields an incremental relation that can be readily accounted for with the proposed element state determination algorithm.

The element formulation is flexibility-based and, thus, relies on the assumption of force interpolation functions along the element. While the final element equations can be arrived at with either the force method or the two-field mixed method, the mixed method is more general and points the way to the consistent numerical implementation of the element state determination.

The element state determination for the determination of the element resisting forces and stiffness matrix that correspond to given nodal displacements consists of an iterative algorithm based on residual deformations. The proposed nonlinear algorithm for the element state determination is general and can be used with any nonlinear constitutive relation. The procedure involves an element iteration scheme that converges to a state that satisfies the material constitutive relations within the specified tolerance. During the iterations the equilibrium of the element is always satisfied in a strict sense. The proposed method proved computationally stable and robust, and able to describe the complex hysteretic behavior of structural members accounting for effects such as strain hardening, "pinching" and softening.

In comparison with other beam elements proposed to date, this flexibility-based model offers some major advantages:

- with the use of the exact force interpolation function along the element, fewer elements are needed in the discretization of the structure;

- the effect of distributed loads on the hysteretic behavior of the element can be accounted for in a rational way by appropriate modification of the force interpolation functions;

- the model can trace softening material response, strength loss and local failure without numerical difficulties;

- the proposed incremental constitutive relation is very flexible and can be calibrated to represent a very broad range of hysteretic behavior by appropriate modification of parameters and corresponding damage indices;

- the element formulation is general and can be applied to any nonlinear constitutive relation, both, purely nonlinear or piecewise linear. It is independent of the global iteration strategy used for the solution of the equilibrium equations of the entire structure.

The element belongs to the family of flexibility based elements, but distinguishes itself by the general and clearly formulated state determination process that does not resort to ad hoc approximations and special solution strategies to avoid numerical difficulties. The generality of the model is already validated in the formulation of a beam-column element with fiber discretization of the cross sections by Taucer et al. (1991), who also demonstrate the implementation of distributed element loads.

Comparisons between the results of the proposed model and experimental data show good correlation. Since the shear deformations are not included in the proposed beam element, the selection of specimens for testing the validity of the model is limited to cases with negligible contribution of shear deformations to the overall response. The correlation studies are also limited to specimens with low axial force, because the model presently assumes that the axial and flexural behavior are uncoupled and that the response to axial forces is linear elastic. The proposed element is, therefore, suitable for the representation of the nonlinear hysteretic behavior of girders and columns under low axial loads. The degradation of the mechanical properties of the constitutive relation is a significant feature of the model. The degradation of the material parameters is based on a damage function that

depends on the weighted sum of normalized plastic energy dissipation and deformation ductility.

The model offers several opportunities for future studies:

- The constitutive law could be extended to include coupling between bending in two orthogonal directions, axial behavior and, eventually, torsion. Similar constitutive laws are available in the literature, but have not been implemented in the formulation of a nonlinear beam element with distributed nonlinearity.

- The constitutive law should be refined to eliminate the physical inconsistencies in Appendix B, namely the violation of Ilyushin's and Drucker's postulates. Similar improvements of the original endochronic theory in the literature show that it is possible to, at least partially, overcome these inconsistencies. It is, however, important to point out that these violations of theory of plasticity postulates do not affect the numerical stability of the constitutive law, or of the beam element state determination.

- It is imperative to carefully select the parameters and damage indices of the proposed endochronic law. In this respect, a formal parameter identification method is an ideal tool. The model can describe a wide range of hysteretic behaviors, but some parameters do not bear a direct relation to physical properties of the structural member. Injudicious choice of parameters can, thus, result in physically unreasonable hysteretic behavior.

- It is important that the degradation parameters of the model be selected by calibration against a large set of experimental results from similar specimens, so as to ensure that numerical failure of the model corresponds to physical failure of the specimen. An extensive parameter study is necessary before the proposed hysteretic model can used in large scale simulation of the seismic response of structures.

- The proposed nonlinear solution algorithm has a wide range of application. Its implementation in elements with different nonlinear constitutive relations should be explored. Similarly, the extension of the algorithm to complex mechanical systems formed by several elements connected in series and/or in parallel should be studied.

- Second order effects should be included in the element.

- The proposed degradation scheme in the nonlinear constitutive relation should be studied in more detail. The damage function should be extended to depend on the plastic energy dissipation of some region of the element, rather than a single section.

The section response of distributed nonlinearity models is known to be sensitive to the number of monitored sections, and localization problems arise under strength softening of a section. This nonlocal extension of the proposed damage model would ensure the independence of the results from the discretization of the member (objectivity).

- The characteristics of the proposed model make it particularly attractive for the probabilistic seismic damage analysis of structures. The proposed endochronic constitutive relation bears great similarities with the Bouc-Wen model, which is extensively used in the random vibration analysis of nonlinear structures. Since the Bouc-Wen model is only used at the global level as a force-displacement relation, while the proposed model addresses the hysteretic response of invididual sections, the latter can be of great use in the identification of damage concentration and the more rational definition of damage indices for members and structures.

REFERENCES

Banon, H. And Veneziano, D. (1982) "Seismic Safety of Reinforced Concrete Members and Structures." *Earthquake Engineering and Structural Dynamics*, Vol. 10, pp. 179-193.

Brancaleoni, F., Ciampi, V. and Di Antonio, R. (1983). "Rate-Type Models for Non Linear Hysteretic Structural Behavior." *EUROMECH Colloquium*, Palermo, Italy.

Carlesimo, L. (1983). "Comportamento Sismico di Telai in Acciaio in Campo Non Lineare." *Tesi di Laurea (B.S. Thesis)*, Facoltà di Ingegneria, Università degli Studi "La Sapienza", Rome (in Italian).

Casciyati (1987). "Nonlinear Stochastic Dynamics in Large Structural Systems by Equivalent Linearization." *5th International Conference on Application of Statistics and Probability in Soil and Structural Engineering*, University of British Columbia, Vancouver, Canada.

Ciampi, V. and Carlesimo, L. (1986). "A Nonlinear Beam element for Seismic Analysis of Structures." *8th European Conference on Earthquake Engineering*, Lisbon.

Ciampi, V. and Nicoletti, M. (1986). "Parameter Identification for Cyclic Constitutive Models with Stiffness and Strength Degradation." *8th European Conference on Earthquake Engineering*, Lisbon.

Dahlquist, G. and Björck, Å. (1974). *Numerical Methods*. Prentice-Hall, New Jersey.

Kaba, S. and Mahin, S.A. (1984). "Refined Modeling of Reinforced Concrete Columns for Seismic Analysis." *EERC Report 84/03*, Earthquake Engineering Research Center, University of California, Berkeley.

Krawinkler, H. and Zohrei, M. (1983). "Cumulative Damage in Steel Structures Subjected to Earthquake Ground Motions." *Computers and Structures*, Vol. 16, No. 1-4, pp. 531-541.

Krawinkler, H. (1987). "Performance Assessment of Steel Components." *Earthquake Spectra*, Vol. 3, No. 1, pp. 27-41.

Kunnath, S.K. and Reinhorn, A.M. (1990). "Model for Inelastic Biaxial Bending Interaction of Reinforced Concrete Beam-Columns." *ACI Structural Journal*, Vol. 87, No. 3, pp. 284-291.

Kwak, H.G. and Filippou, F.C. (1990). "Finite Element Analysis of Reinforced Concrete Structures under Monotonic Loads." *SEMM Report 90-14*, Department of Civil Engineering, University of California, Berkeley.

Lemaitre, J. (1992). *A Course on Damage Mechanics*. Springer Verlag, New York, 1992.

Ma, S.Y., Bertero, V.V. and Popov, E.P. (1976). "Experimental and Analytical Studies on the Hysteretic Behavior of Reinforced Concrete Rectangular and T-Beams." *EERC Report 76/02*, Earthquake Engineering Research Center, University of California, Berkeley.

Mahasuverachai, M., and Powell, G.H. (1982). "Inelastic Analysis of Piping and Tubular Structures." *EERC Report 82/27*, Earthquake Engineering Research Center, University of California, Berkeley.

Mahin, S. and Bertero. V.V. (1981). "An Evaluation of Inelastic Seismic Design Spectra." *Journal of Structural Engineering*, ASCE, 107(ST9), pp. 1777-1795.

Mazars, J. and Pijaudier-Cabot, G. "Continuum Damage Theory, Application to Concrete.", *Journal of Engineering Mechanics*, ASCE, 115, pp. 345-365.

Mondkar, D.P. and Powell, G.H. (1975a). "ANSR 1 Static and Dynamic Analysis of Nonlinear Structures." *EERC Report 75/10*, Earthquake Engineering Research Center, University of California, Berkeley.

Mondkar, D.P. and Powell, G.H. (1975b). "ANSR 1 General Purpose Program for Analysis of Nonlinear Structural Response." *EERC Report 75/37*, Earthquake Engineering Research Center, University of California, Berkeley.

Ozdemir, H. (1981). "Nonlinear Transient Dynamic Analysis of Yielding Structures." *Ph. D. Thesis*, Department of Civil Engineering, University of California, Berkeley.

Park, Y.J. and Ang, A.H.-S. (1985). "Mechanistic Seismic Damage Model for Reinforced Concrete." *Journal of Structural Engineering*, ASCE, 111(ST4), pp. 722-739.

Park, Y.J., Wen, Y.K. and Ang, A.H-S. (1986). "Random Vibration of Hysteretic Systems Under Bi-Directional Ground Motions." *Earthquake Engineering and Structural Dynamics*, Vol. 14, pp. 543-557.

Paronesso, A. (1986). "Un Elemento Finito di Trave a Plasticizzazione Diffusa con Legame Plastico Non Classico." *Tesi di Laurea (B.S. Thesis)*, Facoltà di Ingegneria, Università degli Studi "La Sapienza", Rome (in Italian).

Pian, T.H.H. (1964). "Derivation of Element Stiffness Matrices by Assumed Stress Distributions." *AIAA Journal*, 2, pp. 1333-1336.

Roufaiel, M.S.L. and Meyer, C. (1987). "Analytical Modeling of Hysteretic Behavior of R/C Frames." *Journal of Structural Engineering*, ASCE, 113(ST3), pp. 429-444.

Spilker, R.L. and Pian, T.H.H. (1979). "Hybrid-Stress Models for Elastic-Plastic Analysis by the Initial-Stress Approach." *International Journal for Numerical Methods in Engineering*, Vol. 14, pp. 359-378.

Stroud, A. H. and Secrest, D. (1966). *Gaussian Quadrature Formulas*, Prentice Hall, New Jersey.

Tabarrok, B. and Assamoi, L. (1987). "A New Variational Principle in Elastodynamics." *Computer Methods in Applied Mechanics and Engineering*, Vol. 61, pp. 303-321.

Taucer, F.F., Spacone, E. and Filippou, F.C. (1991). "A Fiber Beam-Column Element for Seismic Analysis of Reinforced Concrete Structures." *EERC Report 91/17*, Earthquake Engineering Research Center, University of California, Berkeley.

Valanis, K.C. (1971). "A Theory of Viscoplasticity Without a Yield Surface, Part I. General Theory." *Archives of Mechanics*, Vol. 23, No. 4, pp. 517-533.

Valanis, K.C. (1980). "Fundamental Consequences of a New Intrinsic Time Measure: Plasticity as a Limit of the Endochronic Theory." *Archives of Mechanics*, Vol. 32, No. 2, pp. 171-191.

Valanis, K.C. (1981). "On The Substance of Rivlin's Remarks on the Endochronic Theory." *International Journal for Numerical Methods in Engineering*, Vol. 17, pp. 249-265.

Valanis, K.C., and Lee, C.F. (1984). "Endochronic Theory of Cyclic Plasticity with Applications." *Journal of Applied Mechanics*, Vol. 51, pp. 367-374.

Wen, Y.K. (1980). "Equivalent Linerarization for Hysteretic Systems Under Random Excitation." *Journal of Applied Mechanics*, ASME, Vol. 47. No. 1, pp. 150-154.

Wen, Y.K. (1986). "Stochastic Response and Damage Analysis of Inelastic Structures." *Probabilistic Engineering Mechanics*, Vol. 1, No. 1, pp. 49-57.

Zeris, C.A. (1986). "Three Dimensional Nonlinear Response of Reinforced Concrete Buildings." *Ph. D. Thesis*, University of California, Department of Civil Engineering, Berkeley.

Zeris, C.A. and Mahin, S.A. (1988). "Analysis of Reinforced Concrete Beam-Columns under Uniaxial Excitation." *Journal of Structural Engineering*, ASCE, 114(ST4), pp. 804-820.

Zeris, C.A. and Mahin, S.A. (1991). "Behavior of Reinforced Concrete Structures Subjected to Biaxial Excitation." *Journal of Structural Engineering*, ASCE, 117(ST9), pp. 2657-2673.

Zienkiewicz, O.C. and Taylor, R.L. (1989). *The Finite Element Method*. Volume 1. Basic Formulation and Linear Problems. Fourth Edition. McGraw Hill, London.

Zienkiewicz, O.C. and Taylor, R.L. (1991). *The Finite Element Method*. Volume 2. Solid and Fluid Mechanics, Dynamics and Non-Linearity. Fourth Edition. McGraw Hill, London.

APPENDIX A

STATE DETERMINATION SUMMARY

A.1 Element State Determination

A step-by-step summary of the state determination algorithm in Chapter 2 is presented below. The summary focuses on a single Newton-Raphson iteration i at the structural degrees of freedom, because the innovative aspect of the present study is the process of element state determination. The remainder of the nonlinear solution algorithm follows well established methods, such as the Newton-Raphson method selected in this study. Alternative solution strategies can be implemented without additional effort, since these are independent of the element state determination. The relation of the Newton-Raphson iteration to the nonlinear solution of the entire structure is illustrated at the top of Figure 2.5, which also shows the relation between the overall solution strategy and the element state determination process with corresponding states denoted by uppercase Roman letters. Figure 2.6 shows in detail the evolution of the state determination process for an element and corresponds to steps **(2)** through **(13)** in the following summary. The flow chart of computations for the entire solution algorithm is shown in Figure A.1, while the flow chart of computations for the element state determination is shown in Figure A.2.

The i-th Newton-Raphson iteration is organized as follows:

(1) *Solve the global system of equations and update the structural displacements.*

At the i-th Newton-Raphson iteration the structure stiffness matrix $\mathbf{K}_s^{i-1}$ at the end of the previous iteration i-1 is used to compute the displacement increments $\Delta\mathbf{p}^i$ for the given load increments $\Delta\mathbf{P}_E^i$ which represent the unbalanced forces from the previous iteration.

$$\mathbf{K}_s^{i-1}\, \Delta\mathbf{p}^i = \Delta\mathbf{P}_E^i$$
$$\mathbf{p}^i = \mathbf{p}^{i-1} + \Delta\mathbf{p}^i$$

(2)   *Calculate the element deformation increments and update the element deformations.*

The element deformation increments Δq^i are determined using matrix L_{ele}, which relates element displacements in the global reference system to element deformations in the local reference system and is defined in Eq. (2.13).

$$\Delta q^i = L_{ele} \, \Delta p^i$$

$$q^i = q^{i-1} + \Delta q^i$$

As discussed in Chapter 2, the new element deformations q^i do not change until the following $i+1$ Newton-Raphson iteration. The remaining operations of the nonlinear solution algorithm make up the element state determination process which establishes the element stiffness and resisting forces for the given element deformations q^i.

(3)   *Start the element state determination. Loop over all elements in the structure.*

The state determination of each element is performed in loop j. The index of the first iteration is $j=1$.

(4)   *Determine the element force increments.*

The element force increments ΔQ^j are determined with the element stiffness matrix K^{j-1} at the end of the previous iteration in loop j

$$\Delta Q^j = K^{j-1} \, \Delta q^j$$

When $j=1$, $K^0 = K^{i-1}$ and $\Delta q^1 = \Delta q^i$ where i-1 corresponds to the state of the element at the end of the last Newton-Raphson iteration. When $j>1$ Δq^j is equal to the residual element deformations of the previous iteration, as determined in Step **(12)**.

(5)   *Update the element forces.*

$$Q^j = Q^{j-1} + \Delta Q^j$$

When $j=1$, $Q^0 = Q^{i-1}$.

(6)   *Determine the section force increments. Steps* **(6)** *through* **(10)** *are performed for all control sections (integration points) of the element.*

The section force increments $\Delta D^j(x)$ are determined from the force interpolation functions $b(x)$. Subsequently, the section forces $D(x)$ are updated.

$$\Delta D^j(x) = b(x) \, \Delta Q^j$$

$$D^j(x) = D^{j-1}(x) + \Delta D^j(x)$$

(7) *Determine the section deformation increments.*

The section deformation increments $\Delta d^i(x)$ are determined by adding the residual section deformations from the previous iteration $r^{j-1}(x)$ to the deformation increments caused by the section force increments $\Delta D^j(x)$. The latter are determined with the section flexibility matrix $f^{j-1}(x)$ at the end of the previous iteration in loop j.

$$\Delta d^j(x) = r^{j-1}(x) + f^{j-1}(x)\,\Delta D^j(x)$$

$$d^j(x) = d^{j-1}(x) + \Delta d^j(x)$$

When $j=1$, $r^0(x) = 0$.

(8) *Section state determination.*

This step may differ depending on the form of the section constitutive law. Assuming for simplicity that this law is explicitly known, from the section force-deformation relation the tangent stiffness matrix $k^j(x)$ and the section resisting forces $D_R^j(x)$ are updated for the new section deformations $d^j(x)$. This stiffness matrix $k^j(x)$ is then inverted to obtain the new tangent flexibility matrix $f^j(x)$ of the section.

$$f^j(x) = \left[k^j(x)\right]^{-1}$$

Two section force-deformation relations and the relevant section state determination procedures are given in Sections A.2.1 and A.2.2 for the beam elements presented in Chapters 3 and 4, respectively.

(9) *Determine the unbalanced forces at the section.*

The section unbalanced forces $D_U^j(x)$ are the difference between the applied forces $D^j(x)$ and the resisting forces $D_R^j(x)$.

$$D_U^j(x) = D^j(x) - D_R^j(x)$$

(10) *Determine the residual section deformations.*

The section unbalanced forces and the new section flexibility yield the residual section deformations $r^j(x)$

$$r^j(x) = f^j(x)\,D_U^j(x)$$

(11) *Determine the element flexibility and stiffness matrices.*

The element flexibility matrix F^j is formed by integration of the section flexibility matrices $f^j(x)$. This matrix is then inverted to obtain the element tangent stiffness

matrix K^j.

$$F^j = \int_0^L b^T(x)\, f^j(x)\, b(x)\, dx$$

$$K^j = \left[F^j\right]^{-1}$$

(12) *Check for element convergence.*

(a) If the convergence criterion is satisfied, the element is considered to have converged. After setting $Q^i = Q^j$ and $K^i = K^j$ the process continues with step **(13)**.

(b) If the convergence criterion is not satisfied, the residual element deformations s^j are determined by integration of the residual section deformations $r^j(x)$.

$$s^j = \int_0^L b^T(x)\, r^j(x)\, dx$$

At this point j is incremented to $j+1$ and a new iteration begins in loop j. In this case Δq^j at step **(4)** is replaced with Δq^{j+1} which is set equal to $-s^j$

$$\Delta q^{j+1} = -s^j$$

and steps **(4)** through **(12)** are repeated until convergence is achieved.

(13) *Add rigid body modes to element stiffness and resisting forces.*

Using matrix L_{ele} the element stiffness matrix K^i_{ele} and resisting force vector Q^i_{ele} in the global reference system with rigid body modes are computed from K^i and Q^i.

$$K^i_{ele} = L^T_{ele}\, K^i\, L_{ele}$$

$$Q^i_{ele} = L^T_{ele}\, Q^i$$

(14) *Determine the resisting forces and the new stiffness matrix of the entire structure.*

When all elements have converged, the i-th step of the Newton-Raphson iteration is complete. The element force vectors are assembled to form the updated structure resisting forces

$$P^i_R = \sum_{ele=1}^{n} Q^i_{ele}$$

where n is the total number of beam elements in the structure and the subscript *ele* is added as a summation index. The new structure stiffness matrix is formed by assembling the current element stiffness matrices

$$k = 1$$

assemble initial structure tangent stiffness matrix $\mathbf{K}_s$

$\Delta \mathbf{P}$ = initial load increment $\Delta \mathbf{P}^{k=1}$

$\Delta \mathbf{P}$ = next load increment $\Delta \mathbf{P}^k$

$$i = 1$$

$\Delta \mathbf{P}$ = unbalanced load $\mathbf{P}_U$

solve $\Delta \mathbf{P} = \mathbf{K}_s \, \Delta \mathbf{p}$

for ele = 1, number of elements

state determination of element ele

next ele

assemble new structure tangent stiffness matrix $\mathbf{K}_s$

assemble structure resisting force vector $\mathbf{P}_R$

compute unbalanced force vector $\mathbf{P}_U = \mathbf{P} - \mathbf{P}_R$

is $\|\mathbf{P}_U\|$ sufficiently small ?

no

next i

next k

yes

FIGURE A.1 FLOW CHART OF STRUCTURE STATE DETERMINATION
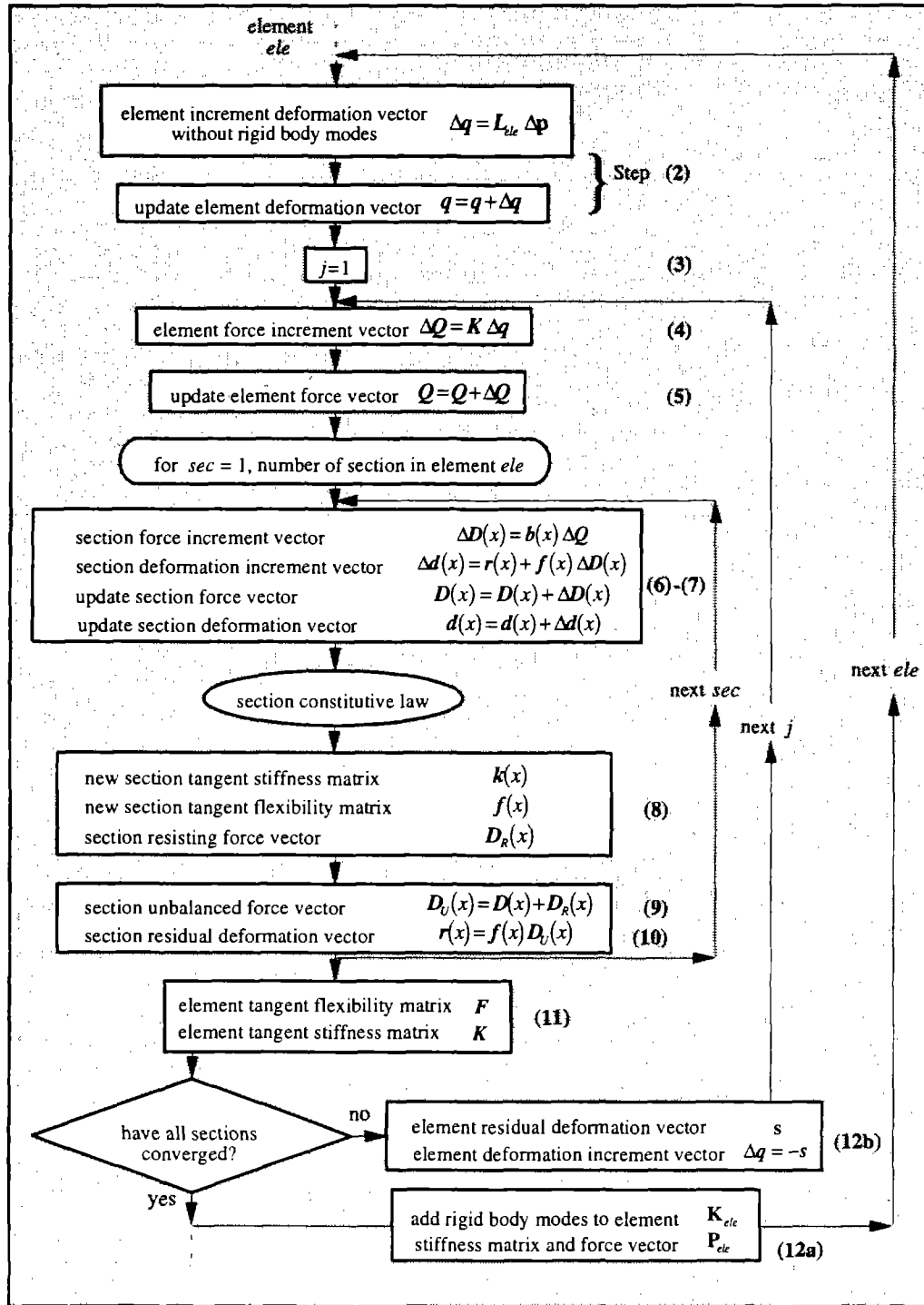
FIGURE A.2   FLOW CHART OF ELEMENT STATE DETERMINATION: THE SECTION
                       CONSTITUTIVE RELATION IS ASSUMED TO BE EXPLICITLY KNOWN

$$\mathbf{K}_s^i = \sum_{ele=1}^{n} \mathbf{K}_{ele}^i$$

The summation symbol in the two previous equations clearly indicate assembly of the element vectors and matrices in the corresponding vector and matrix of the entire structure. At this point the structure resisting forces $\mathbf{P}_R^i$ are compared with the total applied loads $\mathbf{P}_E^k$. If the difference $\Delta\mathbf{P}_U^i$, which is the structure unbalanced force vector, is not within the specified tolerance, i is incremented to $i+1$ and the next Newton-Raphson iteration begins. Steps (1) through (14) are repeated after replacing $\Delta\mathbf{P}_E^i$ with $\Delta\mathbf{P}_E^{i+1} = \Delta\mathbf{P}_U^i$ until convergence takes place at the structure degrees of freedom.

A graphical overview of the entire nonlinear analysis procedure is presented in Figure A.1 and Figure A.2. Figure A.1 provides an overview of the entire process with the nesting of the individual iteration loops and does not differ from conventional nonlinear analysis schemes. The new features of the algorithm are introduced in the element state determination phase, which is singled out for presentation in Figure A.2. Since all integrations along the element are performed numerically, an additional iteration loop over all control sections of the element is introduced in this diagram.

In the interest of clarity the above presentation of the nonlinear analysis procedure refers to an explicit section deformation relation. The following paragraphs describe the section state determination for the section force-deformation relations presented in Chapters 3 and 4.

A.2   State Determination for Section with Differential Constitutive Law

The section state determination of the beam in Chapter 4 mainly involves the determination of the section flexibility and residual deformations. The differential form of the constitutive law does not allow the direct computation of the section resisting forces. Consequently, the numerical integration of the differential equation results in an iterative algorithm for the determination of the flexibility and residual deformations of the section at each element iteration j. In this case the following steps replace steps (8) through (10) of the general element state determination algorithm in the previous section

(8a)   *Compute the error function and its derivatives.*

From the new section deformations $d^j(x)$ and the deformations $d^{i-1}(x)$ at the beginning of the element iterations the new error function ψ^j and its derivatives $(\partial\psi/\partial M)^j$, $(\partial\psi/\partial\chi)^j$ are computed.

(8b) Compute the section flexibility and residual deformations.

From the error function and its derivatives, the new section flexibility matrix and residual deformation vector are computed

$$f^j(x) = -\frac{\left(\dfrac{\partial\psi}{\partial M}\right)^j}{\left(\dfrac{\partial\psi}{\partial\chi}\right)^j}$$

$$r^j = -\frac{\psi^j}{\left(\dfrac{\partial\psi}{\partial\chi}\right)^j}$$

Proceed with step **(11)**

APPENDIX B

COMPARISON OF DIFFERENTIAL CONSTITUTIVE LAW
WITH BOUC-WEN MODEL

B.1   General

The incremental constitutive relation described in Chapter 4 can represent a range of hysteretic behaviors, very similar to the range of the well known Bouc-Wen model (BW model). The BW model is a hysteretic constitutive law that also belongs to the family of endochronic models and has been widely used in the field of nonlinear random vibrations of structures. This model has been thoroughly studied and a large bibliography is available. A detailed description of the model and its applications is presented by Wen (1980 and 1986).

A comparison between the two models is presented in this appendix. The comparison serves several purposes:

- even though the BW model has a wide range of application, it has not been used for the section constitutive relation of a beam element with distributed nonlinearity;

- the proposed beam element could be of significant use in the stochastic analysis of multiple-degree-of-freedom (MDOF) structural systems, much like the BW model has been used in the random vibration analysis of single-degree-of-freedom (SDOF) systems;

- recent studies have extended the original BW model to the biaxial bending case with coupling of the response in the two normal directions (Park et al. 1986, Kunnath and Reinhorn 1990). Similar extensions of the proposed model are also possible. In similar fashion, the model presented in Chapter 4 could be extended to include the coupling of flexural with axial response;

- both models suffer from the same limitations, stemming from the violation of theory of plasticity postulates. The widespread use of BW model and its numerical robustness testify that the numerical implementation of the models and the accuracy

of the results are not affected by this violation.

B.2   Comparison with Bouc-Wen Model

A brief review of the Bouc-Wen model is given based on the schematic illustration of Figure B.1. The model can be considered as the coupling of a linear and a nonlinear element in parallel. Using the notation commonly used in the literature about the BW model, $F_1 = \alpha k u$ is the force resisted by the linear element and $F_2 = (1-\alpha)kz$ is the force resisted by the nonlinear element. Thus, the total restoring force F is given by

$$F = \alpha k u + (1-\alpha)k z \tag{B.1}$$

where z is a displacement parameter that controls the response of the nonlinear element of Figure B.1 and is governed by the differential equation

$$\dot{z} = A\,\dot{u} - \beta\,|\dot{u}|\,|z|^{n-1}z - \gamma\,\dot{u}\,|z|^{n} \tag{B.2}$$
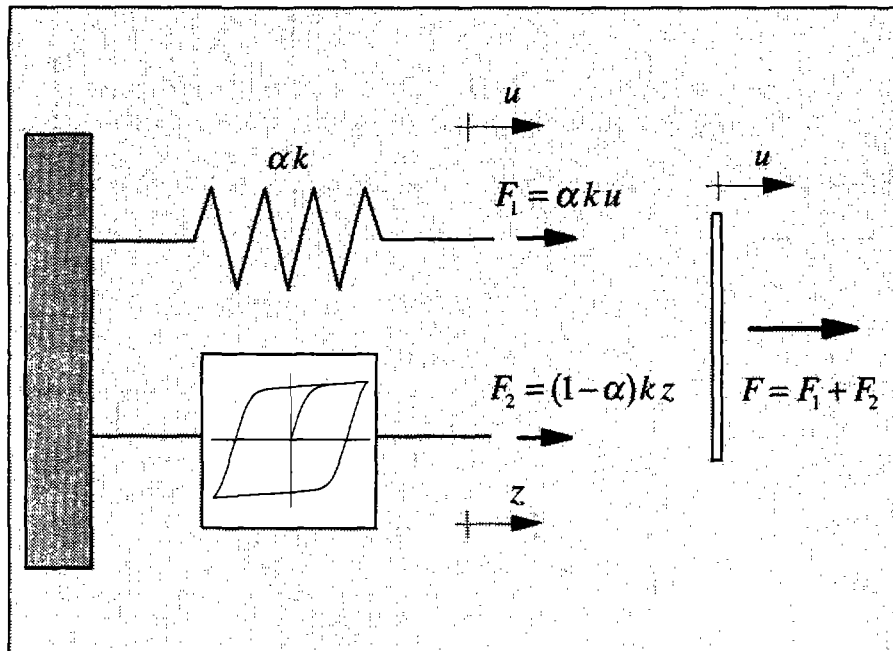
FIGURE B.1   BOUC-WEN MODEL

where A, β, γ and n are a set of parameters that control the hysteretic response of the nonlinear element. If Eq. (B.2) is divided by $\dot{u}$, it becomes

$$\frac{dz}{du} = A - \beta \frac{|\dot{u}|}{\dot{u}} |z|^{n-1} z - \gamma |z|^n \qquad (B.3)$$

The initial stiffness k_0 and the post-yield stiffness k_f are given by the following expressions

$$k_0 = \alpha k + (1-\alpha) k A \qquad (B.4)$$

$$k_f = \alpha k \qquad (B.5)$$

For $A=1$ the initial stiffness k_0 is equal to k. This is the assumption that is adopted in the following in order to facilitate the comparison between the two models. The sharpness of the transition from the linear to the nonlinear range is governed by parameter n. γ and β give different loading-unloading paths and no limits are imposed on the values that these two parameters can assume. To find the differential equation relating F with u, the total restoring force F in Eq. (B.1), is differentiated with respect to u

$$\frac{dF}{du} = \alpha k + (1-\alpha) k \frac{dz}{du} \qquad (B.6)$$

Using Eq. (B.1) and recalling that, for $A=1$, $k = k_0$, the rearrangement of terms results in the following expression for the derivative of the force in Eq. (B.6)

$$\frac{dF}{du} = k_0 \left\{ 1 - (1-\alpha) [sgn(du) \, sgn(z) \beta + \gamma] |z|^n \right\} \qquad (B.7)$$

Eq. (B.7) is the force-deformation differential equation that governs the BW model. It looks very similar to Eq. (4.15) that defines the model discussed in Chapter 4. To compare the two models the notation of Figure 4.1 is changed according to that of Figure B.1. The new notation is shown in Figure B.2. Recall that this change in notation is consistent with the observation that the proposed constitutive law of Figure 4.1 can be used for any force-deformation relation. Using Figure B.2, Eq. (4.15) can be written

$$\frac{dF}{du} = k_0 \left\{ 1 - (1-\alpha) [sgn(du) \, sgn(x) \beta + \gamma] |x|^n \right\} \qquad (B.8)$$

where

$$x = \frac{F}{F_0 (1-\alpha)} - \frac{u \alpha}{u_0 (1-\alpha)} \qquad (B.9)$$

$$k_0 = \frac{F_0}{u_0} \qquad (B.10)$$

F_0 and u_0 are defined exactly as M_0 and χ_0 are defined in Figure 4.2. The derivative of x with respect to u is

$$\frac{dx}{du} = \frac{1}{1-\alpha} \left[\frac{1}{F_0} \frac{dF}{du} - \frac{\alpha}{u_0} \right]$$

(B.11)

Eqs. (B.7) and (B.8) are substituted into Eq. (B.11) which after rearrangement of terms becomes

$$\frac{dx}{du} = \frac{1}{u_0} \left[1 - \beta \frac{|\dot{u}|}{\dot{u}} |x|^{n-1} x - \gamma |x|^n \right]$$

(B.12)

Finally, Eq. (B.12) is multiplied by $\dot{u}$ to yield

$$\dot{x} = \frac{1}{u_0} \left[\dot{u} - \beta |\dot{u}||x|^{n-1} x - \gamma \dot{u}|x|^n \right]$$

(B.13)

The similarities between Eqs. (B.8), (B.12), and (B.13), on the one hand, and Eqs. (B.7), (B.3) and (B.2), on the other, are clearly evident with the following definitions

$$\bar{z} = u_0 x$$

$$\bar{\gamma} = \frac{\gamma}{u_0^n}$$

(B.14)

$$\bar{\beta} = \frac{\beta}{u_0^n}$$
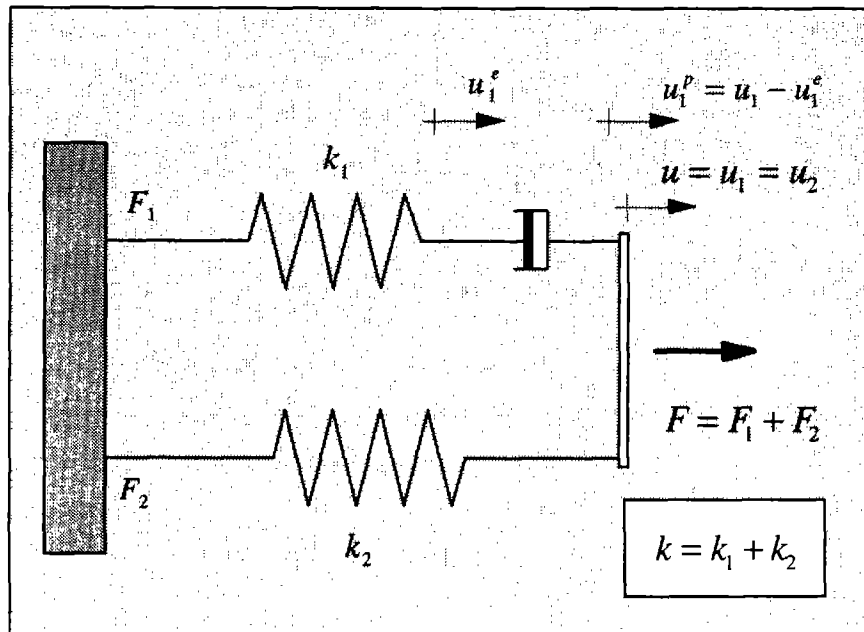
FIGURE B.2   CHANGE IN NOTATION OF MODEL IN FIGURE 4.1

FOR COMPARISON WITH BOUC-WEN MODEL

Then, Eqs. (B.8), (B.12) and (B.13) become

$$\frac{dF}{du} = k_0 \left\{ 1 - (1-\alpha)\left[sgn(du)\, sgn(\bar{z})\, \overline{\beta} + \overline{\gamma} \right] |\bar{z}|^n \right\} \tag{B.15}$$

$$\frac{d\bar{z}}{du} = 1 - \overline{\beta}\, \frac{|\dot{u}|}{\dot{u}}\, \bar{z}\, |\bar{z}|^{n-1} - \overline{\gamma}\, |\bar{z}|^n \tag{B.16}$$

$$\dot{\bar{z}} = \dot{u} - \overline{\beta}\, |\dot{u}|\, |\bar{z}|^{n-1}\, \bar{z} - \overline{\gamma}\, \dot{u}|\bar{z}|^n \tag{B.17}$$

BOUC-WEN MODEL	MODEL OF CHAPTER 4
$\dfrac{dF}{du} = k_0 \left\{ A - (1-\alpha)\left[sgn(du)\, sgn(z)\beta + \gamma \right]|z|^n \right\}$	$\dfrac{dF}{du} = k_0 \left\{ 1 - (1-\alpha)\left[sgn(du)\, sgn(\bar{z})\overline{\beta} + \overline{\gamma} \right]|\bar{z}|^n \right\}$
$\dfrac{dz}{du} = A - \beta\, \dfrac{|\dot{u}|}{\dot{u}}\,|z|^{n-1}\, z - \gamma\,|z|^n$	$\dfrac{d\bar{z}}{du} = 1 - \overline{\beta}\, \dfrac{|\dot{u}|}{\dot{u}}\, \bar{z}\,|\bar{z}|^{n-1} - \overline{\gamma}\,|\bar{z}|^n$
$\dot{z} = A\dot{u} - \beta\, |\dot{u}|\,|z|^{n-1}\, z - \gamma\,\dot{u}|z|^n$	$\dot{\bar{z}} = \dot{u} - \overline{\beta}\,|\dot{u}|\,|\bar{z}|^{n-1}\,\bar{z} - \overline{\gamma}\,\dot{u}|\bar{z}|^n$

TABLE B.1   COMPARISON BETWEEN BOUC-WEN MODEL AND MODEL OF CHAPTER 4

Table B.1 offers a direct comparison of the governing differential equations for the two models. It can be concluded that the BW model with the definition of $\bar{z}$, $\overline{\gamma}$ and $\overline{\beta}$ according to Eq. (B.14) is identical with the proposed model, as long as the condition $A=1$ is imposed.

The BW model is widely used in nonlinear random vibration analysis of structures. Some studies have shown, however, that this model results in physically unreasonable hysteretic behavior when cycled between fixed load or displacement values of unequal magnitude. The proposed model suffers from the same problem. Thus the following discussion of this limitation makes only reference to the proposed model of Chapter 4.

Figure B.3 shows that, when the solid model is cycled between two fixed displacement values, it exhibits force relaxation. Two aspects of the hysteretic behavior of the model disagree with the observed physical behavior of specimens. First, the hysteretic loop of the model does not close, second, hysteretic cycles settle to a zero mean force. Furthermore, the model violates a fundamental plasticity postulate. After recalling that the energy dissipation during displacement reversal is equal to $\oint F\, du$, it is concluded that the model dissipates negative energy during the first displacement cycle in Figure B.3. This energy

corresponds to the area of the cross hatched region in Figure B.3. This behavior violates Ilyushin's postulate, which states, that the energy dissipation has to be positive in any displacement cycle. This phenomenon disappears after a certain number of cycles, when the model stabilizes to a zero mean force and the hysteretic loops close in Figure B.3.

Figure B.4 illustrates a second important shortcoming of these models. The model does not exhibit stable (closed) hysteretic loops when cycled between two fixed load values of unequal magnitude. For $n=1$, the value of drift d in a load cycle $F_1 \to F_2 \to F_1$ (with $F_1 > F_2$) is

$$d = \frac{1}{\beta - \gamma} \log\left(\frac{1-(\beta-\gamma)|F_2|}{1-(\beta-\gamma)|F_1|}\right) + \frac{1}{\beta - \gamma} \log\left(\frac{1+(\beta+\gamma)|F_2|}{1+(\beta+\gamma)|F_1|}\right)$$ (B.18)
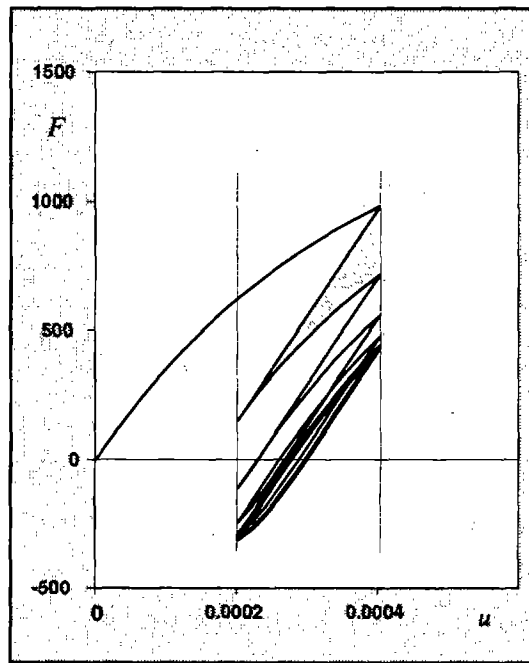
FIGURE B.3   HYSTERETIC BEHAVIOR OF THE MODEL UNDER CYCLING BETWEEN FIXED, ASYMMETRIC DISPLACEMENT VALUES

From Eq. (B.18) it can be concluded that symmetric load cycles do not exhibit drift, but that asymmetric load cycles always exhibit drift. This phenomenon arises for the following two main reasons: first, the model does not distinguish between first loading and reloading. Second, the unloading stiffness is always greater than the loading stiffness. This is evident from Eq. (B.8), which results in the following expressions for the loading stiffness k_l and the unloading stiffness k_u, for $x > 0$:
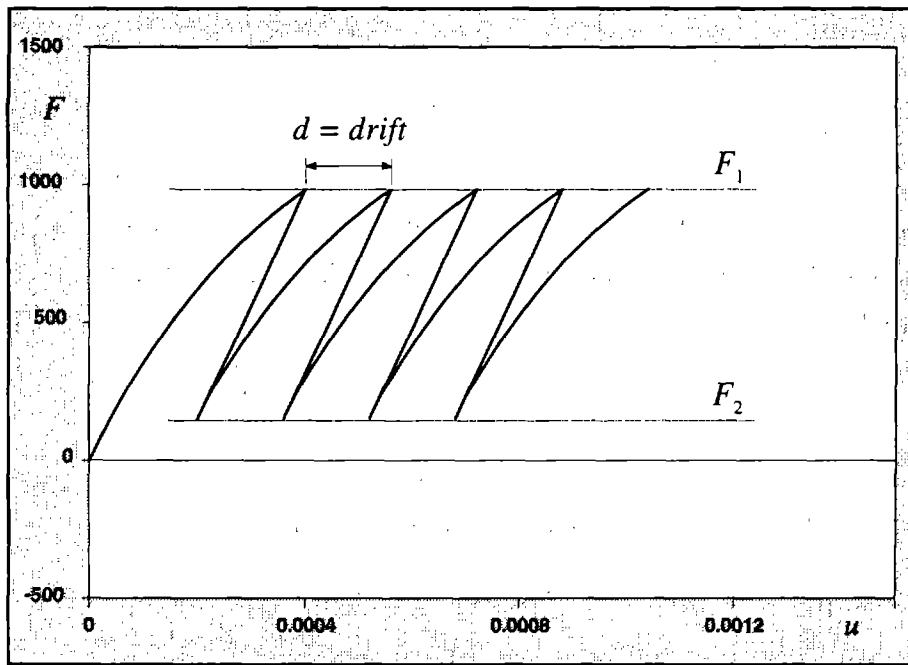
**FIGURE B.4   HYSTERETIC BEHAVIOR OF THE MODEL UNDER CYCLING
BETWEEN FIXED, ASYMMETRIC FORCE VALUES**
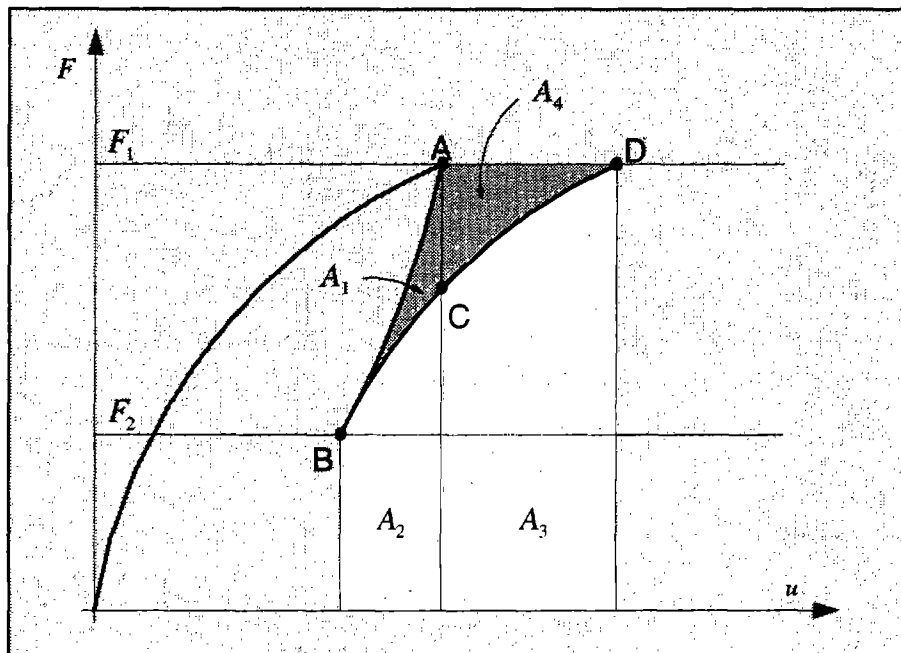
**FIGURE B.5   HYSTERETIC BEHAVIOR OF THE MODEL FOR A SINGLE
LOAD CYCLE BETWEEN ASYMMETRIC FORCE VALUES**

$$k_l = k_0 \left\{ 1 - (1-\alpha) |x|^n \right\}$$

$$k_u = k_0 \left\{ 1 - (1-\alpha)(-\beta + \gamma)|x|^n \right\}$$

Since $\gamma \le 0.5$ and $\beta + \gamma = 1$, the unloading stiffness k_u is always greater than the loading stiffness k_l for the same x. This is the result of the derivation of the dash pot equation Eq. (4.8) to include loading and unloading paths. This phenomenon also leads to violation of Ilyushin's postulate. This can be clearly seen in the hysteretic loop of Figure B.5. When the model describes path ABC, it undergoes a full displacement cycle and dissipates energy equal to $-A_1$, which is again negative.

Drucker's postulate is also violated. It states that for any load cycle with initial and final force level F_1 the following inequality must be satisfied

$$\oint (F - F_1) du \ge 0 \qquad\qquad\qquad (B.19)$$

Since this integral is equal to $-(A_1 + A_4)$ in Figure B.5, the model violates Eq. (B.19). A partial correction of the BW model was proposed by Casciyati (1987), which results in a reduction, but, no elimination of the observed drift, and, thus, again violates Ilyushin's and Drucker's postulates.

The same deficiencies plague the original endochronic theory of Valanis (1971), who found that the problem was caused by the fact that the unloading stiffness at a point of stress reversal is larger than the initial stiffness, while experimental results show that the two values should be approximately equal. In a later work, Valanis (1980) demonstrated that defining the intrinsic time in the plastic-strain space, and not, as in the original formulation, in the total strain space, results in an endochronic formulation that exhibits the correct hysteretic behavior, in satisfaction of Ilyushin's and Drucker's plasticity postulates. More recently, Valanis (1981) argues that the violation of the above plasticity postulates does not diminish the validity of the theory and, goes on to demonstrate that linear viscoelastic materials, as well as frictional materials, violate the same stability postulates.

From these observations it is concluded that:

• both, the Bouc-Wen model and the model proposed in Chapter 4 violate Drucker's and Ilyushin's plasticity postulates when cycled between fixed, but unequal, load or displacement values. This aberrant behavior can be, however, corrected by defining intrinsic time in the plastic strain space, and not in the total strain space;

- the two postulates do not represent strict physical or thermodynamical requirements, and other widely used mechanical models exhibit the same behavior;

- the refinement of the model in Chapter 4 to satisfy the two postulates in accordance with Valanis' recent proposals is beyond the scope of this study. Moreover, extensive numerical simulations with the model have shown that its numerical stability and accuracy is not affected by the violation of Ilyushin's and Drucker's postulates.

, EARTHQUAKE ENGINEERING RESEARCH CENTER REPORT SERIES

EERC reports are available from the National Information Service for Earthquake Engineering (NISEE) and from the National Technical Information Service (NTIS). Numbers in parentheses are Accession Numbers assigned by the National Technical Information Service; these are followed by a price code. Contact NTIS, 5285 Port Royal Road, Springfield Virginia, 22161 for more information. Reports without Accession Numbers were not available from NTIS at the time of printing. For a current complete list of EERC reports (from EERC 67-1) and availablity information, please contact University of California, EERC, NISEE, 1301 South 46th Street, Richmond, California 94804-4698.

UCB/EERC-84/01   "Pseudodynamic Test Method for Seismic Performance Evaluation: Theory and Implementation," by Shing, P.-S.B. and Mahin, S.A., January 1984, (PB84 190 644)A08.

UCB/EERC-84/02   "Dynamic Response Behavior of Kiang Hong Dian Dam," by Clough, R.W., Chang, K.-T., Chen, H.-Q. and Stephen, R.M., April 1984, (PB84 209 402)A08.

UCB/EERC-84/03   "Refined Modelling of Reinforced Concrete Columns for Seismic Analysis," by Kaba, S.A. and Mahin, S.A., April 1984, (PB84 234 384)A06.

UCB/EERC-84/04   "A New Floor Response Spectrum Method for Seismic Analysis of Multiply Supported Secondary Systems," by Asfura, A. and Der Kiureghian, A., June 1984, (PB84 239 417)A06.

UCB/EERC-84/05   "Earthquake Simulation Tests and Associated Studies of a 1/5th-scale Model of a 7-Story R/C Frame-Wall Test Structure," by Bertero, V.V., Aktan, A.E., Charney, F.A. and Sause, R., June 1984, (PB84 239 409)A09.

UCB/EERC-84/06   "Unassigned," by Unassigned, 1984.

UCB/EERC-84/07   "Behavior of Interior and Exterior Flat-Plate Connections Subjected to Inelastic Load Reversals," by Zee, H.L. and Moehle, J.P., August 1984, (PB86 117 629/AS)A07.

UCB/EERC-84/08   "Experimental Study of the Seismic Behavior of a Two-Story Flat-Plate Structure," by Moehle, J.P. and Diebold, J.W., August 1984, (PB86 122 553/AS)A12.

UCB/EERC-84/09   "Phenomenological Modeling of Steel Braces under Cyclic Loading," by Ikeda, K., Mahin, S.A. and Dermitzakis, S.N., May 1984, (PB86 132·198/AS)A08.

UCB/EERC-84/10   "Earthquake Analysis and Response of Concrete Gravity Dams," by Fenves, G.L. and Chopra, A.K., August 1984, (PB85 193 902/AS)A11.

UCB/EERC-84/11   "EAGD-84: A Computer Program for Earthquake Analysis of Concrete Gravity Dams," by Fenves, G.L. and Chopra, A.K., August 1984, (PB85 193 613/AS)A05.

UCB/EERC-84/12   "A Refined Physical Theory Model for Predicting the Seismic Behavior of Braced Steel Frames," by Ikeda, K. and Mahin, S.A., July 1984, (PB85 191 450/AS)A09.

UCB/EERC-84/13   "Earthquake Engineering Research at Berkeley - 1984," by EERC, August 1984, (PB85 197 341/AS)A10.

UCB/EERC-84/14   "Moduli and Damping Factors for Dynamic Analyses of Cohesionless Soils," by Seed, H.B., Wong, R.T., Idriss, I.M. and Tokimatsu, K., September 1984, (PB85 191 468/AS)A04.

UCB/EERC-84/15   "The Influence of SPT Procedures in Soil Liquefaction Resistance Evaluations," by Seed, H.B., Tokimatsu, K., Harder, L.F. and Chung, R.M., October 1984, (PB85 191 732/AS)A04.

UCB/EERC-84/16   "Simplified Procedures for the Evaluation of Settlements in Sands Due to Earthquake Shaking," by Tokimatsu, K. and Seed, H.B., October 1984, (PB85 197 887/AS)A03.

UCB/EERC-84/17   "Evaluation of Energy Absorption Characteristics of Highway Bridges Under Seismic Conditions - Volume I (PB90 262 627)A16 and Volume II (Appendices) (PB90 262 635)A13," by Imbsen, R.A. and Penzien, J., September 1986.

UCB/EERC-84/18   "Structure-Foundation Interactions under Dynamic Loads," by Liu, W.D. and Penzien, J., November 1984, (PB87 124 889/AS)A11.

UCB/EERC-84/19   "Seismic Modelling of Deep Foundations," by Chen, C.-H. and Penzien, J., November 1984, (PB87 124 798/AS)A07.

UCB/EERC-84/20   "Dynamic Response Behavior of Quan Shui Dam," by Clough, R.W., Chang, K.-T., Chen, H.-Q., Stephen, R.M., Ghanaat, Y. and Qi, J.-H., November 1984, (PB86 115177/AS)A07.

UCB/EERC-85/01   "Simplified Methods of Analysis for Earthquake Resistant Design of Buildings," by Cruz, E.F. and Chopra, A.K., February 1985, (PB86 112299/AS)A12.

UCB/EERC-85/02   "Estimation of Seismic Wave Coherency and Rupture Velocity using the SMART 1 Strong-Motion Array Recordings," by Abrahamson, N.A., March 1985, (PB86 214 343)A07.

UCB/EERC-85/03   "Dynamic Properties of a Thirty Story Condominium Tower Building," by Stephen, R.M., Wilson, E.L. and Stander, N., April 1985, (PB86 118965/AS)A06.

UCB/EERC-85/04   "Development of Substructuring Techniques for On-Line Computer Controlled Seismic Performance Testing," by Dermitzakis, S. and Mahin, S., February 1985, (PB86 132941/AS)A08.

UCB/EERC-85/05   "A Simple Model for Reinforcing Bar Anchorages under Cyclic Excitations," by Filippou, F.C., March 1985, (PB86 112 919/AS)A05.

UCB/EERC-85/06   "Racking Behavior of Wood-framed Gypsum Panels under Dynamic Load," by Oliva, M.G., June 1985, (PB90 262 643)A04.

UCB/EERC-85/07   "Earthquake Analysis and Response of Concrete Arch Dams," by Fok, K.-L. and Chopra, A.K., June 1985, (PB86 139672/AS)A10.

UCB/EERC-85/08   "Effect of Inelastic Behavior on the Analysis and Design of Earthquake Resistant Structures," by Lin, J.P. and Mahin, S.A., June 1985, (PB86 135340/AS)A08.

UCB/EERC-85/09   "Earthquake Simulator Testing of a Base-Isolated Bridge Deck," by Kelly, J.M., Buckle, I.G. and Tsai, H.-C., January 1986, (PB87 124 152/AS)A06.

UCB/EERC-85/10   "Simplified Analysis for Earthquake Resistant Design of Concrete Gravity Dams," by Fenves, G.L. and Chopra, A.K., June 1986, (PB87 124 160/AS)A08.

UCB/EERC-85/11   "Dynamic Interaction Effects in Arch Dams," by Clough, R.W., Chang, K.-T., Chen, H.-Q. and Ghanaat, Y., October 1985, (PB86 135027/AS)A05.

UCB/EERC-85/12   "Dynamic Response of Long Valley Dam in the Mammoth Lake Earthquake Series of May 25-27, 1980," by Lai, S. and Seed, H.B., November 1985, (PB86 142304/AS)A05.

UCB/EERC-85/13   "A Methodology for Computer-Aided Design of Earthquake-Resistant Steel Structures," by Austin, M.A., Pister, K.S. and Mahin, S.A., December 1985, (PB86 159480/AS)A10 .

UCB/EERC-85/14   "Response of Tension-Leg Platforms to Vertical Seismic Excitations," by Liou, G.-S., Penzien, J. and Yeung, R.W., December 1985, (PB87 124 871/AS)A08.

UCB/EERC-85/15   "Cyclic Loading Tests of Masonry Single Piers: Volume 4 - Additional Tests with Height to Width Ratio of 1," by Sveinsson, B., McNiven, H.D. and Sucuoglu, H., December 1985, (PB87 165031/AS)A08.

UCB/EERC-85/16   "An Experimental Program for Studying the Dynamic Response of a Steel Frame with a Variety of Infill Partitions," by Yanev, B. and McNiven, H.D., December 1985, (PB90 262 676)A05.

UCB/EERC-86/01   "A Study of Seismically Resistant Eccentrically Braced Steel Frame Systems," by Kasai, K. and Popov, E.P., January 1986, (PB87 124 178/AS)A14.

UCB/EERC-86/02   "Design Problems in Soil Liquefaction," by Seed, H.B., February 1986, (PB87 124 186/AS)A03.

UCB/EERC-86/03   "Implications of Recent Earthquakes and Research on Earthquake-Resistant Design and Construction of Buildings," by Bertero, V.V., March 1986, (PB87 124 194/AS)A05.

UCB/EERC-86/04   "The Use of Load Dependent Vectors for Dynamic and Earthquake Analyses," by Leger, P., Wilson, E.L. and Clough, R.W., March 1986, (PB87 124 202/AS)A12.

UCB/EERC-86/05   "Two Beam-To-Column Web Connections," by Tsai, K.-C. and Popov, E.P., April 1986, (PB87 124 301/AS)A04.

UCB/EERC-86/06   "Determination of Penetration Resistance for Coarse-Grained Soils using the Becker Hammer Drill," by Harder, L.F. and Seed, H.B., May 1986, (PB87 124 210/AS)A07.

UCB/EERC-86/07   "A Mathematical Model for Predicting the Nonlinear Response of Unreinforced Masonry Walls to In-Plane Earthquake Excitations," by Mengi, Y. and McNiven, H.D., May 1986, (PB87 124 780/AS)A06.

UCB/EERC-86/08   "The 19 September 1985 Mexico Earthquake: Building Behavior," by Bertero, V.V., July 1986.

UCB/EERC-86/09   "EACD-3D: A Computer Program for Three-Dimensional Earthquake Analysis of Concrete Dams," by Fok, K.-L., Hall, J.F. and Chopra, A.K., July 1986, (PB87 124 228/AS)A08.

UCB/EERC-86/10   "Earthquake Simulation Tests and Associated Studies of a 0.3-Scale Model of a Six-Story Concentrically Braced Steel Structure," by Uang, C.-M. and Bertero, V.V., December 1986, (PB87 163 564/AS)A17.

UCB/EERC-86/11   "Mechanical Characteristics of Base Isolation Bearings for a Bridge Deck Model Test," by Kelly, J.M., Buckle, I.G. and Koh, C.-G., November 1987, (PB90 262 668)A04.

UCB/EERC-86/12   "Effects of Axial Load on Elastomeric Isolation Bearings," by Koh, C.-G. and Kelly, J.M., November 1987.

UCB/EERC-87/01   "The FPS Earthquake Resisting System: Experimental Report," by Zayas, V.A., Low, S.S. and Mahin, S.A., June 1987, (PB88 170 287)A06.

UCB/EERC-87/02   "Earthquake Simulator Tests and Associated Studies of a 0.3-Scale Model of a Six-Story Eccentrically Braced Steel Structure," by Whittaker, A., Uang, C.-M. and Bertero, V.V., July 1987, (PB88 166 707/AS)A18.

UCB/EERC-87/03   "A Displacement Control and Uplift Restraint Device for Base-Isolated Structures," by Kelly, J.M., Griffith, M.C. and Aiken, I.D., April 1987, (PB88 169 933)A04.

UCB/EERC-87/04   "Earthquake Simulator Testing of a Combined Sliding Bearing and Rubber Bearing Isolation System," by Kelly, J.M. and Chalhoub, M.S., December 1990.

UCB/EERC-87/05   "Three-Dimensional Inelastic Analysis of Reinforced Concrete Frame-Wall Structures," by Moazzami, S. and Bertero, V.V., May 1987, (PB88 169 586/AS)A08.

UCB/EERC-87/06   "Experiments on Eccentrically Braced Frames with Composite Floors," by Ricles, J. and Popov, E., June 1987, (PB88 173 067/AS)A14.

UCB/EERC-87/07   "Dynamic Analysis of Seismically Resistant Eccentrically Braced Frames," by Ricles, J. and Popov, E., June 1987, (PB88 173 075/AS)A16.

UCB/EERC-87/08   "Undrained Cyclic Triaxial Testing of Gravels-The Effect of Membrane Compliance," by Evans, M.D. and Seed, H.B., July 1987, (PB88 173 257)A19.

UCB/EERC-87/09   "Hybrid Solution Techniques for Generalized Pseudo-Dynamic Testing," by Thewalt, C. and Mahin, S.A., July 1987, (PB 88 179 007)A07.

UCB/EERC-87/10   "Ultimate Behavior of Butt Welded Splices in Heavy Rolled Steel Sections," by Bruneau, M., Mahin, S.A. and Popov, E.P., September 1987, (PB90 254 285)A07.

UCB/EERC-87/11   "Residual Strength of Sand from Dam Failures in the Chilean Earthquake of March 3, 1985," by De Alba, P., Seed, H.B., Retamal, E. and Seed, R.B., September 1987, (PB88 174 321/AS)A03.

UCB/EERC-87/12   "Inelastic Seismic Response of Structures with Mass or Stiffness Eccentricities in Plan," by Bruneau, M. and Mahin, S.A., September 1987, (PB90 262 650/AS)A14.

UCB/EERC-87/13   "CSTRUCT: An Interactive Computer Environment for the Design and Analysis of Earthquake Resistant Steel Structures," by Austin, M.A., Mahin, S.A. and Pister, K.S., September 1987, (PB88 173 339/AS)A06.

UCB/EERC-87/14   "Experimental Study of Reinforced Concrete Columns Subjected to Multi-Axial Loading," by Low, S.S. and Moehle, J.P., September 1987, (PB88 174 347/AS)A07.

UCB/EERC-87/15   "Relationships between Soil Conditions and Earthquake Ground Motions in Mexico City in the Earthquake of Sept. 19, 1985," by Seed, H.B., Romo, M.P., Sun, J., Jaime, A. and Lysmer, J., October 1987, (PB88 178 991)A06.

UCB/EERC-87/16   "Experimental Study of Seismic Response of R. C. Setback Buildings," by Shahrooz, B.M. and Moehle, J.P., October 1987, (PB88 176 359)A16.

UCB/EERC-87/17   "The Effect of Slabs on the Flexural Behavior of Beams," by Pantazopoulou, S.J. and Moehle, J.P., October 1987, (PB90 262 700)A07.

UCB/EERC-87/18   "Design Procedure for R-FBI Bearings," by Mostaghel, N. and Kelly, J.M., November 1987, (PB90 262 718)A04.

UCB/EERC-87/19   "Analytical Models for Predicting the Lateral Response of R C Shear Walls: Evaluation of their Reliability," by Vulcano, A. and Bertero, V.V., November 1987, (PB88 178 983)A05.

UCB/EERC-87/20   "Earthquake Response of Torsionally-Coupled Buildings," by Hejal, R. and Chopra, A.K., December 1987.

UCB/EERC-87/21   "Dynamic Reservoir Interaction with Monticello Dam," by Clough, R.W., Ghanaat, Y. and Qiu, X-F., December 1987, (PB88 179 023)A07.

UCB/EERC-87/22   "Strength Evaluation of Coarse-Grained Soils," by Siddiqi, F.H., Seed, R.B., Chan, C.K., Seed, H.B. and Pyke, R.M., December 1987, (PB88 179 031)A04.

UCB/EERC-88/01   "Seismic Behavior of Concentrically Braced Steel Frames," by Khatib, I., Mahin, S.A. and Pister, K.S., January 1988, (PB91 210 898/AS)A11.

UCB/EERC-88/02   "Experimental Evaluation of Seismic Isolation of Medium-Rise Structures Subject to Uplift," by Griffith, M.C., Kelly, J.M., Coveney, V.A. and Koh, C.G., January 1988, (PB91 217 950/AS)A09.

UCB/EERC-88/03   "Cyclic Behavior of Steel Double Angle Connections," by Astaneh-Asl, A. and Nader, M.N., January 1988, (PB91 210 872)A05.

UCB/EERC-88/04   "Re-evaluation of the Slide in the Lower San Fernando Dam in the Earthquake of Feb. 9, 1971," by Seed, H.B., Seed, R.B., Harder, L.F. and Jong, H.-L., April 1988, (PB91 212 456/AS)A07.

UCB/EERC-88/05   "Experimental Evaluation of Seismic Isolation of a Nine-Story Braced Steel Frame Subject to Uplift," by Griffith, M.C., Kelly, J.M. and Aiken, I.D., May 1988, (PB91 217 968/AS)A07.

UCB/EERC-88/06   "DRAIN-2DX User Guide.," by Allahabadi, R. and Powell, G.H., March 1988, (PB91 212 530)A12.

UCB/EERC-88/07   "Theoretical and Experimental Studies of Cylindrical Water Tanks in Base-Isolated Structures," by Chalhoub, M.S. and Kelly, J.M., April 1988, (PB91 217 976/AS)A05.

UCB/EERC-88/08   "Analysis of Near-Source Waves: Separation of Wave Types Using Strong Motion Array Recording," by Darragh, R.B., June 1988, (PB91 212 621)A08.

UCB/EERC-88/09   "Alternatives to Standard Mode Superposition for Analysis of Non-Classically Damped Systems," by Kusainov, A.A. and Clough, R.W., June 1988, (PB91 217 992/AS)A04.

UCB/EERC-88/10   "The Landslide at the Port of Nice on October 16, 1979," by Seed, H.B., Seed, R.B., Schlosser, F., Blondeau, F. and Juran, I., June 1988, (PB91 210 914)A05.

UCB/EERC-88/11   "Liquefaction Potential of Sand Deposits Under Low Levels of Excitation," by Carter, D.P. and Seed, H.B., August 1988, (PB91 210 880)A15.

UCB/EERC-88/12   "Nonlinear Analysis of Reinforced Concrete Frames Under Cyclic Load Reversals," by Filippou, F.C. and Issa, A., September 1988, (PB91 212 589)A07.

UCB/EERC-88/13   "Implications of Recorded Earthquake Ground Motions on Seismic Design of Building Structures," by Uang, C.-M. and Bertero, V.V., November 1988, (PB91 212 548)A06.

UCB/EERC-88/14   "An Experimental Study of the Behavior of Dual Steel Systems," by Whittaker, A.S., Uang, C.-M. and Bertero, V.V., September 1988, (PB91 212 712)A16.

UCB/EERC-88/15   "Dynamic Moduli and Damping Ratios for Cohesive Soils," by Sun, J.I., Golesorkhi, R. and Seed, H.B., August 1988, (PB91 210 922)A04.

UCB/EERC-88/16   "Reinforced Concrete Flat Plates Under Lateral Load: An Experimental Study Including Biaxial Effects," by Pan, A. and Moehle, J.P., October 1988, (PB91 210 856)A13.

UCB/EERC-88/17   "Earthquake Engineering Research at Berkeley - 1988," by EERC, November 1988, (PB91 210 864)A10.

UCB/EERC-88/18   "Use of Energy as a Design Criterion in Earthquake-Resistant Design," by Uang, C.-M. and Bertero, V.V., November 1988, (PB91 210 906/AS)A04.

UCB/EERC-88/19   "Steel Beam-Column Joints in Seismic Moment Resisting Frames," by Tsai, K.-C. and Popov, E.P., November 1988, (PB91 217 984/AS)A20.

UCB/EERC-88/20   "Base Isolation in Japan, 1988," by Kelly, J.M., December 1988, (PB91 212 449)A05.

UCB/EERC-89/01   "Behavior of Long Links in Eccentrically Braced Frames," by Engelhardt, M.D. and Popov, E.P., January 1989, (PB92 143 056)A18.

UCB/EERC-89/02   "Earthquake Simulator Testing of Steel Plate Added Damping and Stiffness Elements," by Whittaker, A., Bertero, V.V., Alonso, J. and Thompson, C., January 1989, (PB91 229 252/AS)A10.

UCB/EERC-89/03   "Implications of Site Effects in the Mexico City Earthquake of Sept. 19, 1985 for Earthquake-Resistant Design Criteria in the San Francisco Bay Area of California," by Seed, H.B. and Sun, J.I., March 1989, (PB91 229 369/AS)A07.

UCB/EERC-89/04   "Earthquake Analysis and Response of Intake-Outlet Towers," by Goyal, A. and Chopra, A.K., July 1989, (PB91 229 286/AS)A19.

UCB/EERC-89/05   "The 1985 Chile Earthquake: An Evaluation of Structural Requirements for Bearing Wall Buildings," by Wallace, J.W. and Moehle, J.P., July 1989, (PB91 218 008/AS)A13.

UCB/EERC-89/06   "Effects of Spatial Variation of Ground Motions on Large Multiply-Supported Structures," by Hao, H., July 1989, (PB91 229 161/AS)A08.

UCB/EERC-89/07   "EADAP - Enhanced Arch Dam Analysis Program: Users's Manual," by Ghanaat, Y. and Clough, R.W., August 1989, (PB91 212 522)A06.

UCB/EERC-89/08   "Seismic Performance of Steel Moment Frames Plastically Designed by Least Squares Stress Fields," by Ohi, K. and Mahin, S.A., August 1989, (PB91 212 597)A05.

UCB/EERC-89/09   "Feasibility and Performance Studies on Improving the Earthquake Resistance of New and Existing Buildings Using the Friction Pendulum System," by Zayas, V., Low, S., Mahin, S.A. and Bozzo, L., July 1989, (PB92 143 064)A14.

UCB/EERC-89/10   "Measurement and Elimination of Membrane Compliance Effects in Undrained Triaxial Testing," by Nicholson, P.G., Seed, R.B. and Anwar, H., September 1989, (PB92 139 641/AS)A13.

UCB/EERC-89/11   "Static Tilt Behavior of Unanchored Cylindrical Tanks," by Lau, D.T. and Clough, R.W., September 1989, (PB92 143 049)A10.

UCB/EERC-89/12   "ADAP-88: A Computer Program for Nonlinear Earthquake Analysis of Concrete Arch Dams," by Fenves, G.L., Mojtahedi, S. and Reimer, R.B., September 1989, (PB92 139 674/AS)A07.

UCB/EERC-89/13   "Mechanics of Low Shape Factor Elastomeric Seismic Isolation Bearings," by Aiken, I.D., Kelly, J.M. and Tajirian, F.F., November 1989, (PB92 139 732/AS)A09.

UCB/EERC-89/14   "Preliminary Report on the Seismological and Engineering Aspects of the October 17, 1989 Santa Cruz (Loma Prieta) Earthquake," by EERC, October 1989, (PB92 139 682/AS)A04.

UCB/EERC-89/15   "Experimental Studies of a Single Story Steel Structure Tested with Fixed, Semi-Rigid and Flexible Connections," by Nader, M.N. and Astaneh-Asl, A., August 1989, (PB91 229 211/AS)A10.

UCB/EERC-89/16   "Collapse of the Cypress Street Viaduct as a Result of the Loma Prieta Earthquake," by Nims, D.K., Miranda, E., Aiken, I.D., Whittaker, A.S. and Bertero, V.V., November 1989, (PB91 217 935/AS)A05.

UCB/EERC-90/01   "Mechanics of High-Shape Factor Elastomeric Seismic Isolation Bearings," by Kelly, J.M., Aiken, I.D. and Tajirian, F.F., March 1990.

UCB/EERC-90/02   "Javid's Paradox: The Influence of Preform on the Modes of Vibrating Beams," by Kelly, J.M., Sackman, J.L. and Javid, A., May 1990, (PB91 217 943/AS)A03.

UCB/EERC-90/03   "Earthquake Simulator Testing and Analytical Studies of Two Energy-Absorbing Systems for Multistory Structures," by Aiken, I.D. and Kelly, J.M., October 1990, (PB92 192 988)A13.

UCB/EERC-90/04   "Unassigned," by Unassigned, 1990.

UCB/EERC-90/05   "Preliminary Report on the Principal Geotechnical Aspects of the October 17, 1989 Loma Prieta Earthquake," by Seed, R.B., Dickenson, S.E., Riemer, M.F., Bray, J.D., Sitar, N., Mitchell, J.K., Idriss, I.M., Kayen, R.E., Kropp, A., Harder, L.F., Jr. and Power, M.S., April 1990, (PB 192 970)A08.

UCB/EERC-90/06   "Models of Critical Regions in Reinforced Concrete Frames Under Seismic Excitations," by Zulfiqar, N. and Filippou, F.C., May 1990.

UCB/EERC-90/07   "A Unified Earthquake-Resistant Design Method for Steel Frames Using ARMA Models," by Takewaki, I., Conte, J.P., Mahin, S.A. and Pister, K.S., June 1990.

UCB/EERC-90/08   "Soil Conditions and Earthquake Hazard Mitigation in the Marina District of San Francisco," by Mitchell, J.K., Masood, T., Kayen, R.E. and Seed, R.B., May 1990, (PB 193 267/AS)A04.

UCB/EERC-90/09   "Influence of the Earthquake Ground Motion Process and Structural Properties on Response Characteristics of Simple Structures," by Conte, J.P., Pister, K.S. and Mahin, S.A., July 1990, (PB92 143 064)A15.

UCB/EERC-90/10   "Experimental Testing of the Resilient-Friction Base Isolation System," by Clark, P.W. and Kelly, J.M., July 1990, (PB92 143 072)A08.

UCB/EERC-90/11   "Seismic Hazard Analysis: Improved Models, Uncertainties and Sensitivities," by Araya, R. and Der Kiureghian, A., March 1988.

UCB/EERC-90/12   "Effects of Torsion on the Linear and Nonlinear Seismic Response of Structures," by Sedarat, H. and Bertero, V.V., September 1989, (PB92 193 002/AS)A15.

UCB/EERC-90/13   "The Effects of Tectonic Movements on Stresses and Deformations in Earth Embankments," by Bray, J. D., Seed, R. B. and Seed, H. B., September 1989.

UCB/EERC-90/14   "Inelastic Seismic Response of One-Story, Asymmetric-Plan Systems," by Goel, R.K. and Chopra, A.K., October 1990, (PB93 114 767)A11.

UCB/EERC-90/15   "Dynamic Crack Propagation: A Model for Near-Field Ground Motion.," by Seyyedian, H. and Kelly, J.M., 1990.

UCB/EERC-90/16   "Sensitivity of Long-Period Response Spectra to System Initial Conditions," by Blasquez, R., Ventura, C. and Kelly, J.M., 1990.

UCB/EERC-90/17   "Behavior of Peak Values and Spectral Ordinates of Near-Source Strong Ground-Motion over a Dense Array," by Niazi, M., June 1990, (PB93 114 833)A07.

UCB/EERC-90/18   "Material Characterization of Elastomers used in Earthquake Base Isolation," by Papoulia, K.D. and Kelly, J.M., 1990, PB94-190063.

UCB/EERC-90/19   "Cyclic Behavior of Steel Top-and-Bottom Plate Moment Connections," by Harriott, J.D. and Astaneh-Asl, A., August 1990, (PB91 229 260/AS)A05.

UCB/EERC-90/20   "Seismic Response Evaluation of an Instrumented Six Story Steel Building," by Shen, J.-H. and Astaneh-Asl, A., December 1990, (PB91 229 294/AS)A04.

UCB/EERC-90/21   "Observations and Implications of Tests on the Cypress Street Viaduct Test Structure," by Bollo, M., Mahin, S.A., Moehle, J.P., Stephen, R.M. and Qi, X., December 1990, (PB93 114 775)A13.

UCB/EERC-91/01   "Experimental Evaluation of Nitinol for Energy Dissipation in Structures," by Nims, D.K., Sasaki, K.K. and Kelly, J.M., 1991.

UCB/EERC-91/02   "Displacement Design Approach for Reinforced Concrete Structures Subjected to Earthquakes," by Qi, X. and Moehle, J.P., January 1991, (PB93 114 569/AS)A09.

UCB/EERC-91/03   "A Long-Period Isolation System Using Low-Modulus High-Damping Isolators for Nuclear Facilities at Soft-Soil Sites," by Kelly, J.M., March 1991, (PB93 114 577/AS)A10.

UCB/EERC-91/04   "Dynamic and Failure Characteristics of Bridgestone Isolation Bearings," by Kelly, J.M., April 1991, (PB93 114 528)A05.

UCB/EERC-91/05   "Base Sliding Response of Concrete Gravity Dams to Earthquakes," by Chopra, A.K. and Zhang, L., May 1991, (PB93 114 544/AS)A05.

UCB/EERC-91/06   "Computation of Spatially Varying Ground Motion and Foundation-Rock Impedance Matrices for Seismic Analysis of Arch Dams," by Zhang, L. and Chopra, A.K., May 1991, (PB93 114 825)A07.

UCB/EERC-91/07   "Estimation of Seismic Source Processes Using Strong Motion Array Data," by Chiou, S.-J., July 1991, (PB93 114 551/AS)A08.

UCB/EERC-91/08   "A Response Spectrum Method for Multiple-Support Seismic Excitations," by Der Kiureghian, A. and Neuenhofer, A., August 1991, (PB93 114 536)A04.

UCB/EERC-91/09   "A Preliminary Study on Energy Dissipating Cladding-to-Frame Connection," by Cohen, J.M. and Powell, G.H., September 1991, (PB93 114 510)A05.

UCB/EERC-91/10   "Evaluation of Seismic Performance of a Ten-Story RC Building During the Whittier Narrows Earthquake," by Miranda, E. and Bertero, V.V., October 1991, (PB93 114 783)A06.

UCB/EERC-91/11   "Seismic Performance of an Instrumented Six-Story Steel Building," by Anderson, J.C. and Bertero, V.V., November 1991, (PB93 114 809)A07.

UCB/EERC-91/12   "Performance of Improved Ground During the Loma Prieta Earthquake," by Mitchell, J.K. and Wentz, Jr., F.J., October 1991, (PB93 114 791)A06.

UCB/EERC-91/13   "Shaking Table - Structure Interaction," by Rinawi, A.M. and Clough, R.W., October 1991, (PB93 114 917)A13.

UCB/EERC-91/14   "Cyclic Response of RC Beam-Column Knee Joints: Test and Retrofit," by Mazzoni, S., Moehle, J.P. and Thewalt, C.R., October 1991, (PB93 120 277)A03.

UCB/EERC-91/15   "Design Guidelines for Ductility and Drift Limits: Review of State-of-the-Practice and State-of-the-Art in Ductility and Drift-Based Earthquake-Resistant Design of Buildings," by Bertero, V.V., Anderson, J.C., Krawinkler, H., Miranda, E. and The CUREe and The Kajima Research Teams,, July 1991, (PB93 120 269)A08.

UCB/EERC-91/16   "Evaluation of the Seismic Performance of a Thirty-Story RC Building," by Anderson, J.C., Miranda, E., Bertero, V.V. and The Kajima Project Research Team,, July 1991, (PB93 114 841)A12.

UCB/EERC-91/17   "A Fiber Beam-Column Element for Seismic Response Analysis of Reinforced Concrete Structures," by Taucer, F., Spacone, E. and Filippou, F.C., December 1991, (PB94 117 629AS)A07.

UCB/EERC-91/18   "Investigation of the Seismic Response of a Lightly-Damped Torsionally-Coupled Building," by Boroschek, R. and Mahin, S.A., December 1991, (PB93 120 335)A13.

UCB/EERC-92/01   "Studies of a 49-Story Instrumented Steel Structure Shaken During the Loma Prieta Earthquake," by Chen, C.-C., Bonowitz, D. and Astaneh-Asl, A., February 1992, (PB93 221 778)A08.

UCB/EERC-92/02   "Response of the Dumbarton Bridge in the Loma Prieta Earthquake," by Fenves, G.L., Filippou, F.C. and Sze, D.T., January 1992, (PB93 120 319)A09.

UCB/EERC-92/03   "Models for Nonlinear Earthquake Analysis of Brick Masonry Buildings," by Mengi, Y., McNiven, H.D. and Tanrikulu, A.K., March 1992, (PB93 120 293)A08.

UCB/EERC-92/04   "Shear Strength and Deformability of RC Bridge Columns Subjected to Inelastic Cyclic Displacements," by Aschheim, M. and Moehle, J.P., March 1992, (PB93 120 327)A06.

UCB/EERC-92/05   "Parameter Study of Joint Opening Effects on Earthquake Response of Arch Dams," by Fenves, G.L., Mojtahedi, S. and Reimer, R.B., April 1992, (PB93 120 301)A04.

UCB/EERC-92/06   "Seismic Behavior and Design of Semi-Rigid Steel Frames," by Nader, M.N. and Astaneh-Asl, A., May 1992.

UCB/EERC-92/07   "A Beam Element for Seismic Damage Analysis," by Spacone, E., Ciampi, V. and Filippou, F.C., August 1992.

16. Abstract This study proposes a beam finite element model with distributed inelasticity and two nonlinear end rotational springs for the nonlinear dynamic analysis of frame structures under earthquake excitations. The beam element is based on the assumption that deformations are small and shear deformations are neglected. The axial behavior is assumed to be linear elastic and is uncoupled from flexural behavior. The element is derived with the mixed method of finite element theory. The force distribution within the element is based on interpolation functions that satisfy equilibrium. The relation between element forces and corresponding deformations is derived from the weighted integral of the constitutive force-deformation relation. While the element can also be derived with the virtual force principle, the mixed method approach has the advantage of pointing the way to the consistent numerical implementation of the element state determination. The constitutive force-deformation relation of the control sections of the beam and of the end rotational springs has the form of a differential relation that is derived by extending the simple standard solid model according to the endochronic theory. The study concludes with a demonstration of the ability of the proposed model to trace the softening response of a cantilever beam without numerical difficulties and with correlation studies of the response of the model with the experimental behavior of two reinforced concrete cantilever beams that highlight the flexibility of the constitutive law in the description of the hysteretic behavior of structural members.

17. Document Analysis a. Descriptors

b. Identifiers/Open-Ended Terms

c. COSATI Field/Group